63-4-2

FTD-TT- 62-1762



# TRANSLATION

PHYSICAL METALLURGY AND HEAT TREATMENT OF STEEL
(SELECTED PARTS)



## FOREIGN TECHNOLOGY DIVISION

## AIR FORCE SYSTEMS COMMAND

**WRIGHT-PATTERSON AIR FORCE BASE**

**OHIO**

# UNEDITED ROUGH DRAFT TRANSLATION

PHYSICAL METALLURGY AND HEAT TREATMENT OF STEEL
(SELECTED PARTS)

BY: M. L. Bernshteyn and A. G. Rakhshtadt

English Pages: 138

SOURCE: Russian Book, Metallovedeniye i Termicheskaya Obrabotka Stali, Spravochnik, Metallurgizdat, Moskva, 1961, pp. 49-58, 592-597, 670-709



PREPARED BY:

TRANSLATION SERVICES BRANCH
FOREIGN TECHNOLOGY DIVISION
WP-AFB, OHIO.

TABLE OF CONTENTS

## Chapter 4

## METHODS OF DETERMINING RESIDUAL STRESSES*

### 1. GENERAL

Stresses that remain in a body after the factors giving rise to them have been withdrawn are known as residual stresses.** The causes of the appearance of residual stresses are irreversible changes (non-uniform plastic deformations, phase transformations, and so forth) that are not uniform throughout the volume of the solid.

A mechanical method of determining residual stresses has been proposed by N.V. Kalakutskiy [2]. It is based on the following considerations. The residual stresses are mutually compensated within the body – their resultant and moment are zero in any section, as proceeds directly from the body's equilibrium conditions. If some part of a stressed body is removed, the stress equilibrium in the rest of it will be disturbed. Elastic deformations will arise in it; on measurement, these will enable us to determine the values of the residual stresses.

The mechanical method has been developed only for bodies of the simplest symmetrical shapes: cylinders, tubes, plates, and so forth, and cannot be applied to bodies with complex shapes, i.e., to the majority of real objects. Moreover, the distribution of the residual stresses depends to a considerable degree on the shape of the body.

Use of the mechanical method is limited further by the fact that the pieces subject to investigation are usually completely or, more rarely, partially destroyed.



TMP TT 60-1769/1+2

THIS
PAGE
IS
MISSING
IN
ORIGINAL
DOCUMENT

residual stresses from the measured deformations.

Below we consider a number of specific cases in which the mechanical method is applied to determine residual stresses of the first kind.

## 2. DETERMINATION OF RESIDUAL STRESSES IN CYLINDRICAL BODIES

Every stressed state is characterized by three principal stresses. For cylindrical bodies, these stresses are axial, radial and tangential (or circumferential). Figure 1 shows a volume element that has been cut out of a cylinder. The arrows indicate the principal-stress vectors. The radial stresses $\sigma_r$ are directed along the radius of the cylinder's circumference, the axial stresses $\sigma_{os}$ along the axis of the cylinder, and the tangential stresses $\sigma_t$ along the normal to the meridional plane.

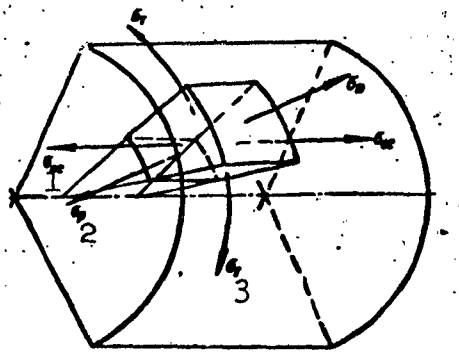


Fig. 1. Diagram of stressed state in cylindrical body. 1) $\sigma_{os}$; 2) $\sigma_r$; 3) $\sigma_t$.

The methods of Zaks [Sachs], Kalakutskiy and Davidenkov are extensively used for investigation of residual stresses in cylindrical objects.

### The Zaks Method

The surface of the cylinder and its faces are ground in such a way that the faces are parallel to one another and perpendicular to the axis of the cylinder. The prepared cylinder is carefully measured: the diameter is measured in three directions in each of three zones and the length along three different symmetrically located generatrices (Fig. 2). After these measurements have been taken, the cylinder is center-drilled through its axis and the diameters and lengths of the cylinder again measured at the same points as previously. Then the hole is bored out progressively (by steps) and the same measurements repeated after each boring operation. The boring steps must be suffi-

ciently small to produce the largest possible number of points for the stress diagrams, but not so small that the deformations produced by the boring cannot be measured with sufficient accuracy.

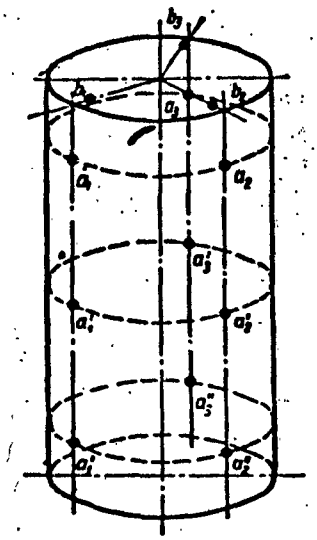

Fig. 2. Diagram illustrating measurement of dimensions of cylinder in determining residual stresses by Zaks method: $a_1$, $a'_1$, $a''_1$, $a_2$, $a'_2$, $a''_2$, $a_3$, $a'_3$, and $a''_3$ are the points of deformation measurement on three diameters meeting at an angle of 120° in three bands; $b_1$, $b_2$ and $b_3$ are the points at which the deformation in length is measured.

The measurements are used as a basis for computing the deformation of the cylinder after each boring operation and the residual stresses in the layer removed are determined from the average values of the cylinder's diametral and length deformations.

The stresses are computed by the following formulas (3):

$$\sigma_{oc} = \frac{E}{1-\mu^2}\left[(U_0 - f)\frac{d\Lambda}{df} - \Lambda\right]; \quad (1)$$

$$\sigma_r = \frac{E}{1-\mu^2} \times$$

$$\times\left[(U_0 - f)\frac{d\Theta}{df} - \frac{f_0 + f}{2f}\Theta\right]; \quad (2)$$

$$\sigma_p = \frac{E}{1-\mu^2}\cdot\frac{f_0 - f}{2f}\Theta, \quad (3)$$

where $f_v$ is the specimen's sectional area with respect to the outside diameter, $f$ is the area of the drilled pole, E is the normal elastic modulus, $\mu$ is Poisson's coefficient,

$$\Theta = \vartheta + \mu\lambda;$$
$$\Lambda = \lambda + \mu\vartheta,$$

where $\vartheta$ is the relative change in the diameter on boring the cylinder and $\lambda$ is the relative change in the cylinder's length.

The derivatives $d\Lambda/df$ and $d\Theta/df$ appearing in Formulas (1), (2) and (3) are computed graphically from curves of the variation of $\Theta$ and $\Lambda$ as functions of the area of the drilled hole $f$ (Fig. 3).

For these curves to be smooth, the experimental data must be cor-

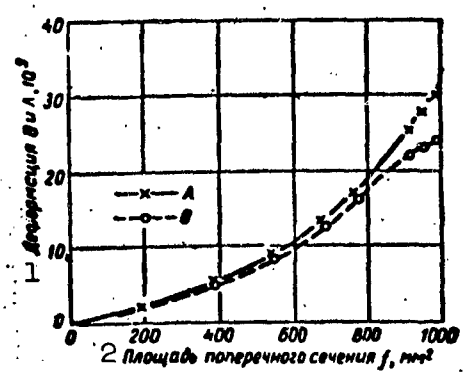


Fig. 3. Example of Λ and θ [sic] as functions of f. 1) Deformations Θ and Λ, $x10^3$; 2) cross-sectional area f, $mm^2$.

rected slightly when they are plotted. For convenience in graphic calculation of the derivatives, the values of Θ and Λ may be increased by a factor of $10^5$.

To compute the derivative at the required point of the curve (for given values of Θ and f or of Λ and f), a tangent is passed and the slope of this tangent to the axis of abscissas is computed. The sign of the derivative is determined by the sign of the tangent in the quadrant in question.

The line is passed tangent to the curve very easily with the aid of a mirror [4]. For this purpose, a mirror standing perpendicular to the paper is adjusted in such a way that the reflection seen in it will be a smooth extension of the curve. Given this condition, the edge of the mirror coincides with the normal to the curve. Once we have located the direction of the normal at the point in question, we may also draw the tangent.

After computing the axial, tangential and radial residual stresses for the various layers, we may plot curves of these stresses over the section of the cylindrical object. The correctness of the stress determination may be established by checking to see whether the resultant of the axial stresses and the moment of the tangential (circumferential) stresses are zero; the sum of the circumferential stresses (or the stresses constructed as a function of the square of the radius) should also be zero.

In determining residual stresses in hollow cylinders (thick-walled tubes), the approach is the same as with solid cylinders, except that

the central holes are not drilled. The stresses are determined by performing successive boring operations on the tube and measuring the diametral and length deformations.

Calculation of the residual stresses with progressive boring-out of the cylinder has a shortcoming in that the magnitude and distribution of the stresses in the surface layer can be obtained only by extrapolation, since the cylinder can be bored out only to a certain limit.

To obtain the complete residual-stress curve, the cylinder-boring experiments must be supplemented by investigations of another specimen, the outer surface of which is turned for measurement of the inside-diameter deformation of the cylinder instead of that of the outside diameter.

When outside layers are removed, the stresses are computed by the following formulas:

$$\sigma_{oc} = \frac{E}{1-\mu^2}\left[(f-f_a)\frac{dA}{df} - A\right]; \qquad (4)$$

$$\sigma_T = \frac{E}{1-\mu^2} \times$$

$$\times\left[(f-f_a)\frac{d\theta}{df} \cdot \frac{f+f_a}{2f}\theta\right]; \qquad (5)$$

$$\sigma_p = -\frac{E}{1-\mu^2} \cdot \frac{f-f_a}{2f}\theta. \qquad (6)$$

Basically, the symbols in these formulas have the same significance as in Formulas (1), (2) and (3); $f_a$ is the area of the cylinder's internal cross section and $f$ is the area of the outside cross section of the cylinder, which changes on turning.

The full stress diagram is constructed by juxtaposing the partial curves obtained on boring and turning the cylinders.

The use of two cylinders can be recommended only when the stress curves in these cylinders are fully identical. However, this is difficult to arrange. Consequently, the complete curve is determined on a single cylinder, which is subjected to successive boring and turning

operations [5]. Here, extrapolation to the surface of the cylinder is supplanted by interpolation over the thin central part of the cylinder that remains after all machining has been completed; this enables us to determine with high precision the superficial stresses, which are usually of the greatest interest.

In this case, the cylinder is first bored and the residual stresses computed for its internal region on the basis of the change in outside diameter and length, using Formulas (1), (2) and (3). Then the remainder of the cylinder is turned and the residual stresses computed for the outside of the cylinder by Formulas (4), (5) and (6) after measuring the changes in its length and inside diameter. However, these residual-stress values will not correspond to the true initial stresses because of the changes that have been wrought by the earlier boring operation. For determination of the true stresses, therefore, it is necessary to compute those residual stresses that were relieved in the cylinder's outside layers during the preliminary boring work, using the formulas

$$\sigma'_{oc} = -\frac{E}{1-\mu^2}\Lambda; \qquad (7)$$

$$\sigma'_{r} = -\frac{E}{1-\mu^2}\cdot\frac{l_0+l}{2l}\theta; \qquad (8)$$

$$\sigma'_{p} = \frac{E}{1-\mu^2}\cdot\frac{l_0-l}{2l}\theta; \qquad (9)$$

$$\Lambda = \lambda_p + \mu\vartheta_p;$$
$$\theta = \vartheta_p + \mu\lambda_p.$$

where $\lambda_r$ and $\vartheta_r$ are the relative changes in the length and outside diameter after preliminary boring of the cylinder.

The true residual stresses in the outer layers of the cylinder are equal to the algebraic sum of the stresses computed by Formulas (4), (5) and (6) in turning the cylinder and the stresses computed by Formulas (7), (8) and (9).

In many cases, it is sufficient to determine only the axial or

only the tangential and radial stresses.

If we study only the axial stresses, they may be computed by Formula (1) or (4), in which $\Lambda$ is replaced by $\lambda$ ($\lambda$ is the relative change in the cylinder's length) and the denominator $(1 - \mu^2)$ may be dropped.

It is necessary, however, to note that with this method of determining the axial stresses, the tangential and radial stresses that are practically always present in cylindrical components are deliberately not taken into account, so that the axial-stress value obtained is usually on the low side.

Like the axial stresses, the tangential and radial stresses may be computed by Formulas (2) and (3) for boring and by Formulas (5) and (6) when the cylinders are turned, replacing $\theta$ by $\vartheta$ and discarding $(1 - \mu^2)$.

If the investigation of residual stresses is to be limited to measurement of only the tangential and radial stresses, the test objects are disks cut from the cylinder. The thickness of such disks should be no greater than 1/5 of its diameter; it is limited to relieve the axial residual stresses [6].

The method set forth above for determining the residual stresses in cylindrical products is well-known in the literature as the Zaks method.

The basic deficiency of the Zaks method, which makes its use particularly difficult in industrial laboratories, consists in the small magnitude of the strains that are subject to measurement and in the extreme sensitivity of the method to temperature factors. The latter prevents undertaking measurements when the object has not been held at the temperature in question for 2-3 hours (depending on its size), and it is necessary to take parallel measurements on some control specimen that remains unchanged during the entire operation.

The method has yet another shortcoming (which, incidentally, is inherent to most other methods). In deriving formulas for calculation of residual stresses, we assumed axial symmetry of the stress distribution and constancy of this distribution on the test length. In many cases, however, the stresses may be distributed asymmetrically. Further, the end effect, which upsets the uniformity of the residual-stress curves along the cylinder axis, arises in determining residual stresses in cylindrical articles. The influence of the end effect for cylinders extends to a depth of the same order as the cylinder diameter [7].

Dependable results may be obtained by the Zaks method only in cases where the cylinder length exceeds its diameter or wall thickness by a factor of at least 5-6 [8].

Together with this, only the Zaks method takes full and irreproachable account of the three-dimensional stressed state, and it is therefore most correct from a theoretical standpoint.

The Method of N.N. Davidenkov

For thin-walled tubes, the Zaks method is rendered virtually useless due to the small magnitude of the deformations subject to measurement.

Consequently, N.N. Davidenkov proposed another method based on measurement of bending deformations rather than tensile or compressive deformations [9].

For determining tangential residual stresses by this method, a segment of tube is slit along one of its generatrices and then layers of metal are removed progressively (for example, by etching) from the outside and inside surfaces of the tube, with measurement of the diameter change each time.

The total initial tangential residual stresses in thin-walled sec-

tions are composed of three components:

$$\sigma_r = \sigma_1 + \sigma_2 + \sigma_3, \tag{10}$$

where $\sigma_1$ are the residual stresses relieved when the ring is split; $\sigma_2$ are the residual stresses that exist in each layer of the tube when removal of all preceding layers is completed; $\sigma_3$ is a correction that takes into account the residual stresses relieved in the layer when all preceding layers are removed.

These components are determined (on removal of internal layers) by the respective formulas:

$$\sigma_1 = \frac{Ea}{2\rho} \cdot \frac{Z' + \frac{\delta^2}{12\rho}}{Z' + \rho} \Delta D; \tag{11}$$

$$\sigma_2 = -\frac{Ea^2\alpha}{3(D-a)^2} \cdot \frac{dD}{da}; \tag{12}$$

$$\sigma_3 = \frac{2E\alpha}{3(D-2a)D}\left[-3a(D_a - D_\delta) + \right.$$

$$\left. + \frac{D-2a}{D} \int_{D_\delta}^{D_a} x dD + \frac{D-a}{D^2} \int_{D_\delta}^{D_a} x^2 dD\right]. \tag{13}$$

In these formulas E is the elastic modulus, $\alpha$ is a coefficient taking into account the impossibility of curvature for the ring walls in the axial plane due to the cylindrical shape: $\alpha = 1/(1 - \mu^2)$; $\mu$ is the Poisson coefficient, $\rho$ is the radius of the median circumference of the ring, Z' is the distance of the layer under consideration from the median circumference, $\delta$ is the thickness of the ring wall, D is the outside diameter of the ring after splitting along a generatrix; $\Delta D$ is the measured change in the outside diameter of the ring on splitting (positive when the diameter increases), which is equal to the spread of the split ends divided by $\pi$, a is the distance between the center of the layer under consideration and the outside surface of the ring, and x is the present coordinate of all layers between $\delta$ and a.

The derivative dD/da is determined graphically from the curve of D = f(a). The quantities $\int_{D_\delta}^{D_a} x dD$ and $\int_{D_\delta}^{D_a} x^2 dD$ are found graphically (or by

rough calculation) from curves of $x = \varphi_1(D)$ and $x^2 = \varphi_2(D)$ constructed on the basis of the experimental data.

To determine the axial stresses, narrow strips are cut from the tube parallel to its axis and the deflection that appears on cutting is measured. Then successive internal layers are removed, e.g., by etching, and the deflection of the strips again measured.

The axial stresses are computed by the formulas

$$\sigma_{cc} = \sigma_1' + \sigma_2' + \sigma_3'; \qquad (14)$$

$$\sigma_1' = \frac{2E\left(\frac{h}{2} - a\right)}{b^2} \cdot f; \qquad (15)$$

$$\sigma_2' = -\frac{Ea^2}{3b^2} \cdot \frac{df}{da}; \qquad (16)$$

$$\sigma_3' = \frac{2E}{3b^2} \int_{f_b}^{f_a} x\,df - \frac{2Ea}{b^2}(f_a - f_b). \qquad (17)$$

where b is half the distance between the supports of the instrument used to measure the deflection, f is the deflection that arises when the strips are cut out (positive if the strip turns its convex side toward the tube axis); the other symbols have the same significance as in the earlier formulas.

The derivatives and integrals are found graphically from the curves of

$$f = \varphi_1(a) \text{ and } x = \varphi_2(f).$$

Since determination of residual stresses by the Davidenkov method presupposes progressive etching away of outside or inside layers, complications arise in study of stresses in tubes whose material does not lend itself to etching or does not etch with sufficient uniformity. Mechanical removal of layers is difficult in this case because secondary plastic deformations may arise in the tube after sectioning along the generatrix (due to its low rigidity). In this case, a special method for mechanical removal of layers may be employed [10].

The tube under study is broken up lengthwise into a number of segments, bored out stepwise to various diameters and then sectioned through these steps. The individual rings with different wall thicknesses obtained in this way are cut along a generatrix and the corresponding diameter changes are measured. Assuming that the magnitude and distribution of the residual stresses are the same in all segments of the tube, we may compute the tangential stresses in the individual rings and thus find their distribution over the thickness of the tube.

Method of N.V. Kalakutskiy

The Kalakutskiy method [2] is used for investigation of tangential stresses in disks (solid or cut from thick-walled tubes). Here it is assumed either that there are no axial stresses in the piece or that they are relieved in cutting out the template, the thickness of which must be as small as possible and, in any event, no greater than 1/5 of the diameter.

Essentially, the method consists in cutting up the disk into a series of concentric rings and measuring the changes in their diameters due to the cutting. These changes (as in the Zaks method) are very small, not exceeding a few hundredths of a millimeter, and are sensitive to temperature fluctuations. Consequently, the measurements should be made with great care. The calculations themselves are quite cumbersome.

The Kalakutskiy method is based on the use of the familiar Lamé formulas for thick-walled cylinders; the technique of the application consists in the following.

After the disk is cut out, its surface is ground and the rings to be cut out of it are scribed on its surface. Marks are made on the centerlines of these rings across three or four diameters (small crossed scratches are made or shallow cores are taken) and a comparator is used

to measure their sizes. Then ring-shaped grooves that separate the future rings are turned through (or marked) and the outside and inside radii of each ring are measured. After this, the rings are cut out and the marked diameters of the central circumferences are again measured on each ring.

The calculations amount to determining the reciprocal pressures experienced by the rings (which are equal to the radial compressive stresses) from the magnitude of the measured (absolute) displacement of the median circumference of the ring $\underline{u}$ according to the formula

$$u = -\frac{1-\mu}{E} r \frac{p_в r_в^2 - p_н r_н^2}{r_н^2 - r_в^2} + \frac{1+\mu}{E} \frac{r_в^2 r_н^2 (p_в - p_н)}{r (r_н^2 - r_в^2)}; \qquad (18)$$

where $\underline{r}$ is the average radius of the ring, $r_в$ and $r_н$ are the outside and inside radii of the ring, $p_в$ and $p_н$ are the inside and outside pressures (positive for compression) which are equal to the radial stresses, E is the elastic modulus, and $\mu$ is the Poisson constant.

The following calculation procedure can be recommended (from the outside ring toward the inside ring*).

The outside ring is free from loads along its external perimeter. Thus, setting $p_{1н} = 0$, we determine $p_1$ from the equation for $\underline{u}$; here (as everywhere in the material that follows), the sign of the variable $\underline{u}$ is reversed, since the deformation forms not under load but when the load is released.

The computed $p_{1в}$ also acts on the second ring. A correction is introduced to account for the finite width of the cut. Assuming that the pressure varies linearly on the small extent of the ring width, we employ linear extrapolation. If the ring width is denoted by $\underline{a}$ and the cut width by $\underline{c}$, the external pressure on the second ring is equal to

$$p_{2n} = p_{1n}\left(1 + \frac{c}{a}\right).$$

Passing through the second ring, for which $p_{2n}$ has already been determined, we find $p_{2v}$ from Eq. (18). As earlier, the correction

$$p_{3n} = p_{2n} + (p_{2n} - p_{2v})\frac{c}{a}.$$

is introduced on passing through the third ring.

Continuing further in the same manner, we finally arrive at the last, inside ring, for which we should find $p_{n_v} = 0$. This result is a check on the measurements and calculations.

After all radial stresses have been determined, the average tangential stresses are computed for each ring of radius $r$ using the formula

$$\sigma_T = -\frac{r_v^2 p_v - r_n^2 p_n}{r_n^2 - r_v^2} + \frac{(p_v - p_n) r_n^2 r_v^2}{r^2 (r_n^2 - r_v^2)}. \qquad (19)$$

The internal stresses are taken for Formula (19) without correction for the cut width.

These complex arithmetical calculations may be simplified considerably (at some cost in accuracy) if it is assumed that the tangential stresses remain constant within the limits of a single ring thickness and the cut width is disregarded, provided that it is sufficiently small as compared with the ring width [11].

In this case the calculations are carried out by the following procedure. For the first, outer (or inner) ring, which are assumed to have no radial stresses, the tangential stresses are computed by the formula

$$\sigma_T = -E\frac{\Delta D}{D}. \qquad (20)$$

where E is the elastic modulus and $\Delta D/D$ is the relative change in ring

diameter after cutting out ($\Delta D$ is taken positive for increasing ring diameter D after cutting out).

For all other rings, which do not face on the outside or free inside surfaces, the influence of radial stresses must also be taken into account in computing the tangential stresses, using the formula

$$\sigma_t = \mu \sigma_r - \frac{\Delta D}{D} E. \qquad (21)$$

The residual stresses are computed successively from the inside ring toward the outside ring or in the reverse order. In the former case, the change in radial stresses $\Delta\sigma'_r$ is found on transition to the second ring by the formula

$$\Delta\sigma'_r = \frac{\delta}{\rho}(\sigma_t - \sigma_r), \qquad (22)$$

where $\delta$ is the distance between the axes of neighboring grooves and $\rho$ is the radius of the groove centerline.

Substituting the value of $\sigma_t$ obtained from Eq. (20) in Eq. (22) and, as before, setting $\sigma_r = 0$, we find the value of $\Delta\sigma'_r$.

Radial stresses $\sigma''_r$ equal to the $\Delta\sigma'_r$ found above act from within on the second ring. Knowing the values of $\sigma''_r$ and $\Delta D/D$, we may determine $\sigma''_t$ for the second ring from Eq. (21).

Having found $\sigma''_t$ and substituted it in Eq. (22), we compute $\Delta\sigma''_r$ for the transition to the third ring. At this point, the radial stress $\sigma'''_r$ acting on the third ring becomes known:

$$\Delta\sigma'_r + \sigma''_r.$$

Continuing in a similar fashion, we may determine successively the tangential and radial stresses for all rings.

If the calculation is carried in the opposite direction – outside to inside – the sign is reversed in the right member of Eq. (22).

Determining the values of the tangential and radial stresses for each ring, we construct the curves of distribution of these stresses

over the cross section of the disk.

If the stress calculation begins with the inside ring, the radial stresses on the outside margin of the next ring should be found to equal zero. If this condition is not met, the erroneously computed value of the radial stresses (if it is not too large) should be distributed evenly among all rings by introducing the appropriate corrections into the tangential-stress values.

The radial stresses on the internal free surface of hollow cylinders (tubes) should also be equal to zero, while the radial stresses in the central ring of a solid cylinder should be equal to the tangential stresses.

Method of N.V. Kalakutskiy as Modified by N.N. Davidenkov

The Kalakutskiy method may be simplified. The measurement of ring deformation on cutting-out may be supplanted by measurement of the deformation that occurs when they are split along one of the radii after cutting out. If we make the quite plausible assumption that the resultant of the tangential stresses is basically relieved when the ring is cut out but that those stresses that create the bending moment are retained, the measured ring deformation after splitting enables us to compute this moment and, consequently, also to determine the slope of the tangential-stress diagram as a function of the median radius of the ring, using the formula

$$\operatorname{tg}\alpha = -\frac{d\sigma_T}{dr} = 2E\frac{\Delta D}{D^2}. \qquad (23)$$

Here, $\Delta D$ is the measured increase in ring diameter after splitting (which is equal to the spread between the cut boundaries, which is simpler to measure, divided by $\pi$).

Knowing the values of these tangents [slopes], we may use them in graphical construction of a curve of the actual stresses (by passing a

smoothing curve over segments of the tangents), or accomplish the same thing analytically assuming that passing a curve over the tangents represents an integration operation.

It must be remembered in this construction that the tangent in this case has the dimensions $kg/mm^2 \cdot mm$, so that it must be constructed taking into account the scales of the stresses (along the axis of ordinates) and lengths (along the axis of abscissas). If, for example, 100 mm is laid off on the axis of abscissas as the length scale, then the value of tan $\alpha$ must be laid off on the axis of ordinates in the stress scale multiplied by 100.

Construction of the curve begins with zero stress. After the entire curve has been plotted, the axis of abscissas is shifted parallel to itself until the positive and negative areas of the diagram become equal, i.e., until the equilibrium condition is satisfied. The ordinates of the curve read off the new axis are what will give the stress values.

The tangent method may also be used to check the curve obtained by the method of rings. However, it is more expedient to use it in combination with direct measurement of the deformation of the outside ring after it has been cut off, the more so because this deformation is usually quite large. Then, using the elementary formula (20), we may determine the tangential stress, and this gives the initial point for construction of the entire diagram. This method dispenses with the necessity of displacing the axis of abscissas and it becomes possible to verify whether the equilibrium condition has been satisfied.

There is also a method for constructing a general diagram from the deformations that arise when the rings are split. However, it involves tedious calculations and will therefore not be described here. For details concerning the above, see [8].

Other Methods for Determining Residual Stresses

Other methods are also known for determining residual stresses, e.g., those of Heyn and Bauer [12], Andersen and Fahlman [13], and Kirchberg [14]. As a rule, however, these methods can be used to investigate either the two-dimensional stressed state and hence to determine only two stress components (tangential and radial), or the linear stressed state, so that only the axial stresses are determined.

In approaching the selection of a method, it is first necessary to form at least a tentative conception concerning the magnitude of the deformations subject to measurement (as a function of the dimensions of the piece and the level of stresses).

It was noted above that the Zaks method enables us fully to define the three-dimensional stressed state in solid and hollow cylinders by determining all three components of the residual stresses – axial, tangential and radial. The Zaks method provides for measurement specifically of small deformations, and its application is limited by the measurement technique. Consequently, this method is practically useless for cylindrical products of large diameter, since boring the first layers of such a cylinder gives rise to such significant deformations at its surface that it is not possible to measure them with sufficient accuracy.

The possibility of using the Zaks method for determining residual stresses may be evaluated as follows.

Let us assume that it is necessary to determine the residual stresses in a disk cut out from a hollow steel cylinder; the inside radius $R_{vn}$ = 20 mm and the outside radius $R_{nar}$ = 60 mm.

Suppose that the minimal tangential stresses on the inside surface of this disk are 10 kg/mm$^2$ (no axial stresses).

Assuming that in this case it is necessary to bore the disks from

the inside, we determine the thickness of the layer by which these disks will be successively bored out. Let us set it equal to ~5% of $R_{nar} - R_{vn}$ (this will enable us to obtain 20 experimental points for plotting the stress diagram), or 2 mm.

When the first layer is removed by boring, the radial stresses relieved may be determined by the formula

$$\sigma_p = \frac{\Delta R}{R_{вн} + \Delta R} \sigma_r.$$

With $\Delta R = 2$ mm,

$$\sigma_p = \frac{2\sigma_r}{R_{вн} + 2}.$$

According to the formula for the radial displacement, the change in the disk's outside diameter is

$$\Delta D = \frac{4R_{вн}^2 R_{нар}\sigma_p}{E(R_{нар}^2 - R_{вн}^2)}.$$

With $E = 2.2 \cdot 10^4$ mm, the elastic deformation on the outside surface of the disk is of the order of 0.0015 mm.

Consequently, if the investigator has at his disposal facilities that enable him to measure elastic deformations with an error no greater than 0.0015 mm, he may use the Zaks method. In practice, however, it is very difficult to attain such accuracy and we may arrive at incorrect conclusions concerning the magnitude of the residual stresses and the manner in which they are distributed.

If the Kalakutskiy-Davidenkov method is used instead of the Zaks method in the case under consideration, we obtain a considerably higher accuracy in determining the stresses.

When the stresses are determined by the simplified Kalakutskiy-Davidenkov method, the smallest deformation for the inside ring is found to be

$$\Delta r = r\sigma_t/E,$$

i.e., the deformation is 0.01 mm in our example, or 6-7 times smaller than according to the Zaks method. Naturally, measurement of such deformations does not involve any complications.

The advantages of the Davidenkov method in applications to thin-walled tubes of small diameter may be evaluated similarly.

## 3. DETERMINATION OF RESIDUAL STRESSES IN PRISMATIC BODIES (BEAMS, PLATES)

The method developed by N.N. Davidenkov to determine axial residual stresses in strips cut out of tubes may be used to determine residual stresses in rectangular-section beams and plates in the uniaxial stressed state. In this case, layers of small thickness are removed successively from one side of the beam or plate (by etching, planing or grinding), and the distortions that arise are measured after each step. The stresses are computed by Formulas (14), (15), (16), and (17).

Subsequently, N.N. Davidenkov improved this method [15], assuming the thickness of the layers removed to be finite rather than infinitesimally small.

The formula for computing the axial stresses in this case takes the form

$$\sigma_{oc} = \frac{E}{\delta^2}\left[\frac{(\delta-a)^2}{3}\cdot\frac{\Delta f}{\Delta a}\varphi - \right.$$
$$- \int_0^{a-\Delta a} S\frac{\Delta x}{\delta-x} - (\delta+\Delta a-2a)\times$$
$$\left.\times f_{a-\Delta a} - \int_0^{a-\Delta a} x\,df\right]. \qquad (24)$$

Here

$$S = \frac{(\delta-x)^2}{3}\cdot\frac{\Delta f}{\Delta x}\varphi;$$
$$\varphi = \frac{1}{1+\frac{\Delta x}{\delta-a}};$$

a is the thickness of the layers removed, δ is the initial thickness of the beam or plate, Δa is the thickness of the layer in which the

stresses are determined, $x$ is the current coordinate, which varies from 0 to $[a - (\Delta a/2)]$, $\Delta x$ is the thickness of the layer situated at depth $x$ below the initial surface, $fa - \Delta a$ is the deflection due to removal of all layers to the depth $(a - \Delta a)$, $\Delta f$ is the deflection due to removal of one layer and $b$ is half the theoretical span of the beam.

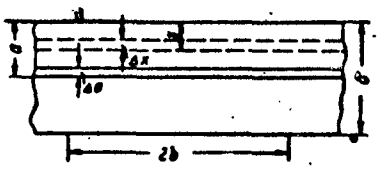

Fig. 4. Diagram illustrating symbols used in computing residual stresses in prismatic body.

All of these symbols will be understood from the diagram shown in Fig. 4.

Calculation of the residual stresses by the improved Formula (24) gives more accurate results than are obtained by Formulas (14), (15), (16), and (17).

In determining residual stresses in prismatic bodies, the layers removed should be as thin as possible for superior reproduction of the stressed state. With large test pieces, however, the deformations that arise on removal of such layers may prove to be so small that they cannot be measured. It is therefore necessary to specify a minimum value for the expected stress and first compute the order of magnitude of the expected strain. Obviously, the more sensitive the instrument, the thinner the layers that may be removed.

Removal of layers over the entire length of the test object represents considerable difficulty, particularly if it is made of hardened steel. Experiments have shown that it is possible to saw the piece to the same depth instead of removing layers [16]. If the number of saw cuts is sufficiently large, the result obtained is the same as if the whole layer had been removed. Thus, if we make cuts at an interval equal to three times the depth, only 5% of the actual stresses remain unregistered by the procedure.

## 4. DETERMINATION OF RESIDUAL STRESSES IN SURFACE LAYERS OF PIECES

Methods for determining residual stresses in any surface zone of a workpiece are also based on measurement of the elastic deformation produced by a change in the stressed state. This change is brought about by specific notching procedures, drilling holes, removing cores, and by other methods [7, 17, 18].

D.G. Kurnosov and M.V. Yakutovich [17] proposed that holes at least 1.5-2 diameters deep be drilled in the stressed surface layer to determine residual stresses in any surface zone of pieces with a flat surface or a surface having a slight curvature.

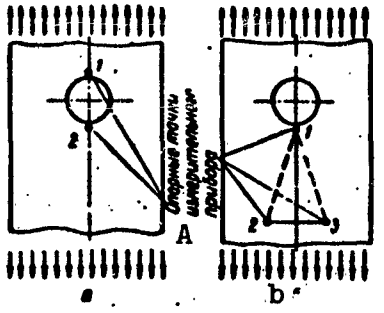


Fig. 5. Diagram illustrating measurement of deformations in determining stresses by hole drilling. A) Flaring points of measuring instrument.

When the hole is drilled, elastic deformations appear as a result of stress redistribution in regions adjoining the outline of the hole.

The hole is drilled normal to the surface of the piece. In many cases, this hole may be drilled without damaging the workpiece beyond tolerances, e.g., in residual-stress determinations on large forgings.

We may compute the residual stresses by determining the radial displacements of points on the outline of the hole.

The deformation measurement may be made in accordance with the schemes shown in Fig. 5; these indicate the placement of the reference points, the distances between which are subject to measurement. Setup a enables us to obtain shifts twice as large as those obtainable with setup b, but the use of setup b is more convenient in practice.

For the deformation measurement, D.G. Kurnosov built a strain tensometer with a 60-mm base and a special appliance for securing it to

the piece being investigated (resistance tensometers can also be used successfully for measurement of deformations, but they must be set up in a different pattern).

For the two-dimensional stressed state, when the directions of both principal stresses and their magnitudes are unknown, the displacements must be made in three directions.

It is convenient to use the following for these directions:

$$\varphi_1 = \vartheta;$$
$$\varphi_2 = \vartheta + 90°;$$
$$\varphi_3 = \vartheta + 45°,$$

where $\vartheta$ is the angle between one of the principal stresses and an arbitrarily selected direction in which the displacement is made.

The general equations for determining the principal stresses take the following form:

$$S = \frac{rE(U\varphi_1 + U\varphi_2)}{2a^2(1+\mu)} + \frac{E(U\varphi_1 - U\varphi_2)}{2\left[\frac{4a^2}{r} - (1+\mu)\frac{a^4}{r^4}\right]\cos 2\vartheta}; \quad (25)$$

$$K = \frac{rE(U\varphi_1 + U\varphi_2)}{2a^2(1+\mu)} - \frac{E(U\varphi_1 + U\varphi_2)}{2\left[\frac{4a^2}{r} - (1+\mu)\frac{a^4}{r^4}\right]\cos 2\vartheta}. \quad (26)$$

where S and K are the principal stresses, $U\varphi_1$, $U\varphi_2$, and $U\varphi_3$ are the displacements in the three directions, r and $\vartheta$ are the polar coordinates of the point on the body whose radial displacement is being measured, and a is the radius of the hole.

If the directions of the principal stresses in the part being investigated are known in advance, e.g., for bodies of simple shape (cylinder, tube, beam, plate, and so forth), then determining their magnitudes requires only measurement of the two corresponding displacements $U_1$ and $U_2$ of the hole contour at a $90^\circ$ angle to one another.

In this case, the stresses are determined by the formulas

$$S = \frac{E[2U_1 + (1-\mu)U_2]}{a(1+\mu)\cdot(3-\mu)}; \qquad (27)$$

$$K = \frac{E[2U_2 + (1-\mu)U_1]}{a(1+\mu)(3-\mu)}. \qquad (28)$$

A pillar may be drilled out with a circular slot to determine residual stresses in the surface layer of a stressed component [18]. The surface deformation of the pillar is measured with wire strain-gauge pickups.

If the measurement is made with simple strain-gauge pickups, it is necessary to core out two pillars, measuring the surface deformation in one direction on each pillar. The measurements may be made on the same pillar by using complex rosette pickups. The pillar diameter should be slightly larger than the pickup base. The depth of the circular slot should be at least 0.7 of the pillar diameter.

The residual stresses are computed by the formulas

$$\sigma_t = -\frac{E}{1-\mu^2}(\varepsilon_t + \mu\varepsilon_{oc}), \qquad (29)$$

$$\sigma_{oc} = -\frac{E}{1-\mu^2}(\varepsilon_{oc} + \mu\varepsilon_t), \qquad (30)$$

where $\varepsilon_t$ and $\varepsilon_{os}$ are the relative deformations measured in the two directions – tangential and axial.

Manuscript Page No.

[Footnotes]

1 Academician N.N. Davidenkov of the Ukrainian SSR was responsible for scientific editing of the paper.

1 The present chapter considers only the mechanical method of determining residual stresses as it applies in the classification of N.N. Davidenkov [1] to stresses of the first kind. Stresses (or, more properly, distortions) of kind II are considered in the chapter entitled "X-Ray Structural Analysis of Polycrystals."

13 N. Kalakutskiy recommends the reverse procedure in the interests of greater accuracy.

REFERENCES


1. N.N. Davidenkov, Sb. Rentgenografiya v prilozhenii k ispytaniyu materialov [Collection. The Application of Roentgenography to Tests of Materials], 1936.
2. N.V. Kalakutskiy, Issledovaniye vnutrennykh napryazheniy v chugune i stali [Investigation of Internal Stresses in Cast Iron and Steel], 1887.
3. G. Zaks, Prakticheskoye metallovedeniye [Practical Physical Metallurgy], Part II, ONTI [United Scientific and Technical Publishing House], 1938.
4. L.A. Glikman, Zavodskaya laboratoriya [Industrial Laboratory], 1936, No. 6.
5. L.A. Glikman and A.N. Babayev, Zavodskaya laboratoriya, 1956, No. 4.
6. M.P. Zheldak and G.V. Kurdyumov, Zavodskaya laboratoriya, 1936, No. 6.
7. S.O. Tsobkallo and D.M. Vasil'yev, Zavodskaya laboratoriya, 1949, No. 2.
8. N.N. Davidenkov, Zavodskaya laboratoriya, 1950, Nos. 2 and 12.
9. N.N. Davidenkov, ZhTF [J. Tech. Phys.], 1931, Vol. 1, No. 1.
10. I. Fox, Engineering, Vol. 136, 1933, p. 375-376.
11. N.N. Davidenkov, Zavodskaya laboratoriya, 1937, No. 8.
12. E. Heyn and O. Bauer, Stahl und Eisen [Iron and Steel], Vol. 31, 1911, pages 760-765.
13. R. Andersen and E. Fahlman. Inst. of Metals, Vol. 32, 1924,

pages 367-383; Vol. 34, 1925, pages 271-300.

14. G. Kirchberg, Farchangshefte Ingenwesen VDI [Engineering Research Numbers, Soc. Germ. Engineers], Vol. 3, 1932.

15. N.N. Davidenkov and Ye.M. Shevandin, ZhTF [Journal of Technical Physics], Vol. IX, 1939, No. 12.

16. F. Staeblen, Kruppische Monat [Krupp Monthly], Vol. 12, 1931, pages 93-99, 52, 1932, pages 15-18.

17. D.G. Kurnosov and M.B., Yakutovich, Zavodskaya laboratoriya, 1939, Nos. 10-11; 1946, Nos. 11-12.

18. L.A. Glikman and M.M. Pisarevskiy, Zavodskaya laboratoriya, 1951, No. 1.

Manu-script Page No.

[List of Transliterated Symbols]

| | |
|---|---|
| 3 | ос = os = osevoy = axial |
| 3 | р = r = radial'nyy = radial |
| 3 | т = t = tangential'nyy = tangential |
| 4 | в = v = vneshniy = outside |
| 7 | р = r = rastochka = boring |
| 13 | н = n = naruzhnyy = outside |
| 13 | в = v = vnutrenniy = inside |
| 18 | вн = vn = vnutrenniy = inside |
| 18 | нар = nar = naruzhnyy = outside |

## Chapter 32

## FORMATION OF AUSTENITE IN HEATING OF STEEL

Study of the processes in which austenite forms on heating were initiated by D.K. Chernov [1] who discovered the critical points of steel.

Initial structure is the most important factor determining not only the kinetics of the transformations, but also, to a certain degree, the positions of the critical points. The transformations with an initial two-phased structure composed of pearlite and sorbite are of greatest practical interest. For this case, the thermodynamic equilibrium in the Fe-C system is determined by the diagram of state. According to the diagram of state, formation of austenite begins when point $A_1$ is reached.

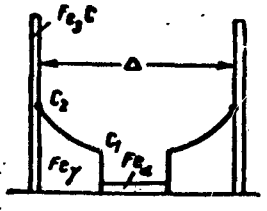


Fig. 1. Distribution of carbon in process of $P \rightarrow A$ transformation at temperature $T_1$.

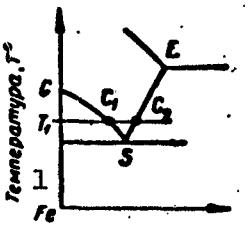


Fig. 2. Positions of $C_1$ and $C_2$ points on Fe-C diagram. 1) Temperature, T°.

Nuclei with the $\gamma$-iron lattice appear and disappear continuously in the ferrite as a result of spontaneous reconstruction of the lattice due to energy fluctuations. However, ferrite can exist in equi-

librium only with austenite whose composition corresponds to the GS line; consequently, only a nucleus with 0.8% C can be a stable nucleus, i.e., a nucleus whose growth is accompanied by a reduction of free energy, for transformation in the region of the $A_1$ temperature.

The probability that such a nucleus will form as a result of spontaneous redistribution of the carbon dissolved in the ferrite is negligibly small as compared with the probability of its formation on the interface with the cementite, in which the carbon concentration is 300 times higher than in the ferrite. Proximity to such a rich source of carbon places the boundary nuclei of the $\gamma$-phase under advantageous conditions and ensures their exclusive development to critical dimensions and beyond. For this reason, the mechanism by which pearlite is transformed to austenite near the $A_1$ point reduces to the appearance of austenite nuclei with 0.8% C at the boundary between the cementite and the ferrite and subsequent diffusive growth of these nuclei.

During isothermal holding at the temperature $T_1$, which is somewhat higher than $A_1$, the austenite is fed by carbon at the expense of the dissolving cementite lamellae and absorbs the ferrite lamella. According to the diagram of state, the carbon concentration at the cementite/austenite interface is $C_2$, while that at the A/F interface is $C_1$ (Figs. 1, 2). The rate at which the austenite front advances is determined by the rate of diffusion of carbon in the austenite,* i.e., at a given temperature, by the diffusion coefficient D and the concentration gradient $(c_2 - c_1)/x$, where $x$ is the distance traversed. When the ferrite disappears, $x = \Delta$, where $2\Delta$ is the interlamellar distance in the pearlite. The smaller $\Delta$ (the finer the pearlite), the higher, accordingly, will be the average rate of austenite propagation. As the initial pearlite (sorbite) becomes finer, therefore, the rate of austenite formation should increase not in proportion to $1/\Delta$, but more

steeply.

The point of thermodynamic equilibrium $A_1$ corresponds to a state in which the free energies of the austenite and pearlite are equal and no transformation at all can take place. Any transformation that takes place at a nonzero rate – whether isothermal or not – proceeds above the point $A_1$. Then two austenite fronts with the concentration $C_1$, i.e., a concentration below the average carbon concentration, are encountered when the ferrite disappears. Thus, the austenite is always still nonhomogeneous at this point in time.

The carbon distribution in the austenite in the transformation process is determined by the differential equation of diffusion. Using this equation to compute the over-all carbon content in the austenite at the moment of ferrite disappearance, it can be shown that under any heating conditions of the pearlite, the cementite will be retained for a certain time after the ferrite lamellae have disappeared completely.

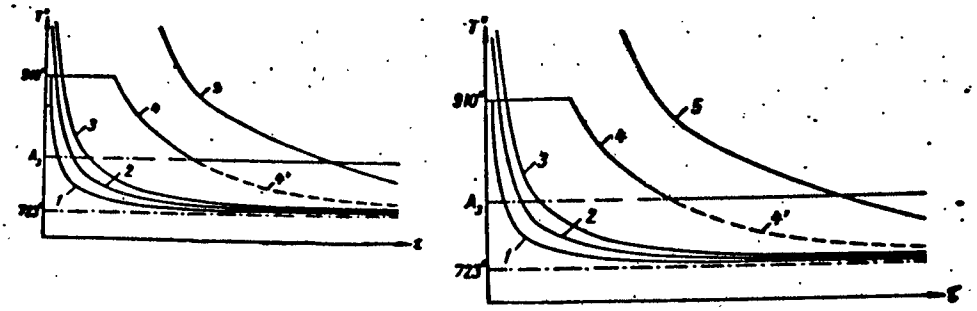

Fig. 3. Diagram of isothermal formation of austenite in hypoeutectoid steel.

In accordance with the above, we may distinguish three stages in the P → A transformation: I) propagation of the austenite through all ferrite gaps; II) solution of the residual cementite; III) equalization of the austenite carbon content.

The relative durations of the individual stages, and particularly of the culminating stage III, are important for practical purposes.

In this stage, concentration equalization is an exponentially damping process. Normally, the process is regarded as complete when the concentration gradient drops below a specified value $\delta_c$. Evaluation on the basis of simplified mathematical diffusion models [21] gives, for example, for isothermal formation of austenite in steel U8 at 800°, $\delta_c = 0.04\%$ (i.e., the austenite is regarded as uniform when its carbon content varies by $\pm 0.02\%$ C from the average) and $2\Delta = 1.2\ \mu$ (coarse pearlite): $t_1 = 0.038$ sec, $t_2 = 0.023$ sec and $t_3 = 0.024$ sec, i.e., all three stages take approximately the same time.

In the presence of structurally free ferrite, the transformation front advances not only into the interlamellar spaces of the pearlite, but also into the free-ferrite grains adjacent to them. However, since the diameter of the grains $D_z \gg \Delta$, the austenite front makes virtually no advance into the ferrite grain during the entire conversion of the pearlite. Thus we may assume that the transformation of the ferrite grain begins after the transformations in the pearlite have been completed. Isothermal transformation of ferrite into austenite consists of two successive stages – first the diffusion front of the transformation reaches the middle of a ferrite grain and the free ferrite vanishes, and then the carbon contents in the former ferrite and pearlite grains are equalized. The durations of both stages are again limited by the rate of carbon diffusion in the austenite. If the average path of the transformation front $\underline{l} \approx D_z/2$, then we may assume in analogy to the corresponding evaluations for pearlite that the transformation time is approximately $(\underline{l}/\Delta)^2$ times longer than the pearlite-transformation time (since the concentration gradient also diminishes in proportion to the increase in diffusion path).

In the general case, the path $\underline{l}$ is determined by the grain size of the ferrite and the quantity of ferrite in the steel. Thus, with an

approximately uniform grain size in a steel with 0.76% C, the measured average was $\underline{l} = 3\ \mu$ [2], while it was 5.1 $\mu$ in a steel with 0.41% C and 8.7 $\mu$ in a steel with 0.24% C. Then, if for isothermal transformation of pearlite at 800°

$$t_p = t_1 + t_2 + t_3 \doteq 0.085 \text{ sec},$$

then for full transformation of the hypoeutectoid steel at 800°, $t_{p+f} = 2.1$ sec with 0.76% C and 5.4 sec with 0.41% C.* According to the diagram of state, the transformation does not go to completion at all if the temperature of the isotherm is below $A_3$.

The sequence of transformations described above is summarized in Fig. 3 in a schematic diagram of isothermal formation of austenite in a hypoeutectoid steel. The diagram applies to initial structures of ferrite + pearlite. The transformation begins immediately on attainment of the point $A_1$.** The lines 1, 2, and 3 refer to transformations in the pearlite: 1 corresponds to the disappearance of the ferrite spaces, 2 to disappearance of the cementite and 3 to homogenization of the austenite in the former pearlite grain. In contrast to the cooling transformations, both the number of centers and the rate of growth increase simultaneously on heating, so that the curves approach the temperature axis monotonically as the temperature rises. The line 4 corresponds to disappearance of the free ferrite (and 4' to suspension of austenite growth at temperatures below $A_3$), and line 5 to homogenization of the austenite throughout the entire volume of the steel. The limiting value of the residual nonuniformity $\delta_c$ must be specified for the homogenization lines 3 and 5.

Such a diagram of state was first constructed for steel U8 by I.L. Mirkin and M.Ye. Blanter [3], who plotted lines 1, 2, and 3 and intermediate lines corresponding to specific austenite percentages. Diagrams were recently constructed [4] for normalized steels with 0.15, 0.34,

0.66% C and a line 4 as well.

The quantity of austenite A in the isothermal transformation P → A varies in time in accordance with the law

$$A = 1 - e^{-\left(\frac{t}{\tau}\right)^q}, \qquad (1)$$

where $t$ is time and $\tau$ and $q$ are constants [4].

The kinetic curves for hypoeutectoid steels have a sharp break corresponding to transition from transformation in the pearlite to transformation of the free ferrite. Both stages follow Eq. (1), but the constant $q$ changes sharply (decreases) when one process is supplanted by the other [4].

In alloy steels, the transformation P → A involves a very long process of redistribution of the alloying elements.* The distribution of the elements between the carbides and ferrites in pearlite is quite nonuniform and depends on the composition of the alloy and its initial heat treatment (annealing, refinement, normalization).** The carbide-forming elements are present preferentially in the carbides, and the noncarbide-forming elements in the ferrites. Thus, the cementite in steel 7Kh3 after tempering at 650° for one hour contains 15% Cr [6]. Here, accordingly, the ferrite will contain only 1.7% Cr. The chromium diffusion coefficient in austenite with 0.8% C at 800° is $D = 2 \cdot 10^{-12}$ $cm^2/sec$ [7], i.e., four orders lower than for carbon. Hence redistribution of the chromium begins for all practical purposes after formation of the austenite has been completed.

If the austenite is regarded as homogeneous when the chromium-concentration variations lie within ±0.05% Cr, then for this steel with pearlite $2\Delta = 1.2$ μ at 800°, an estimate calculation [21] gives a total chromium homogenization time in excess of 15 minutes. It is clear from this example that even for medium-alloy steel, disappearance of

carbides does not attest to uniform distribution of the alloying elements, which requires a much longer holding time. Moreover, austenite that is nonhomogeneous with respect to chromium cannot be homogeneous with respect to carbon either, since here a gradient of carbon activity would arise and cause upward diffusion. Nonuniform distribution of alloying elements inevitably maintains a carbon nonhomogeneity, so that the leveling process proceeds concurrently. As a result, homogenization of alloyed austenite with respect to carbon may take thousands of times longer than in the case of carbon steel.

The influence of alloying on the diagram of the isothermal P → A transformations has not been systematically studied. The carbide-forming elements such as, for example, Cr, W, and Mo, retard the formation of austenite; graphite-forming nickel accelerates it [4, 22].

The kinetics of austenite formation acquires the significance of a decisive heat-treatment factor when production employs heating at high rates with internal heat sources (induction or contact electric heating elements). Here, isothermal holdings are normally not provided, and the kinetics is described by a diagram in which the extent of transformation is represented as a temperature function for a certain constant heating rate. With other heating methods, the heating rate varies with temperature*; the heating rate $v_f$ in the phase-transformation interval should serve as the parameter uniquely defining the kinetics of the transformations.

As a result of the lack of time, equalization of carbon concentration in the austenite is arrived at on continuous heating at temperatures much higher than the equilibrium point. The nonuniformity of the austenite after quick heating changes the kinetics of transformations that take place during cooling and the structure and properties of the transformation products.

With continuous heating of pearlite, the same three transformation stages make their appearance as in isothermal transformation. The higher the heating rate, the higher will be the temperature at which the transformation of pearlite into austenite is completed and the lower will be the carbon concentration in the centers of the former ferrite lamellae at this point in time. Just as in the hypoeutectoid steel, the austenite that forms when the last volumes of ferrite disappear will be poorer in carbon the higher the heating rate.*

The greater the overheating of the untransformed cementite, the higher will be the carbon content in the austenite adjacent to it. The highest concentration is determined by the point of the line SE at the terminal temperature of solution. It does not depend directly on the carbon content in the steel, but is determined by the heating rate and the dispersion of the initial structure. In the diagram of Fig. 5, the upper curve indicates the change in concentration in the richest volumes of the austenite and the lower curve the same variation in the poorest volumes for heating at a constant rate.

In accordance with the diagram of state, the zones of poorest austenite form at the end of stage I, while the richest zones form at the end of II. In stage III, the nonuniformity is leveled. (Concentration leveling also proceeds during stage II, but it affects only the poor volumes, while the maximum concentration is still increasing.) With high heating rates (broken line in Fig. 5), the deviation from the average concentration increases in both rich and poor volumes. The diagram of Fig. 5 is confirmed qualitatively by numerous experimental results. For example, the retention of interlamellar ferrite at rather high overheating temperatures is indicated by the fact that when eutectoid steel with coarse-lamellar pearlite is heated at a rate of 800°C per second, magnetic transformation of ferrite is observed [9], i.e.,

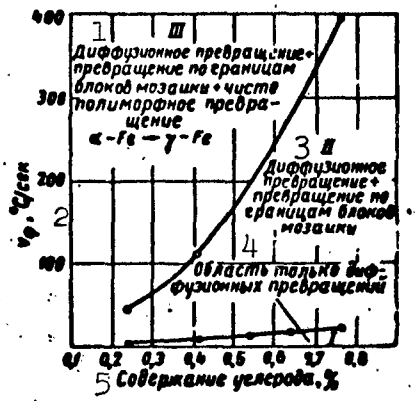


Fig. 4. Regions of existence of various types of austenite-forming processes in heating. 1) Diffusion transformation + + transformation along mosaic-block boundaries + + purely polymorphic α-Fe → γ-Fe transformation; 2) $v_f$, °C/sec; 3) diffusive transformation + + transformation along mosaic-block boundaries; 4) region of exclusively diffusive transformations; 5) carbon content, %.

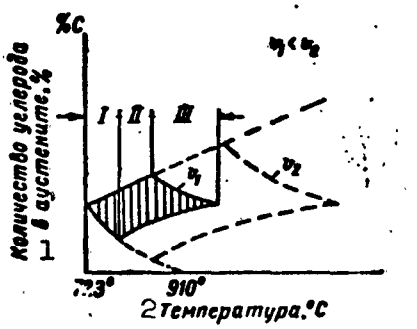


Fig. 5. Range of carbon concentrations in austenite (hatched) during process of P → A transformation during continuous heating (schematic). 1) Quantity of carbon in austenite, %; 2) temperature, °C.

the ferrite lamellae are to some extent retained 50° above point $A_1$.

Reference has already been made to the nonuniformity of martensite in eutectoid steel that has been hardened from induction heating in connection with the formation of a "pseudopearlite" structure with high hardness. Yet another fact: on x-ray diagrams, the doublet due to the tetragonal structure of the martensite after high-frequency hardening is not separated even in cases where there is distinct separation [11] after ordinary hardening. A direct experimental proof is given by analysis of the line shape on the x-ray diagrams [10]. With increasing carbon concentration, the tetragonal structure of the martensite is intensified, so that, in contrast to ordinary hardening, the photometric curve of the (110) line is overlaid in cases of nonuniform martensite by a series of curves of various heights that are similar to it and displaced toward smaller angles $\theta$ (i.e., toward higher carbon contents), which gives rise to asymmetrical blurred lines. The carbon content in the richest volumes of the martensite may be estimated from the degree of smearing. Thus, in steel 20 that has been hardened from

840° at $v_f$ = 130°C/sec, there are zones of martensite with 1% C, which corresponds to completion of the pearlite-solution process no lower than 800°.

In the eutectoid steel, the carbon content rose to 1.95% in isolated volumes of the martensite; this figure corresponds to retention of cementite up to 1130° [11].

Two types of martensite nonuniformity – fine and coarse – are possible in hypoeutectoid steels. The fine nonuniformity occurs only in former pearlite grains and is detected by the presence of hypereutectoid-concentration martensite in them (which is inevitably coupled with the presence of impoverished regions also). Here the carbon concentration fluctuates with a period equal to the interlamellar distance of the initial pearlite. The range of variation may be 0-2.0% C. Coarse nonuniformity consists in differences in carbon content among the former pearlite and ferrite grains. Its period is equal to the size of the initial grain and the range varies from 0 to 0.8% C. The carbon-saturation process of the former ferrite grains in steels with 0.2% C was investigated by the radioautogram method [12]. With a grain size of 0.06-0.08 mm (5 GOST points) and a heating rate of 30°C/sec, the coarse nonuniformity vanishes only toward 1250°.

The nonuniformity of austenite with reference to carbon and alloying elements that arises as a result of rapid heating affects the transformations that take place on cooling.

In all cases, such nonuniformity broadens the interval of the martensite transformation in both directions – both upward and downward (even when the cementite is only partially dissolved). Therefore, as indicated by the diagrams of Fig. 6, electric heating of carbon steel may both raise and lower the quantity of residual austenite as compared with ordinary hardening. In case c (complete solution of ce-

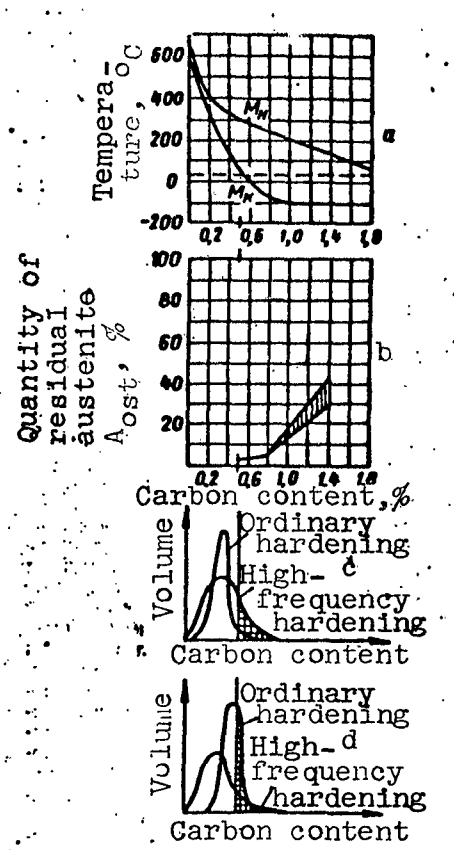


Fig. 6. Formation of residual austenite in carbon steels. a) Position of interval of martensite transformation as a function of carbon content in original austenite [13]; b) quantity of residual austenite (%) as a function of carbon content in original austenite [13]; c) carbon distribution in austenite with full solution of cementite; nonuniformity of austenite contributes to retention of residual austenite; d) carbon distribution in austenite with incomplete solution of cementite after quick heating. % $A_{ost}$ is lower after such heating despite the formation of isolated volumes that are enriched with carbon.

mentite), there is more untransformed austenite (hatched region) after electric heating. In case d (incomplete solution), the average concentration has been shifted toward a smaller carbon content, even though the upper limit of carbon content has not been depressed, and the quantity of untransformed austenite may become lower than after ordinary hardening.

A diagram similar to Fig. 5 may also be used in judging the influence of alloying elements on quantity of residual austenite. After quick heating, there are not only volumes of the austenite that have been impoverished in alloying elements, but also enriched volumes (bordering on the alloyed carbides or occupying their positions after solution has been completed). The percentage of residual austenite depends on their quantitative proportions, which are determined in each specific case by the completeness with which the carbides have dissolved and that of subsequent homogenization.

The difference between the volumes of the phases participating in the transformation creates a stress field about

each growing grain of the phase. Here the tangential stresses are far in excess of the yield point at the transformation temperature. The plastic deformation produced by the volume effect may have various mechanisms – an "athermal" shear mechanism or one of the high-temperature mechanisms (i.e., one that requires thermal activation to a degree such that it limits the rate of the process). The $\gamma \rightarrow \alpha$ transformation on slow cooling is accompanied by plastic deformation of both types: the slide shows a family of slip lines in the grains of the $\alpha$-phase, as well as slip tracks along the grain boundaries (creep type) [14].

In the process of this "phase work hardening" each elementary volume undergoes multiple plastic deformation in many directions, but only by a small amount each time (less than 1%) [15]. The deformed state is thus distinguished from all other forms of plastic deformation by highly uniform distribution of the deformation through the volume and among the slip systems. Such "deconcentration" of the working raises work-hardness and inhibits polygonization and recrystallization.

Austenite that has been work-hardened as a result of the phase transformation recrystallizes on further heating. This is indicated by the refinement of the austenite grain that has been observed by metallographic [16] and x-ray [17] means at temperatures above $Ac_3$ and is accompanied by disappearance of internal texture (i.e., by consistent orientation of the group of $\alpha$-grains that form on subsequent hardening from a single $\gamma$-grain). Thus, a monocrystal of the martensite of steel 35KhGSA is transformed on heating at a rate of 60°C/hour into an austenite monocrystal and then, above 900-950°, into a polycrystal [18]. Another fact: heating of coarse-grained specimens of steels 40KhS and 37KhNZ results in formation of a coarse austenite grain that breaks up to such an extent on subsequent heating above 1150° that a solid ring

is observed on the powder diagram instead of individual reflections [17]. In the alloy of Fe + 30% Ni, where the austenite is easily supercooled to 20°, its recrystallization is detected by the change in hardness at 20°: the $\alpha \rightarrow \gamma$-transformation is completed at about 500°, and a new hardness drop is observed after heating above 1000°; the latter corresponds to recrystallization after phase work-hardening [16].

The temperature range of austenite recrystallization may also occur below the point $A_1$.* Its position depends on the composition and initial structure of the steel, both directly and through the extent of work-hardening produced by the phase transformation.

For carbon steels with an initial martensitic structure heated at a rate of 100°C/sec, the recrystallization temperature diminishes with increasing carbon content:

| Carbon content, % | 0.07 | 0.15 | 1.0 |
|---|---|---|---|
| $T_{rekr}$, °C..... | 1160-1200 | 1000 | 900 |

The recrystallization temperature determined naturally depends on the holding time and, in the case of continuous heating, on the heating rate. Thus, recrystallization had already taken place at $Ac_1$ when steel U8 was heated with the furnace; it occurred at 850° on heating of hardened steel at a rate of 100°C/sec and at 930° with 1000°C/sec [16].

The recrystallization temperature also depends on the extent and mechanism of deformation in phase work-hardening. Thus, when the heating rate of steel ShKh15 (with an initial martensite structure) was raised from 180 to 1000°C/sec, the temperature at which the internal texture is destroyed does not rise, but, quite the contrary, drops from 1050 to 860° as a result of a lower degree of work-hardening in slow heating [16] (most of the deformation is of the creep type).**

Manuscript Page No.

[Footnotes]

26 Like the rate of reactive diffusion in general, the rate of solution of the carbides in the austenite depends on the diffusion coefficients and thermodynamic activities of carbon in both phases. To judge from the appearance of high-carbon martensite at high heating rates of the pearlite (see below), the limiting process in carbon steel would be diffusion of the carbon in the austenite (as will also be pointed out in the subsequent exposition). This assumption may be found inapplicable for low-solubility alloyed carbides. Unfortunately, we cannot indicate the limits of its applicability, since there are no data at all concerning the solubility limits and diffusion coefficients of carbon in carbides.

29 A more exact calculation will give an even longer transformation time, since in this case, in contrast to the $P \rightarrow A$ transformation, the carbon concentration in the original austenite drops even in the first stage. Experimentally constructed diagrams [3, 4, 23] usually give a much longer isothermal-transformation time, since a considerable part of the time is occupied by heating the specimen to the isotherm temperature (provided that special measures are not taken, the heating rate drops off rapidly as we approach this temperature).

29 An incubation period — a time prior to the formation of the first austenite seed — is also theoretically possible, although it has not been detected experimentally. The "incubation period" noted by a number of authors who constructed isothermal diagrams for heating in baths [3, 4] would apparently actually represent the time required to heat the specimen, since it is greatly reduced when the specimen is preheated below $A_1$.

30 The $P + F \rightarrow A$ transformation is of lesser interest, since high-alloy steels usually contain no free ferrite, while in low-alloy steels the original nonuniformity in the alloying-element distribution is of little import.

30 Since many hours of high tempering are frequently required to reach equilibrium distribution of the alloying elements [5], the $A_1$ point of the diagram is determined experimentally, essentially for the initially nonuniform structures. Hence the position not only of $Ac_1$, but also that of the equilibrium point $A_1$ will vary as functions of the prior treatment procedures, and this circumstance must be taken into account in determining the critical points for a steel.

31 The rate drops off particularly sharply in induction heating at the point in time when the magnetic properties are lost, i.e., on passage through the Curie point or with disappear-

Manuscript Page No.

[Footnotes (Continued)]

ance of the ferrite. As a result, it is practically expedient to divide the induction period into two stages [8]. The rate in the second stage is 5 to 25 times smaller than in the first.

32 Formation of austenite by another mechanism is possible at very high heating rates. The retention of free ferrite up to high temperatures may result in seeding of austenite within the volume of carbon and nitrogen segregations along the block boundaries [20] (without an external supply of carbon), and at even higher heating rates to the polymorphic F → A transformation. The region of existence of these processes is indicated on Fig. 4.

37 V.D. Sadovskiy [16] assumes that it is precisely this austenite recrystallization point and not the $Ac_3$ point was discovered by D.K. Chernov and designated as point b.

37 In this case, there is a possibility that the absence of chromium redistribution during tempering in the rapid-heating process is making itself felt here [19], since the fine nonuniformity of the alloy with respect to chromium must retard recrystallization.

Manuscript Page No.

[List of Transliterated Symbols]

28 з = z = zerno = grain

29 п = p = perlit = pearlite

29 ф = f = ferrit = ferrite

35 ост = ost = ostatochnyy = residual

37 рекр = rekr = rekristallizatsiya = recrystallization

REFERENCES


1. D.K. Chernov, Kriticheskiy obzor statey gg. Lavrova i Kalakutskogo o stali i stal'nykh orudiyakh i sobstvennyye D.K. Chernova issledovaniya po etomu zhe predmetu [Critical Summary of the Papers of Messrs. Lavrov and Kalakutskiy on Steel and Steel Implements and D.K. Chernov's Own Investigations on this Subject], Zapiska IRTO [Notes of the Imperial Russian Technical Society], 1868.
2. I.N. Kidin, Fazovyye prevrashchenyye pri uskorenom nagreve stali [Phase Transformations in Accelerated Heating of Steel], Metallurgizdat [State Scientific and Technical Publishing House for Literature on Ferrous and Nonferrous Metallurgy of the USSR], 1957.
3. I. L. Mirkin and M. Ye. Blanter, Metallurg [The Metallurgist], 1937, No. 1.
4. E. Schmidtmann and H. Brandis, Archiv fuer das Eisenhuettenwesen [Iron Metallurgy Archives], Vol. 30, 83, 1959, page 83.
5. S.Z. Bokshteyn, Struktura i mekhanicheskiye svoystva legirovannoy stali [Structure and Mechanical Properties of Alloyed Steel], Metallurgizdat, 1954.
6. Ye.Z. Vintaykin, P.L. Gruzin, Yu.A. Klyachko and A.P. Shotov, Problemy metallovedeniya i fiziki metallov [Problems of Metallurgy and the Physics of Metals], Metallurgizdat, 1955.
7. P.L. Gruzin, Problemy metallovedeniya i fiziki metallov, Metallurgizdat, 1955.

8. I.N. Kidin, Sb. Moskovskogo instituta stali [Collection of the Moscow Steel Institute], No. 33, Metallurgizdat, 1955.
9. G.F. Golovin, ZhTF, Vol. 20, 1950, No. 12.
10. I.N. Kidin, Fizika Metallov i metallovedeniye [Physics of Metals and Metallurgy], Vol. 3, 1956, No. 2.
11. I.N. Kidin, Fizika metallov i metallovedeniye, Vol. 3, 1956, No. 3.
12. I.N. Kidin and Ye.V. Astal'yeva, Nauchnyye doklady vysshey shkoly [Scientific Reports of Higher School], Metallurgiya [Metallurgy], Vol. 1, 1958.
13. Yu. A. Geller, Instrumental'nyye stali [Tool Steels], Metallurgizdat, 1955.
14. P. Lehr, Comptes rendus Acad. sci. [Proceedings of the Academy of Sciences], Vol. 244, 1957, No. 1.
15. N.N. Kidin and M.A. Shtremel', Nauchnyye doklady vysshey shkoly, Metallurgiya, (2), 165, 1959.
16. V.D. Sadovskiy, K.A. Malyshev and B.G. Sazonov, Fazovyye i strukturnyye prevrashcheniye pri nagreve stali, Metallurgizdat, 1954.
17. A.K. Karskaya, N.A. Kompaneytsev, B.K. Sokolov and V.D. Sadovskiy, Fizika metallov i metallovedeniye, Vol. 9, 1960, No. 1.
18. V.D. Sadovskiy, Trudy instituta fiziki metallov UFAN SSSR [Trans. of the Institute of Metal Physics of the Urals Branch of the Academy of Sciences of the USSR], Vol. 20, 1958, p. 303.
19. N.N. Lipchin, Metallovedeniye i termicheskaya obrabotka metallov [Metallurgy and the Heat Treatment of Metals], (II), 19, 1959.
20. I.N. Kidin, Mekhanizm obrazovaniya austenita pri bystrom nagreve [Mechanism of the Formation of Austenite on Rapid Heating], DAN SSSR [Proc. of the Acad. Sci. USSR], Vol. 106, 1956 (6), 1019.

21. I.N. Kidin and M.A. Shtremel', Protsessy obrazovaniya austenita [Processes of the Formation of Austenite], NTO Mashprom [Scientific and Technical Society of the Machine Industry], 1960.

22. V.A. Delle, Legirovannaya konstruktsionnaya stal' [Alloyed Structural Steel], Metallurgizdat, 1953.

23. R.F. Meyl' and U.K. Khagel', Uspekhi fiziki metallov [Progress in Metal Physics], Metallurgizdat, 1960.

## Chapter 35

## THE MARTENSITIC TRANSFORMATIONS

### 1. INTRODUCTION

A transformation of austenite that results in the formation of martensite, which is the basic structural component of hardened steel and determines its properties, is known as a martensitic transformation. The transformation of austenite into martensite (A → M) has a number of special properties that distinguish it clearly from all other transformations in the solid state. These singularities were first detected in steel. It was subsequently found that transformations possessing the characteristic features of the A → M transformation are observed in many metals and alloys and represent one of the chief forms of transformation in the temperature region in which diffusion and self-diffusion processes take place slowly.

The basic criterion of the martensitic transformation – that which determines all of its other special properties – is the unique mechanism by which the crystals of the new phase form. This mechanism consists in cooperative and regular displacement of atoms in which they are shifted relative to one another by distances that do not exceed the interatomic distances; the result of the atomic readjustment is a macroscopic shear (a shape change in the transformed volume in the form of a macroscopic shear). The superficial criterion of this mechanism is the relief that forms as a result of the transformation on a polished surface. The cooperative nature of the atomic displacements in the reconstruction, i.e., its interrelated and ordered nature,

makes the transformation possible at low temperatures at which diffusive migration of the atoms is extremely rare. The order in the atomic displacements also accounts for the retarding effect exerted on the origination and growth of martensite-phase crystals by the appearance of large disruptions in the regularity of the initial-phase structure.

The shearing nature of the lattice reconstruction results in the appearance of considerable elastic deformations during the martensite crystal's growth process and is responsible for the strong influence exerted by stresses on the kinetics of martensitic transformations and a number of other singularities.

The mechanism by which crystals of the new phase form would also appear to be responsible for the limited isothermal course of the transformation, which extends it into a region of temperatures [sic]; this is one of the chief singularities of martensitic transformations.

The intense interest that has long been shown by metallurgists in the nature of the transformation of austenite into martensite is due, on the one hand, to the fact that the problem of hardening of steel is related to it and, on the other hand, by the unusual nature of this transformation. The opinion has been expressed that the special nature of the transformation is to a major degree responsible for the high hardness of quenched steels.

It was known even at the beginning of the present century that an increase in cooling rate results not in an increase in the quantity of untransformed austenite, but, on the contrary, in a reduction; quenching in water produces a larger quantity of martensite in the hardened steel than does quenching in oil. Also extraordinary was the fact that the residual austenite, which remains constant for a long time at room temperature, undergoes transformation into martensite when cooled to the temperature of liquid air.

Study of the nature of the cooling curves [1] and establishment (just before nineteen-twenty) of the fact that the martensitic transformation takes place at temperatures considerably lower than the eutectoid point represented an important stage in the development of research on steel hardening. During the 'twenties, the results of x-ray examination of the crystal structure of martensite [2, 3] gave rise to a conception of martensite as a supersaturated solid solution of carbon in α-iron. It was shown that the transformation of austenite into martensite takes place without decay of the solid solution and consists only in a change in its lattice [4]. During these same years, the strong influence of stresses on the transformation of austenite into martensite was established and an analogy was observed between the nature of martensite-crystal formation and deformation twinning [5-7]. The detection and definition of the laws governing the lattice orientation of martensite with respect to the lattice of the initial austenite [8, 9] provided a basis for developing the crystallography of steel hardening and conceptions as to the mechanism of the atomic readjustment in the process in which austenite becomes martensite. The microkinematic research carried out at the beginning of the nineteen-thirties [10, 11] confirmed the concept of the analogy between the processes of martensite-crystal formation and twinning. The formation time of the martensite crystals was found to be less than a hundredth of a second, and further growth of the crystals was not observed.

During the 'thirties, the kinetics of the austenite-martensite transformation were studied in detail and its peculiar properties established: the transformation takes place basically during cooling; the initial temperature of the transformation (point M) does not depend on cooling rate; this point descends with increasing carbon content, and its position is influenced by alloying elements [12-15]. Ob-

jects of study were the influence of plastic deformation on the transformation and the influence of the manner of cooling on its course; the phenomenon of austenite stabilization and others were established [16-20].

The qualitative laws and singularities of the austenite-to-martensite transformation, which were first established for the most part in the USSR and Germany, were confirmed at the end of the nineteen-thirties by American investigators [21, 22].

Experimental data on the kinetics of the transformation, its crystal-structural and microstructural nature and the great importance of stresses resulted in hypotheses being advanced to the effect that the A → M transformation is not a process in which nuclei form and then grow, that its rate is independent of temperature, that the transformation is an athermal process, and that its mechanism consists in abrupt reconstruction ("inversion") of the lattice. The cause of the transformation itself was sought in the appearance of shearing stresses on cooling [7, 23-25].

Research carried out during the nineteen-thirties into the β-phases of copper-aluminum, copper-tin and copper-zinc alloys indicated that transformations similar to the A → M transformation also take place in other alloys [26-30]. Not only were the same qualitative relationships established for diffusionless β-phase transformations as for the austenite transformation, but a new phenomenon was also detected — the reversibility of the martensite transformations [30-32]. Study of the transformations in these alloys made it possible to regard the martensite phases as crystalline modifications of the solid solution [33]. Since these transformations take place in the absence of diffusive decay processes, i.e., take place without concentration changes, it was suggested that they be treated as phase transformations of single-

component systems similar to the polymorphic transformations of pure metals. A consequence of this was the conception of the martensitic transformation as a process in which nuclei form and subsequently grow [34], one subject to the general laws of phase transformations. The development of this conception and the assumption that martensite crystals grow coherently [35] made it possible during the postwar years to detect new phenomena surrounding the martensitic transformation: the temperature dependence of the rate of martensitic transformations [36] and the thermoelastic equilibrium in such transformations [37].

During the postwar years, the principal research trends were: 1) study of the qualitative laws involved in the temperature-dependence of the martensitic transformation and ascertainment of the nature of the martensite nuclei [56-73, 79-81, 108, 109]; 2) further study of the part taken by stresses in the martensitic transformation and development of a stress theory [74-79]; 3) study of the crystallography of the martensitic transformation and development of conceptions of the crystalline-structural mechanism of the transformations [38, 103-106].

## 2. MARTENSITE

### The Crystal Lattice of Martensite

Martensite is a structural component of steel that appears when it is cooled sharply after heating above the critical point and the one responsible for the high hardness of quenched steel. A large number of martensite crystals form in each grain of the original austenite (Fig. 1); these normally take the form of lamellae. The thickness of the plates is at least one order smaller than their size in directions perpendicular to it. The size of the martensite crystals depends on the state of the austenite grains. The more uniform and perfect the

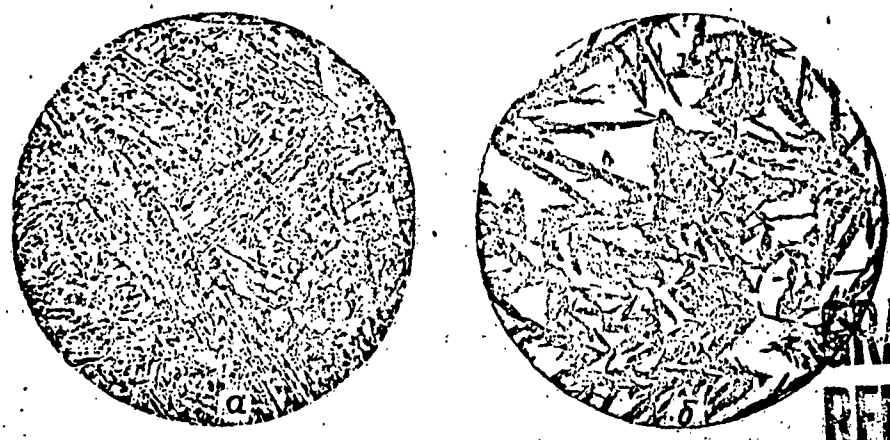




Fig. 1. Characteristic microstructure of martensite. 200 ×. a) Martensite; b) martensite + austenite.

crystalline structure of the austenite, the coarser will be the martensite crystals formed from it. The martensite crystals that form when the austenite-grain structure is highly nonuniform and its crystal structure is imperfect may be very small.

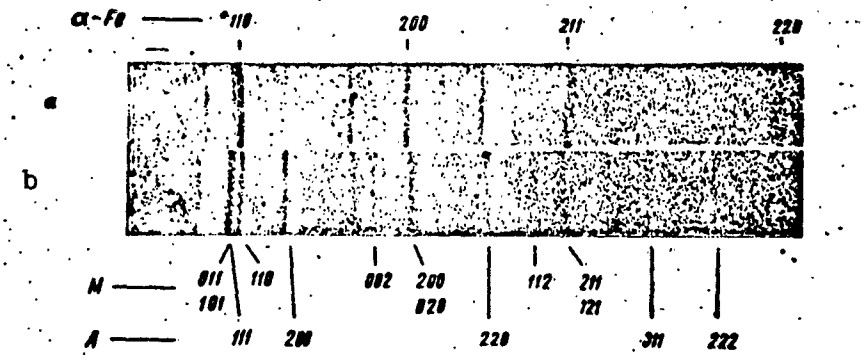


Fig. 2. X-ray diagrams of a) α-iron (lattice of body-centered cube); b) hardened steel with 1.4% C – martensite (body-centered tetragonal lattice) and austenite (face-centered lattice) [111].

Martensite crystals have a centered tetragonal lattice (Fig. 2) similar to the lattice of α-iron and deviating farther from it as the carbon content in the steel rises [2, 3].

The following experimental results from research into the crystal lattice of martensite in carbon steels are important for understanding

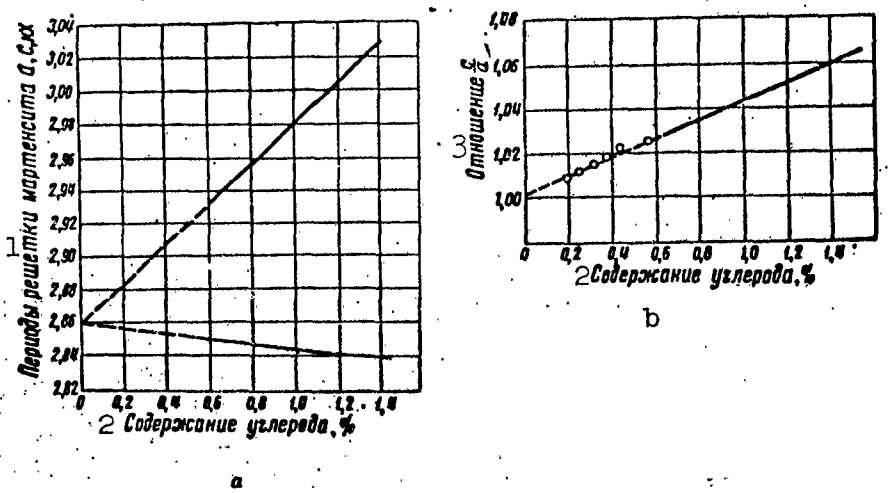


Fig. 3. Lattice parameters a and c of martensite as functions of carbon content: a) for steels containing more than 0.6% C [3, 33] (upper curve for c; lower curve for a); b) for steels containing from 0.2 to 0.6% C [44]. 1) Martensite lattice parameters a and c, kX; 2) carbon content, %; 3) c/a ratio.

the nature of martensite [2-4, 33, 39-41]:

1) the lattice constants do not depend on the hardening temperature for a given steel composition, provided that hardening is conducted from the single-phase austenite region and the cooling rate is high enough;

2) the lattice constants a and c do not depend on cooling rate if the latter is above the critical rate necessary to prevent decay of austenite and tempering of the martensite during cooling;

3) the lattice constants a and c do not depend on the carbon concentration in the steel if hardening is conducted from a given temperature in the heterogeneous region (between $Ac_1$ and $Ac_3$);

4) if the steel is quenched from the single-phase austenite region and the cooling rate is adequate to prevent decay of austenite and tempering of martensite, then the lattice constants a and c depend only on the carbon content in the steel (Fig. 3); this dependence may be described with sufficient approximation by the following equations:

$$c/a = 1 + 0{,}0467p;$$
$$c = a_{Fe} + 0{,}118p;$$
$$a = a_{Fe} - 0{,}015p.$$

where p is the percent by weight of carbon in the steel and $\alpha_{Fe}$ is the lattice constant of α-iron (2.861 A).

It follows from the above experimental data that: 1) martensite is a saturated solid solution of carbon in α-iron; 2) the lattice constants of martensite are determined by the carbon content in the initial austenite; 3) martensite contains in solution as much carbon as was dissolved in the initial austenite. This last conclusion implies that the transformation of austenite into martensite is diffusionless, takes place without changes in the concentration of the solid solution and consists solely of lattice changes.

As in the austenite lattice, the carbon atoms in the martensite lattice are situated in its interstices. They are located in the lattice pores

$$\left[\left[00\tfrac{1}{2}\right]\right] \text{ and } \left[\left[\tfrac{1}{2}\tfrac{1}{2}0\right]\right],$$

between the iron atoms arranged in the direction of the tetragonal axis. The carbon atoms are distributed statistically in these lattice pores.

Structural Singularities of Quenched Low-Carbon Steel

The untempered martensite cannot be fixed by quenching in carbon steels containing less than 0.6% carbon; partial tempering of the martensite has time to occur even during the sharpest quenching process [39]. Untempered martensite is easily obtained in hypereutectoid steels. The lower the carbon content, the higher must the cooling rate be to produce undecayed martensite. This is due to the elevation of the martensite point that occurs when the carbon content diminishes and the sharp increase in the martensite decay rate with rising temperature.

The degrees of decay are different in different crystals because of the propagation of the A → M transformation over a rather wide range of temperatures [4, 39, 42, 33, 53]. This is due to the great nonuniformity of the tetragonal structure of quenched low-carbon steel.

Undecayed martensite with a definite (depending on carbon content) ratio between the axes of the tetragonal lattice can be produced in steels containing even less than 0.6% C by adding alloying elements that lower the martensite point. This method has made it possible to produce undecayed martensite with carbon contents of 0.6-0.2% [43, 44]. The c/a values found conform to the linear relationship established for steels containing less than 0.6% C (Fig. 3b). The ratio between the tetragonal-lattice axes thus is determined by the carbon content in the steel and is virtually independent of the alloying-element concentrations [102].

The decay rate of martensite is governed not only by the mobility of the atoms, which increases rapidly with temperature, but also by the degree of solid-solution supersaturation, which is the motive force for the decay. In steels with very low carbon content (~0.1% and less), therefore, despite the relatively high temperature at which the A → M transformation begins (about 500°), undecayed martensite is nevertheless produced on sharp cooling. This is attested to by the dependence of the width of an x-ray interference line on carbon concentration in low-carbon steels (Fig. 4) [45]. Generally, the sharp cooling in quenching of these steels is necessary not to prevent

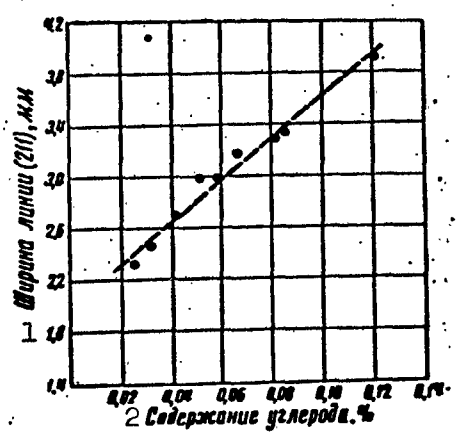


Fig. 4. Width of (211) interference line as a function of carbon content in steel [45]. 1) Width of (211) line, mm; 2) carbon content, %.

decay of martensite, but to delay segregation of ferrite and the normal ("diffusive") $\gamma \rightarrow \alpha$-transformation above the martensite point. Thus the conditions for producing the quenched steel here include not only sharp cooling, but also heating to high temperatures (1000-1200°). The latter is necessary to "heal" crystal-structure disturbances in the austenite, which facilitate formation of $\alpha$-phase nuclei. It has even been possible, by heating above 1150°, to harden iron containing less than 0.01% C, i.e., to prevent "normal" formation of $\alpha$-phase nuclei and effect the $\gamma \rightarrow \alpha$-transformation by the martensitic mechanism [46].

The elementary cell of the martensite lattice in pure iron is obviously the same as in annealed iron. The martensite crystals of pure iron differ from those of annealed iron only as regards their physical state (size, shape, crystal-structure disturbances). The dissimilar physical states are due first to the difference between the crystal-formation mechanisms and, secondly, to the difference between the temperature regions in which they are formed (lower mobility of atoms in martensitic transformation). The martensitic mechanism and the low atomic mobility result in a state that is frequently known as "phase hardening."

At carbon contents as low as about 0.01% and above, the martensite crystals differ from those of annealed $\alpha$-iron not only in physical state, but also by the presence of dissolved carbon. While (up to a certain carbon content) the martensite lattice remains cubic, the carbon atoms are located in the lattice between iron atoms along any of the three tetragonal axes of the cube and, possibly, in other pores as well. Apparently, the martensite lattice remains cubic even with a content of 0.1% C; this has not yet been established by direct measurements of the lattice constants due to the inadequate measurement pre-

cision. At a carbon content as low as 0.2%, the tetragonal lattice is distinctly indicated [44]. Correlation in the carbon-atom distribution and tetragonal symmetry probably appear at carbon contents between 0.1 and 0.2%.

Static Displacements (Distortions of the Third Kind) and Bonding Forces

The presence of carbon atoms that have penetrated into the iron lattice results in shifts of the iron atoms away from their ideal lattice positions. These displacements will obviously be greatest for atoms that are in the immediate vicinity of a carbon atom and will diminish with increasing distance from it. Here, the displacements in the direction of the tetragonal axis should be considerably larger than the displacements in the perpendicular directions [33]. This conclusion follows from the fact that the presence of carbon in solution gives rise to a sharp change in the average distance between iron atoms along the c axis and a slight change along the a axes, as will be seen from the relationship shown above (see Fig. 3) for the lattice constants a and c as functions of carbon content. This is also consistent with the hypothetical coordinates of the carbon atom in the martensite lattice: the distance between carbon and iron atoms in the direction of the c axis is considerably shorter than the distance between them in the perpendicular plane.

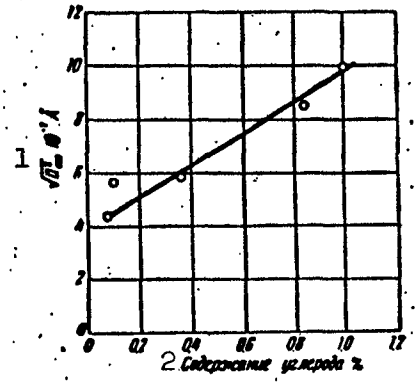


Fig. 5. Static distortions of martensite crystal lattice as a function of carbon content in solid solution [50]. 1) $(\overline{u}^2_{st})^{1/2}\ 10^{-2}$A; 2) carbon content, %.

Determination of the mean-square displacements of the iron atoms from their ideal positions in the lattice has confirmed this hypothesis [47, 48]: the mean-square displacements in the direction of the tetrag-

onal axis were twice as large [49]. Figure 5 shows the mean-square displacement of the iron atoms (without taking anisotropy into account) as a function of the carbon content in the steel [50].

The presence of carbon atoms dissolved in the α-iron not only results in disturbance of the regular periodicity of the atomic arrangement in the lattice, i.e., in static displacements of the atoms in the martensite lattice, but also weakens the interatomic bonding forces, and to a greater degree the higher the carbon content. This follows from the observation that at a given temperature, the mean-square deviations in thermal agitation of the atoms in the martensite lattice are larger than in the α-iron lattice [50]. Accordingly, the Young's modulus of quenched steel diminishes with rising carbon content [51].

Regions of Coherent Scattering and Distortions of the Second Kind

The static displacements of iron atoms in the martensite lattice, i.e., the absence of rigorous periodicity in the arrangement of the atoms at short distances (as we pass from one cell to the adjacent cell), which are due to the presence of carbon atoms interstitial in the iron lattice, is not the only form of disturbance to which the ideal crystal-lattice structure of martensite is subject. It is characteristic for martensite crystals that the regions of coherent x-ray scattering (blocks), i.e., regions of the crystal in which the positions of the atoms are interrelated by the periodicity of the lattice, are extremely small in size – of the order of 200-300 A [52]. Within the limits of measurement error, the size of the martensite-crystal blocks does not depend on the carbon content in the steel – beginning with pure iron (and carbon-free alloyed iron as well) [46] and extending to a steel with 1.4% C. The block size is most reliably determined on martensite crystals that have been electrolytically deposited from quenched steel. In this case, blurring of the lines on the martensite

x-ray diagrams is due chiefly to the small size of the coherent-scattering regions. The entire part of the line broadening that is due to the presence of stresses of the second kind is absent on x-ray diagrams of a powder consisting of isolated martensite crystals [54].

Severe distortions of the second kind, i.e., nonhomogeneous elastic deformation of microregions, is another characteristic of the physical state of the martensite crystals in quenched steel [45, 52]. Evaluated on the basis of line width, the elastic deformation $\Delta a/a$ has a value of $2.5 \cdot 10^{-3}$-$3.0 \cdot 10^{-3}$ even in specimens of steel containing 0.1% C, i.e., it is several times larger than distortions of the second kind in cold-deformed iron. With high carbon contents, the quantity $\Delta a/a$ may reach values near $10^{-2}$ [52].

The magnitude of distortions of the second kind rises sharply as the carbon content in the martensite increases. While the dimensions of the blocks remain the same irrespective of whether the martensite crystals are in a piece of quenched steel or have been electrolytically deposited (isolated), large distortions of the second kind are observed only in monolithic, relatively large specimens, and these distortions are almost completely absent in isolated martensite crystals. This means that each martensite crystal in quenched steel is elastically deformed by forces exterior to it. When it is freed from its environment, the elastic deformation vanishes, together with that part of the line blurring which is proportional to the tangent of the deflection angle and independent of the x-ray wavelength.

Thus, research into the crystalline structure of martensite indicates that such structural details as the magnitudes of the lattice constants a and c and tetragonal symmetry, the significant static displacements of the atoms from their ideal positions in the lattice (distortions of the third kind) and the small size of the coherent-scatter-

ing regions are internal singularities of the martensite crystalline structure. Here, the small block size represents a common property of martensite crystals – both in pure iron (or in alloyed carbon-free iron) and in steel, i.e., in the supersaturated solid solution of carbon in α-iron. The tetragonal lattice constants a and c and the mean-square displacements of the iron atoms in the lattice depend on the carbon content of the solid solution; the values of these fine-structure parameters increase rapidly as the quantity of this element rises. A weakening of the bonding forces with increasing carbon content must also be reckoned among the internal characteristics of martensite crystals; these dictate an increase in the amplitude of thermal agitation.

The lattice constants of martensite, the static displacements and the increased amplitudes of the atomic thermal agitation (dynamic displacement) are thus determined by the presence of carbon atoms interior to the iron lattice. These structural singularities of steel martensite arise as a result of the diffusionless nature of the austenite-to-martensite transformation, i.e., they are the result of formation of a supersaturated solid solution of carbon in iron. The small size of the blocks is apparently governed by the growth mechanism of the martensite crystals, i.e., by the mechanism of regular collective readjustment of the iron atoms during the process of their growth. The details of this mechanism are not yet sufficiently clear. The small block size is not a result of formation of the supersaturated solid solution. As we noted, it is also characteristic for the martensite of pure iron and carbon-free alloyed iron.

Large distortions of the second kind are not a mandatory structural characteristic of martensite crystals. They arise as a result of the influence exerted by some of the austenite grains on others due to shape changes in microregions resulting from both the shearing nature

of the lattice reconstruction and the increase in volume that accompanies it. They vanish when martensite crystals are isolated. Since martensite crystals take the form of lamellae, it is most probable that their elastic deformation consists in bending of these elements.

However, distortions of the second kind may serve as a characteristic of the martensite crystal's strength properties. They may be a measure of the elastic-deformation limit of these crystals. As we have shown, this limit depends heavily on the carbon concentration in the martensite. Due to the presence of carbon atoms in the lattice, therefore, the emergence and advance of elementary plastic-deformation events (emergence and motion of dislocations) under the influence of external forces is rendered difficult [55].

Nature of High Hardness of Quenched Steel

Two kinds of structural peculiarity inherent to quenched steel arise during quenching. Firstly, a characteristic micro- and submicrostructure forms as a result of the martensitic crystal-growth mechanism: a large number of martensite lamellae within each austenite grain (in low-carbon steels, the austenite is transformed almost completely); submicroscopic dimensions of the coherent-scattering regions within these lamellae; nonuniform elastic deformation of the lamellae; a consistent crystal-orientation relationship that governs the retention of some of the importance of the original austenite grain in the behavior of the quenched steel. Secondly, as a result of the diffusionless nature of the martensitic transformation, the martensite crystals represent a supersaturated solid solution of carbon in α-iron that does not exist in the stable state of steel and is absent in slowly cooled carbon steel.

Structural changes of the first kind have the same effect on the behavior of the metals under load as does cold plastic deformation. If

the martensitic transformation in its pure form takes place when they are quenched, quenched alloyed iron and quenched pure iron have strength characteristics similar to those that these materials acquire in the annealed state with high degrees of cold plastic deformation. Only the micro- and submicrostructures change in these materials as a result of the martensitic transformation, in much the same way as occurs in cold plastic deformation, while the chemical composition of the α-phase remains unchanged. The properties of α-phase crystals do not change within small volumes.

When steel is quenched, a change also takes place in the properties of the α-phase crystals themselves in small regions, together with the above changes in micro- and submicrostructures, since their chemical composition undergoes changes (as a result of the formation of the supersaturated solid solution of carbon in α-iron). Here, the deformation resistance of the crystals themselves increases sharply: the limit of their elastic deformation rises.

The higher deformation resistance of martensite crystals in steel as compared with the crystals of α-iron is obviously due chiefly to the presence of carbon atoms interstitial in the iron lattice.

Thus, the increase in the steel's deformation resistance as a result of quenching is due, on the one hand, to the formation of a characteristic fine micro- and submicrostructure in the grain and, on the other hand, to the high elastic-deformation limit of the actual martensite crystals that results from the presence of the carbon dissolved in them. The first factor exerts an influence that depends little on carbon content, while the second becomes more important as the carbon content in the martensite rises and is the principal factor governing the high hardness of quenched steel [55].

## 3. TRANSFORMATION OF AUSTENITE INTO MARTENSITE

### Transformation on Cooling

The basic qualitative laws and singularities of the A → M transformation during continuous cooling are illuminated in References [4, 7, 10, 13, 16, 24, 33-35, 38, 56]. Given sufficiently rapid cooling, the decay of austenite with formation of the α-phase and carbides may be delayed, and the austenite may be supercooled to a temperature considerably lower than the eutectoid point. In carbon and low-alloy steels, however, it is impossible to cool austenite to room temperature under any set of cooling conditions and thereby obtain pure austenite after quenching. Below a certain temperature, which depends on the chemical composition of the austenite, a process occurs in which the austenite is transformed to martensite. The process consists in formation, within the austenite grains, of considerably smaller martensite crystals (sizes of the order of $10^{-3}$ to $10^{-4}$ cm), which usually take the form of lamellae, which accounts for the acicular microstructure of the ground section. The martensite crystals that have appeared do not grow, and the transformation continues by formation of new crystals, extending over a broad temperature range. Stopping cooling results in cessation of martensite-crystal formation. It is necessary to depress the temperature further to permit the transformation to resume. The progress of the martensitic transformation on cooling may be represented by a "martensite curve," which expresses the quantity of martensite as a function of temperature. The initial temperature of the martensitic transformation (the point M or, from earlier investigations, the Ar" point) is known as the martensite point. Depending on the position of the martensite point relative to room temperature, the result of quenching may be a greater or lesser quantity of residual austenite.

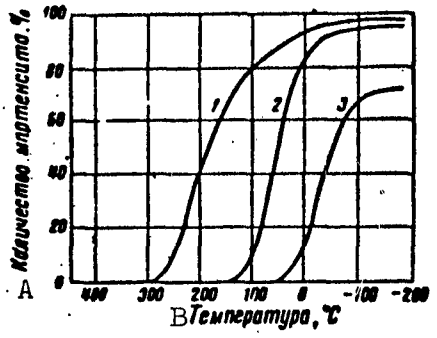


Fig. 6. Martensite curves of manganese steels [79]. 1) 0.64% C; 1.0% Mn; 2) 0.62% C; 5.1% Mn; 3) 0.60% C; 8.6% Mn. A) Quantity of martensite, %; B) temperature, °C.

The position of the martensite point on the temperature scale and the shape of the martensite curve are determined chiefly by the chemical composition of the austenite. For low-carbon steels (containing less than 0.4% C), the curve lies above room temperature, and practically no residual austenite is detected at room temperature. For high-carbon steels, on the other hand, most of the curve is located below room temperature. The majority of alloying elements likewise displace the martensite curve toward lower temperatures. Figure 6 shows martensite curves for certain steels.

The Isothermal Transformation

As we noted above, the transformation ceases when cooling is stopped. However, the formation of martensite crystals does not stop immediately on the specimen's acquiring the temperature of the bath. For a certain amount of time, isothermal transformation of austenite to martensite takes place at a rapidly diminishing rate. The quantity of isothermally formed martensite is very small in most steels with technical applications and ranges from fractions of a percent to several percent. In certain cases, however, for example in the room-temperature region for steels with martensite points below 100°, it is reckoned in tens of percent. Thus, in the case of a martensitic steel containing 0.95% C and 3.5% Mn and having a martensite point at about 85°, 20% of the specimen's volume is converted into martensite at room temperature within 10 minutes [57]. A considerable quantity of the austenite present in a carbon steel with 1.6% C is transformed to mar-

tensite isothermally at room temperature, and the transformation goes on for a long time [58].

In some steels with martensite points below 0°, the transformation may be completely suppressed with sufficiently rapid cooling to the temperature of liquid nitrogen. In this case, the A → M transformation may take place on heating to room temperature or by soaking in a temperature region between that of liquid nitrogen and room temperature [36, 59].

For this temperature region, the kinetics of the A → M transformation become similar to the kinetics of the transformations associated with diffusion processes: the rate of the transformation depends on temperature, diminishing as it rises and going practically to zero at sufficiently low temperatures. Together with this, one of the principal singularities of the kinetics is retained in this temperature region as well: the A → M transformation does not go to completion at the given temperature, but ceases despite the presence of austenite in large quantities. It resumes at the lower temperature.

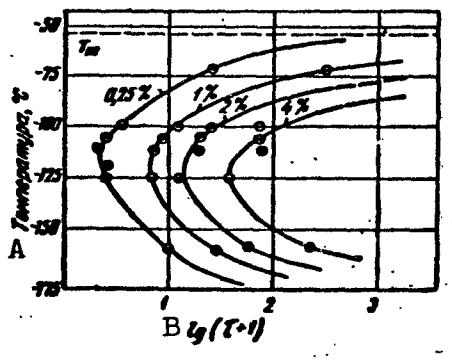


Fig. 7. C-curve diagram of isothermal transformation of austenite in martensite temperature region for N24G3 alloy (23.8% Ni, 3.2% Mn) [59]. A) Temperature, °C; B) log (τ + 1).

An incubation period [60, 61, 62] may be observed in the isothermal transformation. In this case, the martensite point can no longer be characterized as the temperature at which the transformation begins on cooling, since its position depends heavily on cooling rate. For such steels, it should obviously be designated as the temperature below which the transformation may take place with sufficiently long holding.

The isothermal A → M transformation may be described by diagrams similar to those that characterize the isothermal transformation in pearlite, and particularly in the intermediate region, i.e., by curves showing the temperature dependence of the time required for transformation of a certain fraction of the austenite, such as 1, 5, 25% and so forth (Fig. 7). It is advisable to construct such diagrams for those steels in which it is possible by rapid cooling to preserve all of the austenite until the bath temperature is reached [59, 63].

For steels with martensite points lying between 150 and 200°, the percentage of martensite that can be formed isothermally is not large. It may reach a few percent in the initial segment of the martensite curve, i.e., above 100°, and at low temperatures — below −50°. At room temperature, there is practically no isothermal transformation in this case [19, 64, 65, 83, 107].

Influence of Plastic Deformation

Plastic deformation of austenite when cooling is stopped below the point M normally gives rise to further transformation of the austenite to martensite. The quantity of martensite formed when this happens increases with increasing degree of deformation [17, 66].

Transformation of austenite into martensite also takes place as a result of plastic deformation at temperatures above the martensite point. However, the farther the deformation temperature is from the martensite point, the greater is the degree of deformation necessary for martensite to appear. Above a certain temperature that is quite well-defined for each specific steel, plastic deformation no longer causes the A → M transformation (this temperature is frequently known as the $M_d$ point) [7, 67].

Plastic deformation above the martensite point, which does not produce the A → M transformation, exerts considerable influence on the

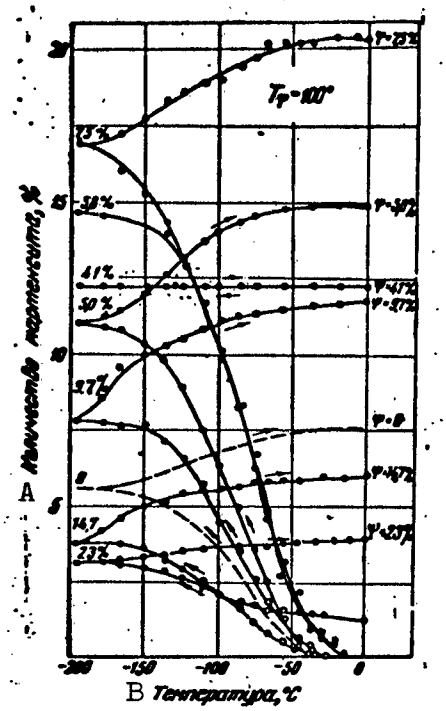

Fig. 8. Transformation of austenite to martensite on cooling to −196° and heating to 20° after varying amounts of preliminary plastic deformation effected at 100°. Alloy Kh18N8 (18.1% Cr, 8.1% Ni) [72]. A) Quantity of martensite, %; B) temperature, °C.

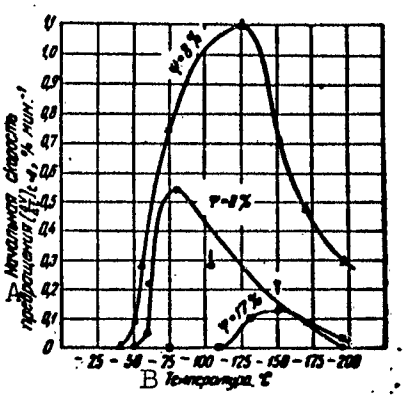

Fig. 9. Curves showing temperature dependence of initial rate of isothermal martensitic transformation (b) for the undeformed ($\psi = 0$) state and the 8% and 17% deformed states. Deformation temperature 100°. Steel Kh17N9 (17.2% Cr, 9.1% Ni) [72]. A) Initial rate of transformation $[\Delta V/\Delta t]_{t=0}$, $\%\cdot min^{-1}$; B) temperature, °C.

subsequent course of the transformation at temperatures below the deformation temperature (below $M_d$) [66, 68-73]. The position of the point M and the shape of the martensite curve also change, as does the nature of the isothermal transformation. Here, the martensitic transformation may be activated (i.e., the point M raised, the quantity of martensite increased, and the rate of the isothermal transformation raised) [69, 71] and, conversely, suppressed [66, 68, 70]. Stimulation of the A → M transformation normally takes place at relatively low degrees of deformation. If the degree of deformation is progressively increased, the activation effect first rises, then reaches a maximum and finally drops to zero. A further increase in degree of deformation gives rise to the reverse

effect – a drop in the quantity of martensite formed on cooling and a reduction of the isothermal-transformation rate – see Figs. 8 and 9 [69].

Research has led to the conclusion that as a result of plastic deformation at temperatures above the martensite point, two types of structural changes arise simultaneously in the austenite: some of these activate the transformation on further cooling, while others have the opposite effect. Here, the changes of the former type are unstable and vanish during the holding time at temperatures around room temperature and below. The second-type changes are more stable and are eliminated at considerably higher temperatures. An effect similar to the austenite stabilization to be described below arises as a result of holding of plastically deformed austenite at temperatures somewhat above the point M. The relationship between the structural changes of the first and second types depends on the deformation temperature, the degree of deformation and the elastoplastic properties of the alloy [69, 72, 73].

Given a sufficiently high elastic limit of the austenite, the structural changes of the first type prevail at first over those of the second type as the degree of deformation is increased (at a constant temperature), and the effect registered is that of activation of the transformation. At a certain degree of deformation, the maximum transformation-activation effect is achieved; here, any further increase in the degree of deformation reduces the effect to zero (here the opposed effects offset one another). However, the existence of both types of structural change is readily ascertained by holding at relatively low temperatures (here, the changes of the first type vanish, while those of the second remain). As the degree of deformation is further increased, the structural changes of the second type prevail and retard the transformation. Holding at moderate temperatures

intensifies this effect [69, 72].

Neutron bombardment of austenite produces effects similar to those produced by plastic deformation (as regards the laws governing the development of activation and retardation of the A → M transformation) [80, 81].

Stabilization of Austenite

Stopping cooling of steel in the martensite range usually results in the A → M transformation not taking place during subsequent cooling within a certain temperature region, resuming only after a certain amount of supercooling (Fig. 10) [18]. This phenomenon is known as stabilization of austenite [7, 18, 82]. Stabilization occurs irrespective of whether or not the isothermal transformation takes place when cooling is suspended. If, however, this transformation does occur, the temperature at which the transformation resumes will be lower, and the more so the larger the quantity of isothermally formed martensite [83, 107]. Further transformation is retarded particularly sharply when cooling is stopped in a region below room temperature.

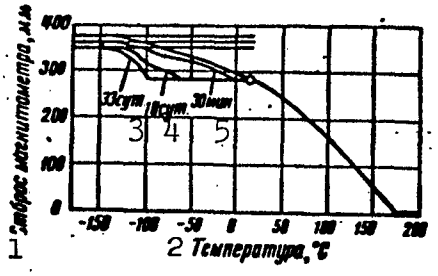


Fig. 10. Influence of holding at room temperature on martensitic transformation during further cooling. Steel with 1.17% C [18]. 1) Magnetometer deflection, mm; 2) temperature, °C; 3) 33 days; 4) 10 days; 5) 30 minutes.

Stoppage of cooling also frequently results in lowering of the entire low-temperature part of the curve and, consequently, in an increased quantity of residual austenite.

The process responsible for stabilization of austenite takes place in time. With prolongation of holding when cooling is stopped, the amount by which the initial temperature of the subsequent transformation is depressed (hysteresis) increases, and the rate of this

increase becomes smaller with increasing holding time, so that the process dies out. The rate of the processes governing stabilization rises with increasing holding temperature [84].

Crystallography of the Transformation

A large number of martensite crystals appear within the austenite grain as a result of the transformation. Their size depends on the perfection of the crystal structure of the original austenite grain. The presence of imperfections and inhomogeneity of structure reduces the size of the martensite crystals, sometimes to such an extent that the characteristic acicular structure is lost.

A boundary passing along the martensite needle ("center line") and frequently a transverse twin structure are observed in well-formed martensite crystals. The martensite crystals are regularly oriented with respect to the crystallographic axes of the original austenite grain. The orientational relationship between the lattices of the martensite and the original austenite is expressed as follows:

$$(101)_M \parallel (111)_A;$$
$$[11\bar{1}]_M \parallel [\bar{1}10]_A.$$

i.e., the (101) plane of the martensite is parallel to the (111) plane of the austenite, and one direction of the martensite-lattice space diagonal $[11\bar{1}]$, lying in the $(101)_M$ plane, is parallel to the $[\bar{1}10]$ direction of the austenite lattice lying in the $(111)_A$ plane. Since there are four combinations of (111) planes in the austenite lattice and the martensite lattice may be oriented in six different ways with retention of parallelism of the $(101)_M$ face to one of these four faces, the martensite lattice may be oriented in 24 different ways in the same grain [9].

Regularity is observed in martensite-crystal orientation not only as regards lattices, but also as regards the orientation of the lamel-

lae themselves, i.e., orientation of the external shapes of the crystals. However, the plane of the martensite lamella is less strictly oriented, and the planes of the austenite parallel to which the martensite planes are oriented are not simple [38]. For steels with 0.5-1.4% C, this plane is near $(225)_A$, while it is near $(259)_A$ for higher carbon contents.

The appearance of relief on a polished specimen surface is characteristic for the transformation of austenite to martensite. Study of the nature of this relief indicates that the formation of martensite crystals is associated with shear in much the same way as in mechanical twinning [35-38]. The presence of shear is also indicated by changes in the shape of scratches on a polished section that has been subject to the transformation. Breaks appear in the scratches on formation of the martensite crystal, but they remain continuous.

## 4. MARTENSITIC TRANSFORMATIONS IN METALS AND ALLOYS

Transformations that possess the kinetic singularities of the $A \rightarrow M$ transformation take place in a number of metals (Fe, Co, Ti, Zr, Li) and alloys [35, 38]. These include first of all the $\gamma \rightarrow \alpha$ transformation of iron alloys, the $\beta$-phase transformations of eutectoid Cu-Al and Cu-Sn alloys and those of the $\beta$-phase of Cu-Zn alloys, the $\beta \rightarrow \alpha$ transformation in alloys based on titanium and zirconium, the $\beta \rightarrow \alpha$ transformation in alloys based on cobalt, those in Li-Mg alloys, and others. Common features in the kinetics of these transformations include the following: 1) the absence of diffusive migration of atoms; 2) the limited scale of the isothermal transformation, i.e., its cessation in the presence of a large quantity of the initial phase and the resulting extension of the transformation over a range of temperatures; 3) shaping of the crystals of the new phase in a manner similar to the formation of mechanical twins and the resulting shear in the displace-

ments of the material during the transformation.

In cases where the single-phased state of the alloy is stable only at high temperatures, the phases formed as a result of the martensitic transformation are metastable as a result of the diffusionless nature of the martensitic transformation. They have lattices that differ from those of stable phases (for example, $\beta'$ and $\gamma'$ in Cu-Al alloys, $\beta'$ and $\beta''$ in Cu-Sn alloys, $\beta'$, $\beta''$ and $\alpha'$ in Cu-Zn alloys). If the alloy is also single-phased at low temperature (for example, the $\alpha$-phase of alloyed iron, the $\alpha$-phase in alloys based on Ti, Zr, Co), then, as in the case of pure metals, the result of the martensitic transformation is formation of crystals with the lattice of a phase that is stable at low temperatures. In such cases, transformation of the high-temperature phase to the low-temperature phase may take place as a function of cooling conditions or as a martensitic transformation, or as a transformation with "normal" kinetics [56]. In the latter case, the transformation proceeds isothermally to completion and crystal growth is similar to the grain growth that occurs on recrystallization. The possibility of transformations of both types is most clearly established on the example of the $\gamma \rightarrow \alpha$ transformation of alloyed iron.

A "reversibility" effect of this process was observed in investigation of the martensitic transformations in copper alloys: the transformation of the martensitic phases into the initial phases on heating may proceed like the martensitic transformation as regards kinetics and the crystal-structure mechanism. In isolated cases, a phenomenon of thermoelastic equilibrium and the appearance of "elastic" crystals of the martensitic phases have been observed [37]. This phenomenon consists in the fact that the new-phase crystals grow only on cooling. The growth ceases when cooling is stopped and resumes when the temperature is further depressed. A rise in temperature, on the other hand,

results in a decrease in the dimensions of the crystal and finally in their complete disappearance. Such phenomena were first detected for the $\beta_1 \rightarrow \gamma'$ transformation in Cu-Al alloys with manganese or nickel additives, and then in Au-Cd alloys and others.

## 5. NATURE OF MARTENSITIC TRANSFORMATIONS

Understanding of the nature of the austenite-to-martensite transformation requires establishment of the causes and motive forces of the transformation, its mechanism, and the causes of the following basic singularities of the transformation kinetics:

1) the high rate of formation of the individual martensite crystals and their subsequent failure to grow;

2) rapid damping-out of the process in which new martensite crystals appear when cooling is stopped and the extension of the transformation over a region of temperatures.

Also requiring explanations are such effects as the anomalous influence of cooling rate on the course of the austenite-to-martensite transformation, the progress of the transformation during plastic deformation, and stabilization of austenite.

### Causes and Motive Forces of the Transformation

The causes of the martensitic transformation of austenite are the same as for any other phase transition in the solid state, namely: below a certain temperature, there exists a state of the alloy that possesses a smaller free energy than the high-temperature state. Since the martensitic transformation takes place without changes in the concentration of the solid solution, it may be regarded as a transformation in a single-component system. Austenite and martensite represent, from this point of view, crystalline modifications of a solid solution that are similar to the polymorphic modifications of pure metals or chemical compounds [35]. The free energy of each of these modifications

($F_A$ and $F_M$) has its own temperature curve. The position of the intersection point of the temperature curves of free energy ($T_0$), which determines the stability of the phase in question, depends on the chemical composition of the solid solution and may be computed from data on the thermal properties of the two solid-solution modifications [95, 110]. For iron-carbon alloys, the temperature $T_0$ diminishes rapidly with increasing carbon content (Fig. 11) [35] and is found below the eutectoid line above a certain carbon content.

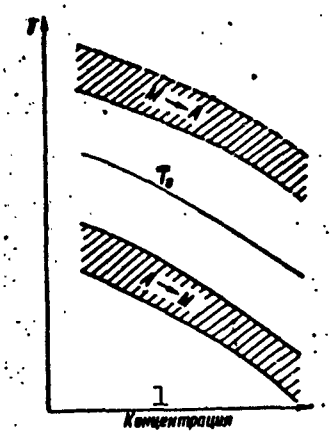


Fig. 11. Schematic diagram of forward and reverse martensitic transformations for solid solutions of various concentrations: $T_0$ is the temperature of metastable equilibrium between the two crystalline modifications of the solid solution [35]. 1) Concentration.

If there are no diffusive solid-solution decay processes, a motive force appears below $T_0$ and makes the $A \rightarrow M$ transformation possible; this motive force is the stronger the greater the difference between the free energies $F_A$ and $F_M$ of the austenite and martensite. However, the transformation does not begin immediately after passage through $T_0$, but at a point M situated considerably (in steels, about 200°) lower than the $T_0$ point. When martensite is heated above the point $T_0$, the quantity $F_A$ is found to be lower, and it would be expected that the reverse transformation of martensite to austenite would take place. The condition for transition in either direction is suppression of the process of solid-solution diffusive decay, since the $T_0$ point is the point of equilibrium between the two modifications only for a solid solution of a given concentration.

In the case of steel, however, it is very difficult to satisfy

this condition because of the high decay rate of martensite. Observation of the reverse transition is further complicated as a result of the wide hysteresis of the transformation, which amounts to several hundred degrees.

The reverse transformation of a martensitic phase into the initial phase was first observed during heating of the β'-phase in copper-aluminum alloys [87, 88]. Favorable conditions prevail in this case: the low rate of solid-solution decay (no decay occurs on cooling and heating in air) and the slight hysteresis of the transformation (a few tens of degrees). The martensitic nature of the reverse $\beta' \rightarrow \beta_1$ transformation was established in References [31, 85]. It has also been possible to observe the reverse transition in other cases of the martensitic transformation by setting up the necessary conditions [35]. It is difficult to observe the transformation of martensite into austenite in steels even with very high heating rates, due to the great speed with which martensite decays. The reverse martensite transition has been observed in carbon-free alloys of iron [89, 90]. Here, decay of the solid solution takes place very slowly. The results of investigation of the reversibility of the martensite transformation in alloys based on iron indicate great hysteresis of the transformation, which is apparently characteristic for transformations of face-centered lattices into body-centered lattices.

This hysteresis makes it difficult to determine the point $T_0$ by experiment. For example, the martensite point for cooling lies below room temperature for an alloy of iron with 30% Ni. The reverse transition, on the other hand, begins above 300°, and the point $T_0$ should be somewhere in between.

The chief reason for the strong hysteresis in the martensite transformation is the appearance of a considerable elastic-deformation

energy ("elastic energy") during formation of the martensite crystals. Deep supercooling is required so that the gain in free energy due to lattice changes can be offset by the energy going into the elastic deformation ("elastic energy").

It is known that the A → M transformation is possible even above the point M in plastic deformation of austenite. Moreover, the farther the deformation temperature is removed from the M point, the greater the degree of deformation necessary for the A → M transformation, and above a certain temperature no amount of plastic deformation is capable of producing the A → M transformation.

From the viewpoint of the conceptions described above concerning the motive force of the martensitic transformation, external factors, including plastic deformation, may cause formation of martensite only in that temperature region in which the martensite lattice is thermodynamically more stable, i.e., below $T_0$. Thus, by determining the deformation temperature at which the austenite is still just capable of going over to martensite, we can establish the point $T_0$, i.e., the temperature below which martensite is thermodynamically stable, more accurately.

It might be expected that plastic deformation above $T_0$ would produce the opposite effect, i.e., cause transition of the martensitic phase to austenite at temperatures below the normal transition usually observed on heating. Research has confirmed this conclusion and indicated the possibility of experimental determination of the temperature above which austenite is thermodynamically stable. It has thus been made possible to determine the concentration dependence of $T_0$ for cobalt-nickel and iron-nickel alloys [91, 95].

Consequently, the cause of the A → M transformation is the higher

thermodynamic stability of the martensite lattice as compared with the austenite lattice below a certain temperature; on the other hand, the motive force of the transformation is the difference between the A and M free energies. However, higher thermodynamic stability indicates only the direction of the transformation's motive force and not the possibility of the transformation. The actual accomplishment of the transition and its kinetics are determined by the singularities of the transition mechanism at the conditions under which the transformation takes place. Then all other factors, including stresses, cannot be regarded in themselves as either causes or motive forces of the transformation. They do not govern the transformation and are important only to the extent that they exert considerable influence on its kinetics.

Mechanism of the Transformation

Formation of crystals of M as a result of lattice readjustment.

The martensitic transformation, which represents formation of crystals of the new phase within an old phase, should take place, like any process of a similar kind, by formation of nuclei and their subsequent growth. Experimental data on the transformation of austenite into martensite, and in particular the analogy between martensite-crystal formation and formation of twins as a result of deformation, as well as the rigorously consistent orientation of the martensite lattice, enable us to conclude that growth of martensite-phase crystals consists in regular reconstruction of the lattice in which atoms do not change places, but are only shifted relative to one another by distances not in excess of the interatomic distance. Yet another confirmation of this proposition is to be found in the following fact: when the original state is an ordered solid solution, the martensite phase is also an ordered solid solution.

On the basis of this conception of the M-formation mechanism, it has been possible to compute in advance the coordinates of the atoms forming the solid solutions in the elementary cells of the martensite phases (for example, the $\gamma'$-phase in Cu-Al alloys and the $\alpha'$-phase in Cu-Zn alloys). The calculated atomic-position coordinates have been confirmed by experimental data [92, 93].

The concept of regular lattice reconstruction enables us to understand the high speed with which martensite crystals form (at low temperatures), the "stepwise" nature of their genesis. In such a mechanism (readjustment), there is no need for diffusive atomic displacements, the rate of which is very low for iron at temperatures below $300^{\circ}$.

The actual readjustment is obviously effected in such a way that the material displacements are of the shear type, as is observed in study of the microrelief that appears on polished surfaces on transformation [90, 94].

The atomic-structural mechanism of the readjustment should correspond to experimentally secured crystal-geometry phase relationships between the martensite and austenite (lattice orientation, lamella orientation, direction and extent of shear). At the present time, the details of the mechanism cannot be regarded as established.

Conjugation of A and M lattices on growth of M. One of the most important hypotheses as to the nature of the atomic readjustment is that coherence or conjugation is preserved during the readjustment between the lattices of the austenite and the growing martensite crystal [35, 56]. A definite order in the arrangement of the atoms is maintained at all times at the moving boundary. Atoms that were neighbors in the austenite lattice remain neighbors at the boundary of the growing crystal as well. On this assumption, if we take into account the shear type of lattice readjustment, large shearing stresses must inev-

itably arise and increase during the process of martensite-crystal growth.

A high growth rate is observed only if coherence is preserved. When the stresses reach a certain (large) magnitude, coherence is upset, i.e., the order is disturbed in the arrangement of the atoms on the phase boundary and conjugation of the lattices vanishes.

The high growth rate with preservation of conjugation is due to the cooperative nature of the readjustment, in which the atomic displacements are similarly directed (consistent) and mutually related. Violation of coherence should result in cessation of growth, since the disordered growth due to individual, noncooperative atomic displacements proceeds at a very low rate at low temperatures.

The coherent-growth hypothesis has made it possible to explain, on the one hand, the high rate with which the individual martensite crystals form and, on the other hand, their failure to grow subsequently when coherence is violated. Coherence and the appearance of large stresses also account for the shape of the crystals: it must be such that for a given martensite-crystal volume, the elastic-deformation energy that arises as a result of the transformation will be minimal [96].

Elastic crystals. The coherent-growth concept has made it possible to predict and then observe experimentally the effect of "thermoelastic equilibrium" in the martensitic transformation and "elastic crystals" in the martensite phase.

The possibility of this effect proceeded from the following considerations. With the shearing nature of the readjustment that occurs during growth of a martensite crystal, the stresses rise rapidly in the region surrounding the growing crystal. The motive force of the transformation is determined by the difference between the free ener-

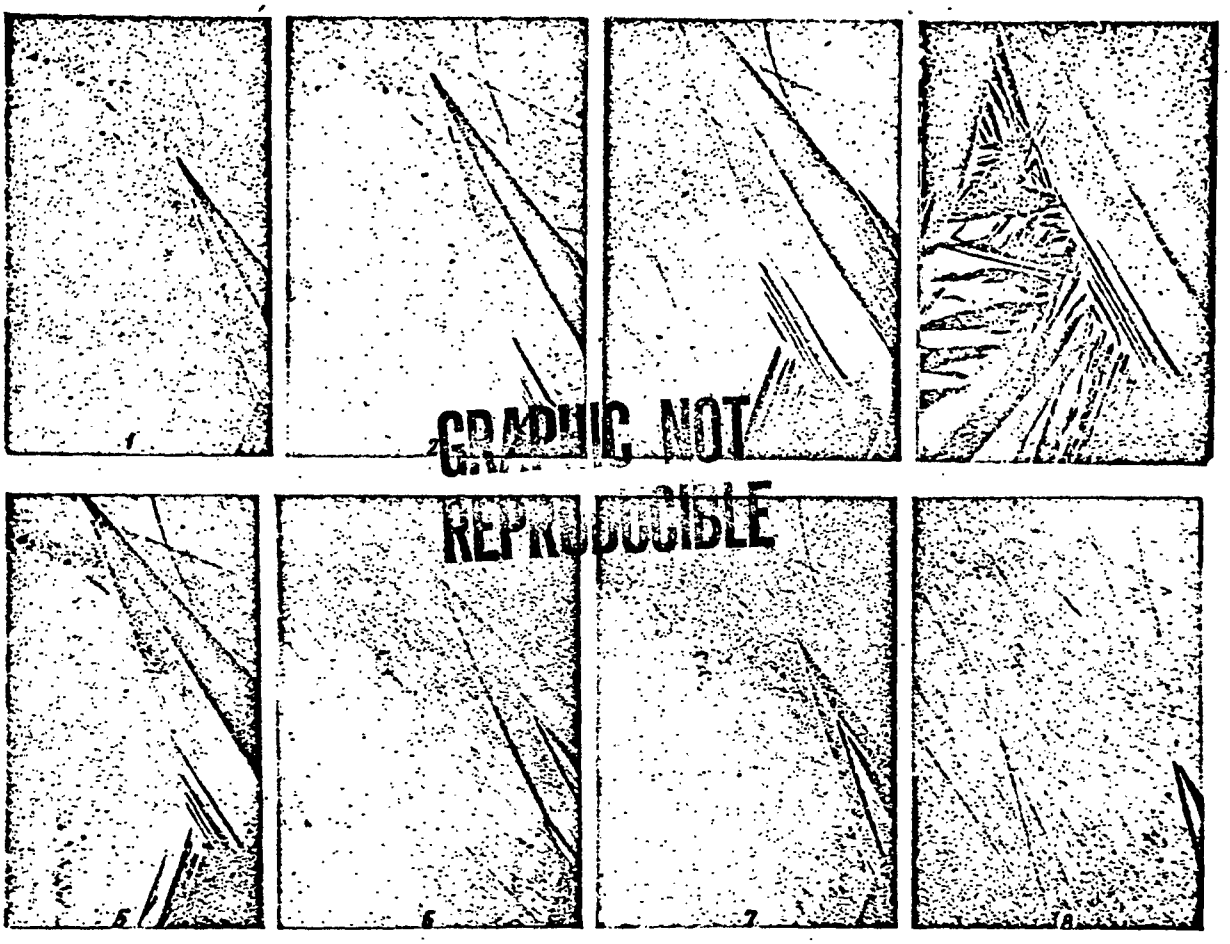


Fig. 12. Elastic martensite crystals. Aluminum bronze (relief). 70 × [37]: 1-4) Cooling; 5-8) heating.

gies of the alloy before and after the lattice change. During growth, however, a considerable "elastic energy" appears and increases rapidly as the crystal grows (as the thickness of the lamella increases). Growth continues as long as this energy is smaller in absolute magnitude than the difference between the free energies of the two lattices. If coherence is not violated during growth, the elastic energy may be found equal at a certain crystal size to the difference between the free energies of the two lattices. Then the motive force of the transformation vanishes, growth ceases, and thermoelastic equilibrium is established [35]. Such a crystal retains the ability to undergo further changes in size if a motive force appears again, for example, on

a temperature change, since this results in a change in the difference between the free energies of the two lattices. A drop in temperature results in growth of the crystal, and a rise in temperature reduces its dimensions [35].

Such a phenomenon has actually been observed in the $\beta_1 \rightarrow \gamma'$ martensitic transformation in Cu-Al alloys with Ni or Mn additives (Fig. 12) [37], and subsequently in certain other alloys as well. The conditions necessary to produce thermoelastic equilibrium are a high elastic limit in the material and a slow increase in stresses as the crystal grows.

Temperature Dependence of Transformation Rate

The premise that the transformation is due to the difference between the free energies of the phase lattices enables us to assume that the formation of nuclei is likewise not an athermal process, i.e., that the rate of this process must, as with any other transformation, depend on the energy of atomic thermal agitation [35].

It has actually been possible to ascertain the temperature dependence of transformation rate as a result of detailed investigations of the martensite transformation below room temperature [36]. It was found that certain phenomena that had been regarded as characteristic for the martensite transformation vanish in this temperature region. The following facts were established: 1) here, the transformation may proceed isothermally for a long time; 2) the rate of the transformation is a function of temperature and diminishes as it is depressed; 3) the transformation may be totally suppressed by rapid cooling to the temperature of liquid nitrogen; 4) austenite that has been cooled rapidly to the temperature of liquid nitrogen is transformed to martensite on heating to room temperature (Fig. 13) [36] at a rate that depends on temperature.

Moreover, it has been shown that the following characteristic features of the martensitic transformation are retained even in this temperature region: 1) martensite crystals in steel grow at an enormous rate (in the plane of the martensite lamella) even at low temperature; 2) the transformation of austenite into martensite extends over a region of temperatures: when cooling stops, only a certain part of the austenite is transformed, the isothermal transformation dies out and ceases, and the process makes further progress only at a lower temperature.

The temperature dependence of transformation rate is determined by the temperature dependence of the rate at which martensite nuclei form, and cessation of the isothermal transformation by nonformation of nuclei capable of growth at the temperature in question. The decline in the transformation rate with diminishing temperature indicates that thermal oscillations of the atoms are an important factor in the formation of martensite nuclei. The possibility of supercooling the austenite in certain steels to the temperature of liquid nitrogen indicates that the nuclei do not form when the atoms have low vibration energies. The transformation begins on heating, as soon as the energy of thermal vibration has become large enough, and proceeds more rapidly the higher the temperature, i.e., the larger this energy. This indicates that formation of the nuclei is thermal.

The fact that the temperature curve of nucleus formation rate is the same as in any other phase transformation is important for understanding the nature of the transformation: the rate of the isothermal transformation first rises below the martensite point, reaches a maximum on further reduction of the temperature and then diminishes (Fig. 14) [59]. However, it is not possible to measure the rate of the isothermal transformation over the entire temperature region unless the

martensite point occurs at a sufficiently low temperature. This rate is easily measured on the descending branch of the curve at temperatures below $-50^{\circ}$. At higher temperatures, the thermal-vibration energy has already become so large that when cooling stops in this region all of the nuclei that can form at the temperature in question are realized in a short interval of time.

On the ascending branch of the curve, slow formation of nuclei takes place slightly below the martensite point, and the rate of the process has become immeasurably high on cooling a few tens of degrees below the point M. The low speed of the transformation near the martensite point is dictated by the large size of the critical nucleus (the large work of formation of the nucleus), i.e., by the necessity that large thermal fluctuations arise. As we go farther from point M, the work of formation drops off rapidly and the transformation rate rises. For ordinary steels, therefore, the isothermal transformation is observed only in a region somewhat lower than the M point and in a region below $-50^{\circ}$. In this interval, there is a region of temperatures in which this process goes with high speed, which is what gave rise to the idea that the martensitic transformation is athermal in nature.

At temperatures below $-50^{\circ}$, the factor determining the low rate of nucleus formation and making it possible to observe the isothermal transformation is the low energy of thermal vibration. The action of this factor is intensified as the temperature drops. In the temperature region about the point M, the factor that makes it possible to observe the isothermal transformation is the large work of nucleus formation. Its action falls off with diminishing temperature, since the work of nucleus formation drops rapidly with increasing distance from $T_0$ [73].

The temperature region in which the basic factor is the first

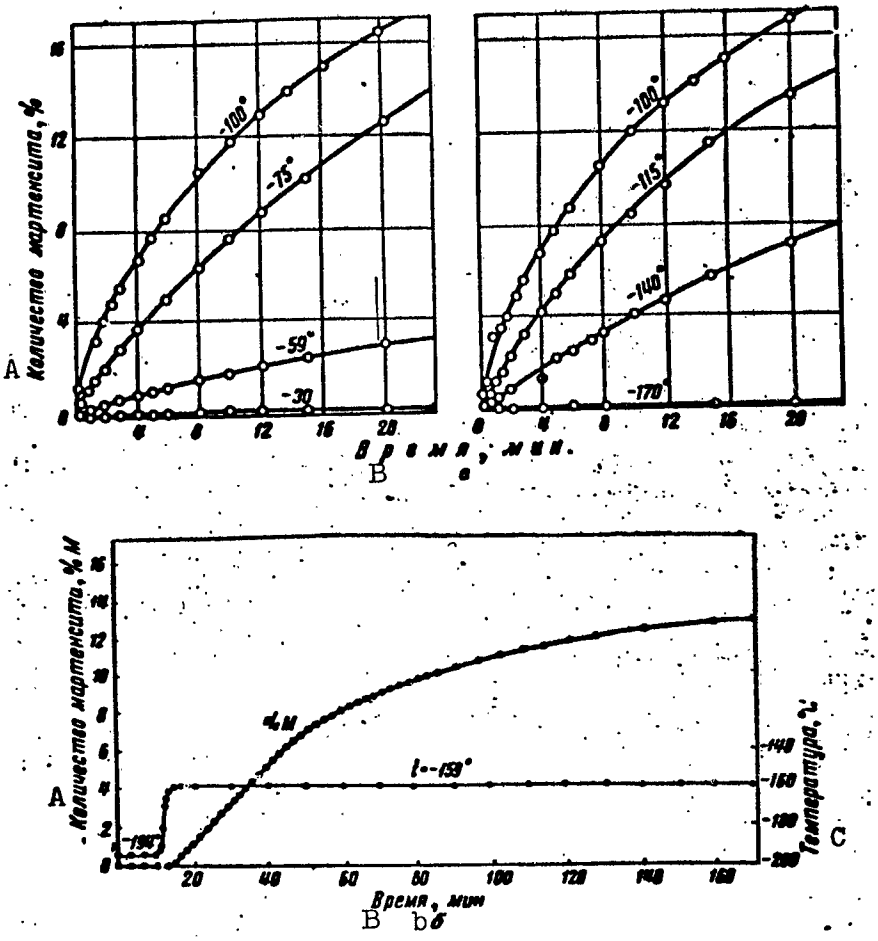


Fig. 13. Isothermal transformation of austenite to martensite. a) Transformation at various temperatures. Iron-nickel-manganese alloy (22.5% Ni, 3.4% Mn); b) transformation at −159° after supercooling in liquid nitrogen. Manganese steel (0.7% C, 6.5% Mn, 2.0% Cu) [36]. A) Quantity of martensite, %; B) time, minutes; C) temperature, °C.

given above is determined by the magnitude of the atom's thermal-vibration energy, i.e., by the absolute temperature. On the other hand, the temperature region in which the second factor predominates depends on the position of the point $T_0$ and, consequently, that of the M point. Thus, by lowering the point M (by an appropriate change in the alloy's composition), we may shift the temperature region of essential importance of the second factor to a temperature region near room temperature, thus making possible measurement of the rate of the isother-

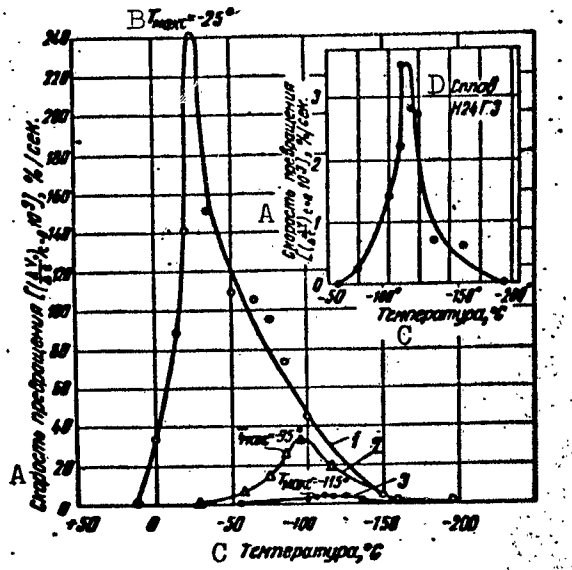


Fig. 14. Temperature dependence of initial rate of isothermal martensitic transformation of iron-nickel-manganese alloys having various martensite points: 1) N23G3 (22.7% Ni, 3.1% Mn), $T_m = +12^o$; 2) N23G4 (22.5% Ni, 3.4% Mn), $T_m = -30^o$; 3) N24G3 (23.8% Ni, 3.2% Mn), $T_m = -55^o$ [59]. A) Transformation rate $[(\Delta V/\Delta t)_{t=0} \cdot 10^3]$, %/sec; B) $T_{max} = -25^o$; C) temperature, $^oC$; D) N24G3 alloy.

mal transformation at its maximum. In this case, there is no region with an athermal transformation. The curve of transformation rate as a function of temperature becomes normal in nature (Fig. 15) [59].

Thus, thermal vibration of the atoms takes an important part in the kinetics of martensite-nucleus formation, just as in other phase transformations. The high rate of nucleus formation at such low temperatures as room temperature, when diffusion processes have been frozen out, is determined by the fact that the atomic displacements required for formation of a martensite nucleus require lower activation energies. This last is apparently linked with the small relative dis-

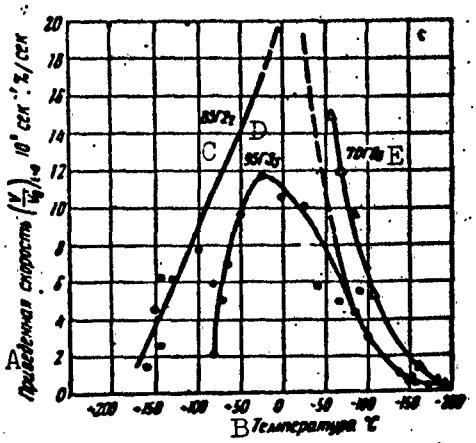


Fig. 15. Temperature dependence of initial reduced rate of isothermal martensitic transformation of manganese alloys having different martensite points: 1) $85G2_2$ (0.85% C, 2.2% Mn), $T_m = 155^\circ$; 95G3 (0.95% C, 3.5% Mn), $T_m = 85^\circ$; $70G6_5$ (0.70% C, 6.5% Mn), $T_m = 50^\circ$ [59]. A) Reduced rate $(V/V_0)_{t=0} \cdot 10^2$ $sec^{-1}$ × × %/sec; B) temperature, °C; C) $85G2_2$; D) $95G3_5$; E) $70G6_5$.

placements of the atoms and the ordered nature of the atomic transformations when the martensite nucleus forms.

The low rate of formation of the nuclei, coupled with the tremendous rate at which the martensite crystals grow at temperatures far below room temperature, indicates that a very small activation energy is required in growth of the martensite crystals, i.e., it is necessary to overcome very low barriers during this growth. Apparently, the height of the barriers diminishes as the crystals grow as a result of the appearance of stresses at the boundary of the growing crystal. During the initial stages, therefore, the rate of crystal growth may not be as large as it becomes when the crystal acquires microscopically visible dimensions.

The stresses may act unequally in directions lying in the plane

of the martensite lamella and in directions perpendicular to it. In the latter case, they may assist in raising the barriers and retarding the growth process. (A lower growth rate over the thickness of the lamella has been observed in certain alloys in investigation of martensite-crystal growth.) It is possible, however, that the low activation energy of crystal growth is related to the singularities of the growth mechanism in itself, concerning which it is necessary to have more detailed information.

Causes of Extension of Propagation over a Region of Temperatures

One of the principal characteristic features of the martensitic transformation consists in the fact that it extends over a region of temperatures, and that only part of the initial phase goes over into the new phase at any temperature in this region. Since the martensite crystals cease growing once they reach certain sizes, stoppage of the transformation implies cessation of nucleus formation.

There are two kinds of factors that might govern this phenomenon: 1) a change in the state of the remaining austenite in which formation of new nuclei or growth of nuclei is inhibited; 2) the appearance of nuclei not at any point in the volume, but only at points at which their formation is made easy.

Factors of the first kind might, for example, include the appearance of a hydrostatic pressure, which would lower the $T_0$ point, as well as structural disturbances that interfere with the formation of nuclei of the critical size or with their growth. The second group of factors would include nonuniformity of the state of the austenite – frozen concentration fluctuations of a dissolved element; various types of structural nonuniformity due to local stresses that tends to reduce the work of formation of nuclei of the new phase; shearing stresses with a region of stressed-state nonuniformity having a size of the same

order as that of the martensite crystals or larger, and so forth.

Factors of the first kind can hardly be of significance for the initial stages of the martensite curve, since the state of all of the untransformed austenite could hardly have undergone any substantial change with such a small quantity of martensite present. However, they may exert substantial influence on the second half of this curve. For the first half, therefore, the principal factors should be those of the second type. On passage through the M point, the nuclei first form at those points where the work of their formation is lowest (due to a favorable structure or concentration deviation). After nuclei have been realized at these points, the process stops. As the temperature is lowered further, the size of the critical nucleus is reduced, with the result that realization at other points favoring nucleus formation becomes possible.

As we have already noted, a stressed state arises and new structure disturbances that favor the formation of martensite nuclei make their appearance after partial transformation in the remaining austenite (apparently in the regions surrounding martensite crystals).

The results of research into the influence exerted by prior plastic deformation of the austenite above the M point, which does not produce any direct transformation [69], and into the influence of neutron bombardment on the kinetics of the subsequent transformation of austenite into martensite [80, 81] confirm the concept in which the martensite nuclei form not throughout the entire volume, but in places where the structure deviates from the mean. Both of these treatments of austenite give rise to the appearance of structural disturbances that facilitate formation of martensite nuclei. However, these disturbances are unstable and gradually disappear during holding even at room temperature (they do so more rapidly at high temperatures). The

latter testifies to large local stresses and small dimensions of these regions, which act as the points of easy nucleus formation. Partial relaxation of such stresses may take place at relatively low temperatures – such as room temperature and even lower.

As a result of plastic deformation or neutron bombardment, and in the process of the actual transformation, structural disturbances of a different, transformation-inhibiting type also make their appearance; these include, for example, disturbances at the boundaries of coherent-scattering regions or other types of cumulative structural disturbances.

It is possible, however, that the austenite-crystal structural disturbances that facilitate the formation of martensite nuclei and inhibit it are of the same type. As long as these disturbances are minor and concentrated only at certain points, they facilitate the cooperative displacement of atoms that is necessary for formation of martensite-crystal nuclei. When these disturbances become numerous, however, and when they are distributed in a certain manner, reducing the region with a regular lattice, they come to represent an obstacle to the formation of nuclei and to growth of nuclei in its initial stages.

From this standpoint, activation of the transformation at low degrees of plastic deformation or bombardment is due to the relatively small number of disturbances that facilitate formation of crystal nuclei and do not inhibit their growth. Holding at room temperature or at moderately elevated temperatures should result in redistribution of the stresses, in more uniform distribution of these stresses, and in a lessening of the local disturbances. As a result, the activating effect is reduced and the inhibiting effect is enhanced (due to the smaller size of the regular-lattice regions). With high degrees of plastic deformation, a large number of the disturbances block cooperative readjustment of atoms in the region required for further growth.

Only at high temperatures do the disturbances vanish and, accordingly, only at these temperatures is the original ability of the austenite to undergo the martensitic transformation restored [97].

Structural disturbances similar to those that are caused by plastic deformation also arise as a result of formation of a new martensite crystal in a region surrounding a crystal that already exists. This must result in easier formation of new nuclei; it appears that stabilization of the austenite when cooling is halted is connected with a change in the distribution of these disturbances and a reduction in local stresses (stress peaks) during holding.

The high disturbance density of the austenite grain's crystal structure arises as a result of forward and reverse martensitic transformations. Here, the local stresses cannot be particularly large because of the high temperature of the reverse transformation. This type of structure renders formation of nuclei and their growth difficult during subsequent cooling below the martensite point [97, 98].

Experimental data indicate that regularity disturbances in the crystal structure represent a major factor in the kinetics of the martensitic transformation. Growth of a martensite nucleus when its dimensions have become greater than critical takes place most easily in an austenite crystal with a regular structure. However, the genesis of martensite crystals in an austenite crystal without structural disturbances is much more difficult. This is apparently associated with the large work of nucleus formation in the "cooperative" displacements of atoms in the ideal lattice as a result of counteraction of the elastic forces. Thus, supercooling far below $T_0$ is necessary to reduce this work at the expense of an increase in $\Delta F$ and to make it possible for fluctuation formation of a martensite nucleus to occur in the ideal austenite lattice. However, this supercooling may be found so great

that even the average thermal-vibration energy in this temperature region will be small for sufficiently frequent formation of the necessary fluctuations. Since for the martensitic transformation, this temperature region lies below room temperature, the martensitic transformation may not occur at all at temperatures below room temperature in an austenite with the ideal lattice, despite great supercooling.

Under such conditions, vitrification of the liquid takes place on transition from the liquid state to the solid. This is observed, for example, in salol: salol that has been thoroughly purified or subjected to impurity deactivation does not crystallize, since the work of formation of its nuclei becomes quite small in a temperature region in which the atomic mobility is already low [99]. In this case, it is necessary to introduce solid particles for crystallization. The genesis of nuclei is made easier in their presence, i.e., the work of their formation is reduced, and this results in reduced supercooling. A similar phenomenon occurs in saturated solid solutions. For example, in determining solubility limits below a definite temperature, the process in which the second phase segregates out is frozen. The experimental solubility curve is found to be vertical. However, by applying preliminary plastic deformation (lowering the work of formation of the segregating phase and raising the mobility of the atoms), we may cause the segregation process to proceed even at lower temperatures and determine the solubility curve experimentally [100].

The above leads us to the conclusion that the martensitic transformation may take place even in an ideal lattice if the point $T_0$ is sufficiently high. Then, even with deep supercooling, which is necessary for a sufficient lowering of the work of nucleus formation, the absolute temperature and, consequently, the thermal-vibration energy will be found high enough for purely fluctuation-type formation of the

nucleus. With certain disturbances to the structure of the austenite crystal, however, the work of nucleus formation is reduced sharply due to reduction of the work done against elastic forces. The supercooling necessary for purely fluctuation-type nucleus formation is sharply reduced in this case.

The subsidence and resumption of the isothermal transformation is accounted for from this standpoint by the initial use of points that have the most severe disturbances or a combination of disturbances that results in the greatest reduction of the work of nucleus formation. When nuclei arise at these points, the isothermal transformation ceases, since the martensite crystals do not grow after violation of coherence and no new nuclei appear. As the temperature is further depressed, the reduced work of nucleus formation for the ideal lattice results in the use of points with less severe structural disturbances. A further depression of the temperature is necessary for subsequent transformation, and so forth. As a result, the transformation is extended over a region of temperatures.

The temperature curve of martensite-crystal generation rate indicates that the principal role in formation of nuclei in such previously "primed" places is taken by thermal oscillations, and that energy fluctuations are necessary even for formation of a nucleus that is capable of growth at such points. This may be observed particularly distinctly at the low martensite point when it has been possible to inhibit the transformation completely by rapid cooling to the temperature of liquid nitrogen. This means that nuclei do not have time to form during cooling at "primed" positions, and that the average energy of vibration is very small at the temperature of liquid oxygen. On the other hand, raising the temperature, i.e., increasing the energy of thermal vibration, increases the probability that the necessary fluctuation will

form at these points and the probability of nucleus formation. The rate of realization of these points is higher the higher the temperature. It increases with increasing temperature until the work of nucleus formation begins to increase more rapidly than the average thermal energy of the atomic oscillations, to the extent that supercooling has been reduced. From this point in time on, the rate of the transformation diminishes with rising temperature.

The appearance of a stress field about the growing crystals is characteristic for the martensitic transformation; this is due chiefly to the shearing property of the atomic readjustment. It follows from this that supercooling below $T_0$ is necessary not only to reduce the work of formation of the critical-sized nucleus, i.e., the nucleus that is capable of growth (after formation of such a nucleus, growth might also take place with less supercooling) at the expense of an increase in $\Delta F$. It is also necessary in order to compensate, at the expense of $\Delta F$, the large elastic energy that arises after formation of a martensite crystal with finite dimensions. Consequently, "primed" positions cannot be used above a certain temperature, at which $\Delta F$ becomes smaller in absolute magnitude than the elastic energy that arises on formation of the entire crystal. This temperature is apparently what constitutes the martensite point.

However, martensite crystals can also form above the point M if the elastic energy is completely or partially offset in the system in question on external application of a stress field opposed to that which arises during the process of formation of the martensite crystal. It is possible that formation of martensite crystals on plastic deformation above the point M is due not only to the emergence of disturbances that stimulate formation of nuclei, but also to the creation of such a field. As the temperature rises, increasingly large plastic

deformations are required to form martensite. However, raising the degree of deformation tends to increase the resistance of the austenite to plastic deformation (strain-hardening) and makes it possible to create higher stresses in it. The nearer the deformation temperature to $T_0$, the greater the externally applied stress required (due to the decrease in $\Delta F$) to offset the stresses that arise as a result of formation of martensite crystals.

Stresses that are sufficiently uniform in a region having dimensions of the order of the martensite-lamella length and oriented in a definite manner should undoubtedly facilitate formation of martensite crystals. Stresses that are uniform over a large volume would give rise to a situation in which not all of the possible orientations of the martensite crystals are equiprobable. Orientations for which the stress direction favors shear will be realized preferentially when external forces are applied.

Thus, the factors that facilitate nucleus formation include local disturbances in very small regions, which are capable of vanishing at relatively low temperatures, and stresses that are uniform in microregions and macroregions.

If the number of structural disturbances is very large and their distribution results in the formation of small coherent-scattering regions (blocks), difficulties then arise in formation of nuclei and the initial stages of their growth. This is probably due to impediments to the cooperative displacement of atoms when there are large crystal-structure disturbances. There is a certain analogy with plastic deformation in regard to the dual nature of the lattice-disturbance effects. In an ideal lattice, plastic deformation requires large forces whose magnitude attains that of the theoretical strength. The presence of dislocations at low dislocation densities is responsible for deforma-

tion by small forces. When, on the other hand, the dislocation density becomes large as a result of the deformation itself, the resistance to deformation also rises considerably (strain hardening).

For steels with medium and high carbon contents, and for iron-nickel alloys, the point M lies approximately 200° below $T_0$. This is due, as we indicated earlier, to the elastic energy that arises on formation of the martensite crystal. In pure and alloyed irons, the point $T_0$ is high (900° or slightly below). At the same time, the martensite points for these alloys lie in a region around 500°. The point M has not been measured for pure iron, but to judge from the dependence of this point on carbon concentration, we may assume that it is below 600°. The increase in hysteresis is probably due to instability and rapid disappearance of severe local structural disturbances at high temperatures (above 500-600°), so that there are no points at which the work of nucleus formation is sharply reduced.

The above conception as to why the transformation extends over a region of temperatures is based on consideration of the cooperative nature of the atomic readjustment in the martensitic transformation, the conjugation between the lattices as the martensite crystals grow, and the general laws of these transformations.

The temperature dependence of the transformation rate indicates that the vibration energy of the atoms plays a major role in the formation of critical-sized nuclei at "primed" points, as in other phase transformations. Structurally primed positions, i.e., places in which formation of nuclei is easier, have the same importance here as the undissolved impurities in crystallization of liquids.

REFERENCES


1. A.L. Baboshin, Metallografiya i termicheskaya obrabotka stali i chuguna [Metallography and Heat Treatment of Steel and Cast Iron], Metallurgizdat [State Scientific and Technical Publishing House for Literature on Ferrous and Nonferrous Metallurgy], 1940.
2. N.Ya. Selyakov, G.V. Kurdyumov and N.T. Gudtsov, ZhPF [Journal of Applied Physics], 1927, No. 2, page 51.
3. G.V. Kudryumov and E.E. Kaminiskiy, Zh. prikl. fiz. [Journal of Applied Physics], 1929, No. 2, page 47.
4. G.V. Kudryumov, Vestnik metallopromyshlennosti [Herald of the Metals Industry], 1932, No. 9, page 20.
5. E. Scheil and G. Tamman, Zs. anorg. allg. chem. [Journal of Inorganic and General Chemistry], Vol. 157, 1926, page 1.
6. E. Schell, Arch. Eisenhuettenw. [Iron Metallurgy Archives], Vol. 2, 1928, page 375.
7. E. Schell, Zs. anorg. allg. Chem. [Journal of Inorganic and General Chemistry], Vol. 183, 1929, Nos. 1-2, page 98.
8. A.A. Ivensen and G.V. Kurdyumov, Vestnik metallopromyshlennosti [Herald of the Metals Industry], 1930, No. 9-10, page 163.
9. G.V. Kurdyumov and G. Zaks, Zs. Phys. [Journal of Physics], 1930, Vol. 64, page 325; Vestnik metallopromyshlennosti, 1930, Nos. 9-10, page 165.
10. H. Haneman and H. Wiester, Arch. Eisenhuetenw. [Iron Metallurgy Archives], 1931-1932, Vol. 5, page 377.
11. H.H. Wiester, Zs. Metallkde [Journal of Metallurgy], 1932, Vol.

24, No. 11, page 276.

12. F. Wever and N. Engel, Mitteil. K.W. Inst. Eisenforsch. [Bull. Kaiser Wilhelm Inst. for Iron Research], 1930, Vol. 12, page 93.
13. S.S. Shteynberg, Metallurg [The Metallurgist], 1930, No. 4-5, page 506.
14. F. Wever, Arch. Eisenhuettenw., 1931-1932, Vol. 5, page 367.
15. S.S. Shteynberg, ZhTF [Journal of Technical Physics], 1935, Vol. 5, No. 2, page 362.
16. E. Schell, Zs. anorg. allg. Chem., 1932, Vol. 207, No. 1, page 21.
17. S.S. Nosyreva and M.V. Burakova, Trudy UFAN SSSR [Urals Branch of the Acad. Sci. of the USSR], 1937, No. 9, page 25.
18. M.M. Bigeyev, Trudy UFAN SSSR, 1937, No. 9, page 13.
19. V.D. Sadovskiy and N.V. Shtishevskaya, Trudy UFAN SSSR, 1937, No. 9, page 45.
20. A.P. Gulyayev, Metallurg, 1939, No. 14, page 64.
21. A.B. Greninger, A.R. Troiano, Trans. AIMME, 1939, Vol. 133, page 204.
22. A.B. Greninger, A.R. Troiano, Trans. AIMME, 1940, Vol. 307, page 140.
23. S.S. Shteynberg and V.I. Zyuzin, Metallurg, 1936, Vol. 11, No. 8, page 3.
24. S.S. Shteynberg, Metallurg, 1937, Vol. 12, No. 10, page 58.
25. S.S. Shteynberg, Termicheskaya obrabotka stali [Heat Treatment of Steel], Metallurgizdat, 1945.
26. N.V. Ageyev and G.V. Kudryumov, Metallurg, 1932, Vol. 7, No. 9, page 3.
27. V. Bugakov, I. Isaychev and G. Kurdyumov, Metallurg, 1934, No. 1, page 35.
28. G.V. Kurdyumov and T.I. Stelletskaya, ZhTF, 1935, Vol. 5, page 395.

29. E.Z. Kaminskiy and G.V. Kurdyumov, ZhTF, 1936, Vol. 6, page 984.
30. G.V. Kurdyumov, Izv. AN SSSR, ser. khim. [Bulletin of the Acad. Sci. USSR, Chemical Series], 1936, No. 2, page 271.
31. V.N. Grindev and G.V. Kurdyumov, ZhTF, 1937, Vol. 7, page 2091.
33. G.V. Kurdyumov, Sbornik dokladov sektsii metallovedeniya i termicheskoy obrabotki metallov. VNITO metallurgov [Collected Works of Section on Metallurgy and Heat Treatment of Metals. All-Union Scientific, Engineering and Technical Society of Metallurgists], 1940, page 96.
34. G.V. Kurdyumov, Fizicheskiye osnovy termicheskoy obrabotki stali. Trudy II Vsesoyuznoy konferentsii [Physical Fundamentals of Heat Treatment of Steel. Trans. of the Second All-Union Conference], Leningrad, 1941, page 4.
35. G.V. Kurdyumov, ZhTF, 1948, Vol. 18, No. 8, page 999; Problemy metallovedeniya i fiziki metallov, Metallurgizdat, 1949, page 132.
36. G.V. Kurdyumov and O.P. Maksimova, DAN SSSR, 1948, Vol. 61, page 83.
37. G.V. Kurdyumov and L.G. Khandros, DAN SSSR, 1949, Vol. 19, page 761.
38. B.A. Billby, J.W. Christian, Inst. of Metals, Monograph and Report Series, No. 18, page 121-172, London, 1956, Symposium "Mechanism of Phase Transformations in Metals."
39. A. Ivensen and G. Kurdyumov, ZhFKh [J. Phys. Chem.], 1930, Vol. 1, page 41.
40. F. Oehman, J. Iron Steel Inst., 1931, Vol. 123, No. 1, page 445.
41. G. Haegg, J. Iron Steel Inst., 1934, Vol. 130, page 439.
42. G.V. Kurdyumov and N.L. Oslon, ZhTF, 1939, Vol. 9, No. 21, page 1891.
43. G.V. Kurdyumov, P. Nekrashevich and V.V. Nechvolodov, Stal'

[Steel], 1935, No. 4, page 84.

44. E.Z. Kaminskiy and M.D. Perkas, Problemy metallovedeniya i fiziki metallov [Problems of Metallurgy and Metal Physics], Metallurgizdat, 1949, page 211.

45. G.V. Kurdyumov, M.D. Perkas and A.Ye. Shamov, DAN SSSR, 1953, Vol. 92, page 955.

46. G.V. Kurdyumov and M.D. Perkas, DAN SSSR [Proc. Acad. Sci. USSR], 1956, Vol. 3, page 818.

47. H. Lipson, A.M.B. Parker, Iron Steel Inst., 1944, Vol. 150, No. 1, page 123.

48. V.A. Il'yina, V.K. Kritskaya and G.V. Kurdyumov, DAN SSSR, 1952, Vol. 85, page 197.

49. M.P. Arbuzov, L.I. Lysak and Ye.G. Nesterenko, DAN SSSR, 1953, Vol. 90, No. 3, page 375.

50. V.K. Kritskaya, G.V. Kurdyumov and N.M. Nodina, ZhTF, 1955, Vol. 25, No. 2, page 177.

51. V.K. Kritskaya, N.M. Nodina and Yu.A. Osip'yan, Fizika metallov i Metallovedeniye [Metal Physics and Metallurgy], 1958, Vol. 6, No. 1, page 177.

52. G.V. Kurdyumov and L.I. Lysak, ZhTF, 1947, Vol. 17, No. 9, page 993.

53. G.V. Kurdyumov and L.I. Lysak, ZhTF, 1946, Vol. 16, No. 11, page 1307.

54. M.P. Arbuzov, DAN SSSR, 1950, Vol. 74, No. 6, page 1085.

55. G.V. Kurdyumov, ZhTF, 1954, Vol. 24, No. 7, page 1254, Problemy metallovedeniya i fiziki metallov [Problems of Metallurgy and Metal Physics], No. 4, Metallurgizdat, 1955, page 321.

56. G.V. Kurdyumov, Problemy metallovedeniya i fiziki metallov, No. 3, Metallurgizdat, 1952, page 9.

57. O.P. Maksimova, Ye.G. Ponyatovskiy, N.S. Rysina and L.G. Orlov, Problemy metallovedeniya i fiziki metallov, Metallurgizdat, No. 5, 1958, page 25.

58. A.P. Gulyayev and Ye.V. Petunina, Metallograficheskoye issledovaniye prevrashcheniya austenita v martensit. Trudy TsNITMASh [Metallographic Investigation of the Conversion of Austenite into Martensite. Trans. of the Central Scientific Research Institute of Technology and Machinery], No. 47, Mashgiz, 1952.

59. G.V. Kurdyumov and O.P. Maksimova, Izv. AN SSSR, OTN [Acad. Sci. USSR, Division of Tech. Sci], 1957, No. 6, page 4.

60. C.H. Shih, B.L. Averbach, M. Cohen, J. Metals, 1955, No. 2, page 183.

61. J. Philbert, C. Crussard, Iron Steel Inst., 1955, Vol. 180, No. 5, page 39.

62. O.P. Maksimova and A.I. Nikonorova, Problemy metallovedeniya i fiziki Metallov, No. 5, Metallurgizdat, 1958, page 56.

63. R.E. Cech, J.H. Hollomon, Trans. AIMME, 1953, Vol. 197, page 685.

64. G.V. Kurdyumov and O.P. Maksimova, DAN SSSR, 1951, Vol. 81, No. 4, page 565.

65. O.P. Maksimova, Trudy nauchno-tekhnicheskoy konferentsii VNITOMASh [Trans. of Sci.-Tech. Conf. of All-Union Scientific Engineering and Technical Society of Mechanical Engineers], Nos. 2,3, 1952; Problemy metallovedeniya i fiziki metallov, No. 3, Metallurgizdat, 1952, page 45.

66. G.V. Kurdyumov, O.P. Maksimova and T.V. Tagunova, DAN SSSR, 1950, Vol. 73, No. 2, page 307; Stal', 1951, No. 2, page 164.

67. A.W. Mc Reynolds, Journ. Appl. Phys., 1949, Vol. 20, No. 10, page 896.

68. O.P. Maksimova, A.I. Nikonorova and G.K. Pogorelov, Problemy

metallovedeniya i fiziki metallov, No. 4, Metallurgizdat, 1955, page 144.

69. G.V. Kurdyumov, O.P. Maksimova and A.I. Nikonorova, DAN SSSR, 1957, Vol. 114, No. 4, page 768.

70. M.G. Gaydukov and V.D. Sadovskiy, Metallovedeniye i obrabotka metallov, 1958, No. 4, page 2.

71. H.C. Fiedler, B.L. Averbach, M. Cohen, Trans. ASM, 1954, page 47.

72. G.V. Kudryumov, O.P. Maksimova, A.I. Nikonorova, Z.D. Pavlenko and A.M. Yampol'skiy, Fizika metallov i metallovedeniye, 1958, Vol. 6, No. 1, page 95.

73. G.D. Kurdyumov, Sovremennyye problemy metallurgii [Contemporary Problems in Metallurgy], Izd. AN SSSR, 1958, page 34.

74. A.P. Gulyayev, Termicheskaya obrabotka stali [Heat Treatment of Steel], Mashgiz, 1953.

75. A.N. Alfimov and A.P. Gulyayev, Izv. AN SSSR, OTN, 1954, No. 3, page 88.

76. A.N. Alfimov and A.P. Gulyayev, Izv. AN SSSR, OTN, 1954, No. 4, page 93.

77. V.G. Vorob'yev and A.P. Gulyayev, ZhTF, 1951, Vol. 21, No. 10, page 1164.

78. A.P. Gulyayev and A.P. Akshentseva, ZhTF, 1955, Vol. 25, No. 2, page 299.

79. V.G. Vorob'yev, Termicheskaya obrabotka stali pri temperaturakh nizhe nulya [Heat Treatment of Steel at Temperatures Below Zero], Oborongiz [State Publishing House for Literature of the Defense Industry], 1954.

80. O.P. Maksimova and A.I. Zakharov, DAN SSSR, 1957, Vol. 114, No. 6, page 1195.

81. A.I. Zakharov and O.P. Maksimova, Izv. AN SSSR, OTN, 1958, No. 7,

page 3.

82. W.J. Garris, M. Cohen, Trans. AIMME, Vol. 180, 1949, page 447.

83. P.P. Petrosyan, DAN SSSR, 1948, Vol. 59, No. 6, page 1109.

84. S.G. Glover, T.B. Smith, The Mechanism of Phase Transt. in Metals, London Inst. Met. No. 18, 1956, page 265. V.V. Nechvolodov, Stal', 1935, No. 4, page 84.

85. V.N. Gridnev, Metallurg [The Metallurgist], 1938, No. 4.

86. V.I. Arkharov, Kristallografiya zakalki stali [Crystallography of Steel Hardening], Metallurgizdat, 1951.

87. G. Wassermann, Metallwirtsch. [Metals Economy], 1934, Vol. 13, page 133.

88. E.Z. Kamenskiy, G.V. Kurdyumov and V.Ye. Neymark, ZhTF, Vol. 4, 1934, page 1774.

89. V.N. Grindev, ZhTF, 1941, Vol. 11, Nos. 13-14, page 1226.

90. Ya.M. Golovchiner, Problemy metallovedeniya i fiziki metallov [Problems of Metallurgy and Physics of Metals], No. 2, Metallurgizdat, 1951, page 119.

91. J.B. Hess, C.S. Barrett, Trans. AIMME, 1952, Vol. 194, page 645.

92. E.Z. Kaminskiy and G.V. Kurdyumov, ZhTF, 1936, Vol. 6, page 984.

93. G. Kurdyumov, V. Miretskiy and T. Stelletskaya, ZhTF, 1938, Vol. 8, page 1959.

94. G.V. Kurdyumov and L.G. Khandros, ZhTF, 1949, Vol. 19, No. 5.

95. L. Kaufman, M. Cohen, J. Metals, 1956, Vol. 8, No. 10, page 1393.

96. M.V. Yakutovich and E.S. Yakovleva, ZhTF, 1939, Vol. 9, page 884.

97. Ya.M. Golovchiner and Yu.D. Tyapkin, DAN SSSR, 1953, Vol. 93, No. 1, page 39.

98. O.P. Maksimova and A.I. Nikonorova, Problemy metallovedeniya i fiziki metallov, No. 4, Metallurgizdat, 1955, pages 123-143.

99. V.I. Danilov, Problemy metallovedeniya i fiziki metallov, No. 1, Metallurgizdat, 1949, pages 7-44.

100. S.T. Konobeyevskiy, Izv. AN SSSR, 1937, Vol. 5, page 1209.

101. S.F. Yur'yev, Udel'nyye ob'yemy faz v martensitnom prevrashchenii austenita [Specific Volumes of Phases in Martensite Transformation of Austenite], Metallurgizdat, 1950.

102. A.P. Gulyayev and Ya.E. Sanchuk, ZhTF, 1952, Vol. 22, No. 11.

103. M.S. Wechler, D.S. Lieberman, T.A. Read. Trans. AIMME, 1953, 197, page 1503.

104. F.C. Frank, Acta Metallurg., 1953, Vol. 1, page 15.

105. J.K. Mackemzie, J.S. Bowler, Acta Metallurg., 1954, Vol. 2, page 138.

106. J.S. Bowler, J.K. Mackenzie, Acta Metallurg., 1954, Vol. 2, page 224.

107. P.P. Petrosyan, Termicheskaya obrabotka stali kholodom [Heat Treatment of Steel in the Cold], Mashgiz [State Scientific and Technical Publishing House], 1957.

108. G.N. Bogacheva and V.D. Sadovskiy, DAN SSSR, 1952, Vol. 83, page 569.

109. V.D. Sadovskiy and G.N. Bogacheva, DAN SSSR, 1952, Vol. 83, No. 2, page 221.

110. C. Zener, Metals Technology, 1946, Vol. 13, page 1.

111. G.V. Kurdyumov, ZhTF, 1930, Vol. 1, page 281; Zs. Phys. [J. Phys.], 1929, 55, page 187.

## Chapter 36

## THEORY OF TEMPERING OF QUENCHED STEEL

Heat treatment in which decay of the state of steel fixed by quenching – the oversaturated solid solution of carbon in α-iron, or martensite, as well as of the residual austenite, takes place is known as tempering. The result of this process is transition to a more stable state. Structures that represent decay products of martensite and austenite – a mixture of α-iron and carbides – form in the steel. The properties of the steel change accordingly: plasticity and toughness are increased, hardness is reduced, and internal (residual) stresses are reduced.

Tempering is accomplished by heating quenched steel to a temperature lying below the $Ac_1$ point, soaking at this temperature, and subsequent cooling. The results of tempering are determined basically by the heating temperature and, to a lesser degree, by the soaking time. The cooling rate has no substantial influence on the result, but if the steel has a tendency toward tempering brittleness, cooling should be quite rapid.

Low, medium and high tempering are distinguished on the basis of heating temperature. Low tempering (heating to 120-250°) has as its purpose reduction of internal stresses in workpieces of which retention of high hardness and wear resistance is demanded. Here, the brittleness of the steel is reduced considerably, while its hardness is hardly affected at all. Medium tempering (heating to 300-500°) is used for products that must possess high elastic limits, strength, and wear-

resistance, as well as rather high toughness (springs, shock absorbers). High tempering (heating to 450-670°) is used for articles that experience rather large impact and vibration loads in operation; it delivers a highly favorable combination of toughness, plasticity and strength properties.

1. PROCESSES TAKING PLACE IN QUENCHED STEEL DURING TEMPERING

Tempering processes are essentially processes of solid-solution decay — decay of martensite and residual austenite — that return the steel to a more stable state. Four stages are distinguished in tempering; of these, the first two correspond to two stages of martensite decay. Decay of martensite takes place over a broad temperature range — from room temperature to 300-350°. The first (below 150°) and second (150-300°) stages of this decay differ as regards mechanism and kinetics.* The processes that unfold in the third and fourth stages of tempering are developed in the temperature ranges from 300 to 450° and from 450° to $Ac_1$. The temperature boundaries of the stages are arbitrary. They may shift in one direction or the other, depending on heating rate, holding time, and the composition of the steel. Certain tempering processes do not go to completion in their specific stages, but extend into later stages.

First Stage of Tempering (First Stage of Martensite Decay)

The first stage of tempering consists in segregation of highly dispersed carbide particles from the martensite. Once they have formed, the nuclei grow until the regions surrounding them have become rather severely impoverished in carbon and the influx of atoms of this element ceases as a result of the low rate of diffusion from the solid solution. Solid-solution regions with carbon concentration lower than the original concentration form about the carbide particles; these are in a state of temporary, unstable "colloidal" equilibrium [2] with the

dispersed carbide particles. These carbon-impoverished regions are surrounded by a solid solution that has the initial carbon concentration. Since a new solid solution with a lower carbon concentration arises and coexists with the original concentration, martensite decay in the first stage is said to be two-phased (or heterogeneous). Almost no regions with intermediate concentrations are observed. The quantity of solid solution that has been impoverished in carbon increases not by growth of the regions, but by an increase in their number. Thus, the progress of the process in time is governed practically exclusively by the number of carbide-phase nuclei that form, and the rate of decay is determined by the rate of generation of carbide particles.

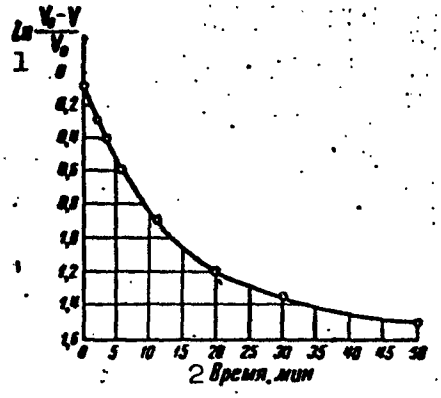


Fig. 1. Variation of quantity of martensite that has undergone partial decay during tempering at 120° [3]. 1) $\ln(V_0 - V/V_0)$; 2) time, minutes.

The kinetics of the process is characterized by the curve of Fig. 1 [1, 3], where $V_0$ is the initial volume of the solid solution (specimen volume), V is the total volume of the impoverished part of the solid solution surrounding the carbide nuclei (the volume of decayed solid solution). The temperature dependence of the decay rate is described by the general equation of crystallization of supersaturated solutions, taking into account the work of formation of the nucleus. The rate of the process is characterized by the half-decay time, i.e., the time necessary for transition of half of the initial solid solution to the new solid solution. For high-carbon steel, the half-decay time at room temperature is reckoned in terms of several years; it is about 8 hours at 80°, 50 minutes at 100°, 8 minutes at 120°, and 45 sec at 160°. Calculations indicate that at 0°, the half-decay time is 340 years, and that it is

6.4 years at 20°, 2.5 months at 40°, and 3 days at 60° [3, 4].

Carbide inclusions take the form of extremely thin lamellae a few lattice constants thick. The lattices of the carbide and the α-solid solution are coherent. Since the crystal lattices and specific volumes of the carbide and the α-phase are different, elastic stresses arise between them (Fig. 2) [5].

A structural state of the steel known as tempered martensite forms as a result of the first stage of decay. In this state, the steel exhibits a fine nonuniform structure, and the α-solid solution is still slightly oversaturated with carbon and has a tetragonal lattice. The activation energy corresponding to the first decay stage is about 33,000 cal/g·mole, while the work of formation of a carbide-phase nucleus is 1000 cal/g·mole (for 120°).

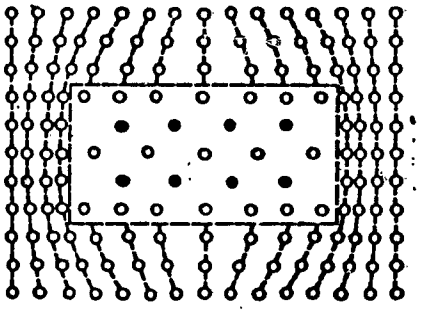

Fig. 2. Diagram showing genesis of lattice distortions on formation of carbide-phase nucleus within martensite crystal. The lattices of the martensite and carbide are coherent [5].


Fig. 3. Diagram showing arrangement of dislocations of coherent lattices of carbide and solid solution [9]. 1) Initial martensite (primary); 2) zone of concentration change; 3) low-carbon martensite; 4) low-temperature carbide.

Data of foreign investigators [6-8] and an attempt to apply dislocation theory to account for the mechanism of tempering processes in this stage [9] do not introduce any substantial changes into the conception set forth above, which is based chiefly on the work of Soviet scientists and primarily that of G.V. Kurdyumov and his colleagues [1]. The pattern in which the dislocations are arranged between the coherent lattices of the carbide and the martensite matrix is illustrated by Fig. 3. It is assumed that the carbide nuclei occur at the boundaries of the martensite crystals, and that the carbide crystals are lamellar [9].

Second Stage of Tempering (Second Stage of Martensite Decay)

The second tempering stage is observed in carbon steel in the range from 150 to 300°. The rise in tempering temperature and the resulting increase in the atomic-migration rate are responsible for further segregation of carbon from the martensite. Decay of the solid solution takes place in this stage by progressive segregation of carbon from the solid solution and a certain amount of carbide-particle growth as a result. This is accompanied by a concurrent coagulation (coalescence) process of the carbide particles – solution of the finer particles and growth of the larger ones with diminishing concentration of the solid solution. The process is homogeneous, single-phased, and continuous. Its rate is determined by the rate of diffusion of carbon atoms and the growth rate of the carbide granules. Precipitation of the carbon first takes place rapidly and then, as the holding time increases, it drops off (Fig. 4) [10]. A definite quantity of carbon remaining in solid solution corresponds to each tempering temperature. The coherence of the carbide and solid-solution lattices is retained. Lattice distortions are reduced but remain significant. Figure 5 [11] shows the variation of the severity of distortions of the second kind

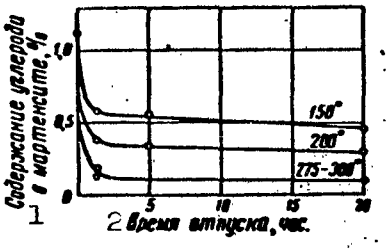


Fig. 4. Carbon content in martensite as a function of tempering time at various temperatures for steel with 1.1% C [10]. 1) Carbon content in martensite, %; 2) tempering time, hours.

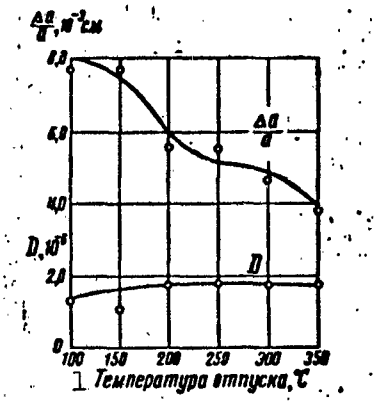


Fig. 5. Size of coherent regions (D) and magnitude of lattice distortions ($\Delta a/a$) as functions of tempering temperature [1, 11]. 1) Tempering temperature, °C.

and the size of the coherent-scattering regions. At 200-300°, the martensite is a slightly oversaturated (at 250°, 0.06% C) solid solution with disperse carbide particles distributed in it.

Decay of Residual Austenite ("Second Transformation" in Tempering)

In high-carbon and many alloyed medium-carbon steels that contain a large quantity of residual austenite, the process of carbon separation from the martensite, which takes place in the range from 150 to 300°, has superimposed upon it the decay process of this austenite. However, the decay of small quantities of austenite does not appear distinctly on the property-variation curves. The rate of the residual-austenite decay process as a function of temperature and tempering time is illustrated by Fig. 6 [8].

Decay of residual austenite begins at higher temperatures than that of martensite, since the passages of carbon atoms from one interstice into another in the γ-lattice (austenite) are constricted to a greater degree than in the α-lattice (martensite), although the interstices themselves are larger in the austenite lattice than in the

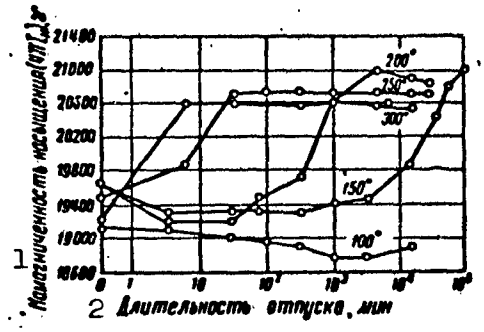


Fig. 6. Kinetics of residual-austenite decay in steel with 0.8% C. Saturation magnetization as a function of tempering time at various temperatures [8]. 1) Saturation magnetization ($4\pi I_n$), gausses; 2) tempering time, minutes.

α-iron lattice [12]. On a considerable increase in the tempering time, the initial decay temperature of the residual austenite is shifted into a lower temperature region [8]. It is assumed that as a result of residual-austenite decay, the same phases form in carbon steel as in tempering of martensite at the same temperature, although the coherence of the solid solution and the carbide phase may not be the same in both of these cases.

State of the Carbide Phase in Tempered Steel

The question as to the composition and structure of the carbide segregated out at low tempering temperatures cannot be regarded as adequately clarified at the present time.

Results of x-ray investigations. For a long time, it was not possible to ascertain the presence of carbide by experimental means in low-tempered steel. Carbide lines were observed on x-ray patterns only after tempering at temperatures above 300° [13]. G.V. Kurdyumov and M.P. Arbuzov [14] were the first to succeed in detecting the presence of a carbide in low-tempered martensite; as regards its crystal structure and, apparently, its chemical composition, this carbide differs from cementite. The new carbide was designated $Fe_xC$. On the basis of this investigation, the considerable loss in volume and other changes in the properties of the steel on tempering at about 300° were accounted for by transition of the carbide $Fe_xC$ to $Fe_3C$ [15, 43].* According to the calculations of Ya.S. Umanskiy and Ye.I. Onishchik [16, 17], an interstitial phase with a compact hexagonal lattice is present

in low-annealed steel: its composition is defined approximately by the formula $Fe_3C$. On the basis of research into the crystal structure of steel in various stages of tempering, which was completed in 1961, M.P. Arbuzov established that the carbide phase precipitating out at low tempering temperatures has a close-packed hexagonal lattice that is regularly oriented with respect to the austenite crystal axes. Two carbide phases exist in the range from 200 to 400°: the low-temperature carbide and a carbide having a rhombic lattice; above 400°, there is only one carbide phase — rhombic cementite. Yu.A. Bagaryatskiy [20] showed that continuous transition from the martensite lattice to the cementite lattice is possible when the carbide lattice is somewhat deformed and retains its orientation relative to the martensite lattice. According to M.P. Arbuzov [37], the low-temperature carbide crystallizes with a carbon deficiency and has a smaller volume than cementite. It is known that the reaction between carbon monoxide and iron results in formation of a carbide of the type $Fe_2C$ [21] or $Fe_{20}C_9$ [22] (the percarbide).

Two modifications of the carbide $Fe_2C$ have been produced synthetically: the low-temperature modification $\varepsilon$-$Fe_2C$, which forms at 170-230° with a hexagonal lattice and a Curie point of 380°, and the high-temperature $\chi$-$Fe_2C$, which forms as a result of the former's decay at 200° with a rhombic [27] lattice and a Curie point of 265° [28].

Observing the same interference pattern as G.V. Kurdyumov and M.P. Arbuzov, Jack [22] also concluded that it corresponds to the hexagonal lattice; he regards the composition of the carbide as near $Fe_3C$. He proposed that this carbide be termed the $\varepsilon$ carbide because of its structural similarity to the $\varepsilon$ nitride of iron. This carbide is coherent with the matrix. It is transformed to cementite at 260-360°. Lement [7] determined the composition of this carbide as $Fe_{2.4}C$ (8.22%

C) by calculation.

The hexagonal ε-carbide of iron was also observed by a number of investigators who used the electron-diffraction method [24-27, 38]. Yu.A. Skakov and others [26] define its composition as $Fe_4C$ (see also [18]).

Results of chemical investigations. The carbides produced in tempering at 200-400° correspond as regards chemical composition to cementite [29]. The results obtained by N.V. Gudkova and others [27] differ from those obtained by N.M. Popova. Lement et al. [62] consider that the determination error may be as high as ±0.3% C in these cases and may mask small changes in the carbide's carbon content during the tempering process.

The results of the magnetometric investigations of I.N. Bogachev and V.G. Permyakov [30] showed that in tempering below 250°, a carbide other than cementite forms in steel. According to V.G. Permyakov [31-33], the carbide $Fe_xC$ has a Curie point of 370° and a value of 2 for x. At 270-400°, it goes over into an intermediate carbide that has a Curie point of 260°, and at 400-550° it becomes cementite. B.A. Apayev [34, 35] indicates that the carbide ε-$Fe_xC$ and a small quantity of cementite exist in low-carbon steel that has been tempered at 100-200°; as the tempering temperature is raised, the quantity of ε-$Fe_xC$ is reduced and that of $Fe_3C$ increases. In high-carbon steel, the carbide ε-$Fe_xC$, which is transformed on heating into χ-$Fe_xC$ and cementite, forms from the martensite; subsequently, the χ-$Fe_xC$ disappears and the quantity of cementite increases. Crangle and Sucksmith identify χ-$Fe_xC$ with synthetic χ-$Fe_2C$ [36].

The research results set forth above embody a number of serious contradictions. Thus, M.P. Arbuzov notes [37] that it is difficult to explain why a new phase that is richer in carbon than cementite should

appear at low tempering temperatures in the presence of cementite and then be turned into cementite at higher temperatures. The causes of the great reduction in the steel's volume on tempering at 300° are not yet fully clear: it cannot be accounted for by the carbide transformation alone. The displacement of the Curie points is accounted for by many investigators in terms of lattice distortions of a carbide coherent with the α-phase [38, 62]. The same effect is observed in annealed steel after plastic deformation [39]. B.A. Apayev [35] objects to these statements, referring to References [40, 41 and 42]. Ya.S. Umanskiy et al. [17] regard the proposition that coherence of the carbide may result in a Curie-point shift as inadequately substantiated.

In summarizing, it must be acknowledged that there are many substantial contradictions concerning the most important problems of the state of the carbide in low-tempered steel. There is no consistent opinion concerning the crystalline structure (of ε-$Fe_xC$ and $Fe_3C$ with distorted lattices, and so forth), none as regards composition ($Fe_2C$, $Fe_{2.4}C$, $Fe_3C$, $Fe_4C$), and there is not even agreement as regards the explanation for the property changes (and, in particular, those in the magnetic properties). Clarification of these questions requires new research.

Third Stage of Tempering ("Third Transformation")

The third stage of tempering takes place in carbon steel in the temperature range from 300 to 450°. Rapid growth of carbide granules begins in this stage (Fig. 7) [19]. Up to about 350°, this growth takes place without disturbance of coherence between the carbide and the surrounding solid solution. Above 350°, the carbide granules increase rapidly to dimensions such that the stresses reach values sufficient to make the distortion energy greater than the energy of interface formation. Then coherence is violated, an interface appears be-

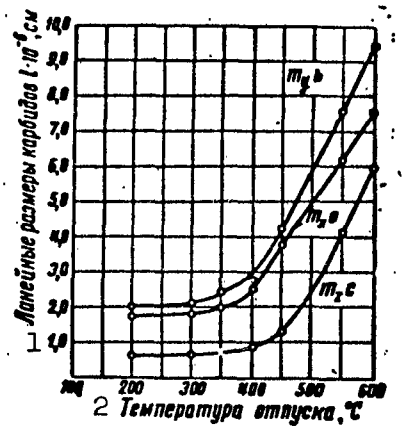


Fig. 7. Variation in dimensions of iron-carbide crystals in carbon steel as a function of tempering temperature: $m_x a$ — along x-axis; $m_y b$ — along y-axis; $m_z c$ — along z-axis [19]. 1) Linear dimensions of carbides, $l \times \times 10^{-6}$, cm; 2) tempering temperature, °C.

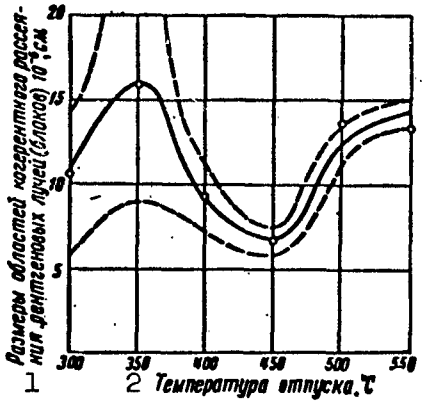


Fig. 8. Change in size of α-phase regions that scatter x-rays coherently as a function of tempering temperature [4]. 1) Dimensions of regions of coherent x-ray scattering (blocks), $10^{-6}$, cm; 2) tempering temperature, °C.

tween the phases, and the carbide crystals and mosaic blocks of the α-phase separate. The size of the α-phase regions that scatter x-rays coherently decreases (Fig. 8) [4]. In the temperature region above 450°, the α-phase blocks again increase in size (grow), since diffusion processes take place intensively at these temperatures.

This process of coherence violation is accompanied by a decrease in stresses; its temperature of completion is the temperature at which stresses of kind II are relieved (Fig. 9) [4], which contributes to significant volume [44] and thermal [45] effects. In the same temperature range, distortions of kind III are also extensively relieved [47].

A diminution of the α-phase blocks may occur in the temperature range of the third tempering stage not only as a result of loss of lattice coherence, but also as a consequence of relief of elastic stresses by plastic shears in microregions of the metal. These shears take place under the influence of the rather high elastic stresses present in the steel, provided that the metal's plasticity is made high enough. Block size, distortions of the second kind,

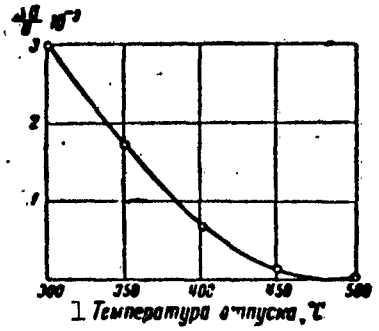


Fig. 9. Variation of distortions of the second kind ($\Delta a/a$) in α-phase lattice as a function of tempering temperature [4]. 1) Tempering temperature, °C.

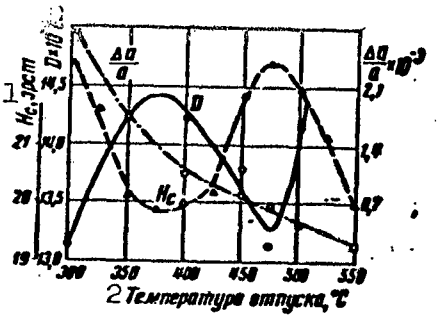


Fig. 10. Variation in block size (D), coercive force ($H_c$) and distortions of the second kind ($\Delta a/a$) in hardened steel with 0.7% C, as a function of tempering temperature [46]. 1) $H_c$, oersteds; 2) tempering temperature, °C.

and coercive force are compared in Fig. 10 [46]. The temperature region in which pulverization of the blocks is observed and the corresponding temperature region in which the mechanical properties and coercive force undergo significant changes may be shifted under the influence of a change in the elastic stresses of the crystal lattice, which, in turn, are determined by the degree of deformation, carbon and alloying-element contents in the steel, and other factors (compare Fig. 12) [46]. The initial stages of recrystallization of the α-solid solution, which is deformed as a result of intraphase work-hardening, may take place in this same stage of tempering [44, 46, 48, 49].

A number of authors link the change in physical properties in the third stage of tempering with transition of the low-temperature carbide into cementite [30-35 and others].

Fourth Stage of Tempering

Coagulation (more properly, coalescence) of the carbides takes place basically during this stage. Beginning in a carbon steel at the temperatures of the second stage, these processes develop intensively above 350°. They were investigated in detail by S.Z. Bokshteyn [50].

In the first stages of tempering, the carbides are precipitated in the form of lamellar granules, since the elastic energy is at its minimum in this case. If the particles were to assume a spherical shape, the surface-energy value would be reduced. The elastic energy is proportional to particle volume, while surface energy is proportional to the area of the phase segregated. The interaction between the two forms of energy results in spheroidization being observed only after prolonged tempering at a rather high temperature. Then the diameter of the carbide particles increases by a factor of approximately 1000, which gives rise to large changes in total surface and in the crystal-chemical relationships between the phases, as well as a considerable change in properties. The coagulation process was analyzed theoretically by S.T. Konobeyevskiy [2]. In isothermal tempering, the fine particles undergo solution continuously, the large ones grow, and the medium-sized particles first grow larger at the expense of the fine ones, and then are also dissolved, unless they attain the critical size as a result of their growth. The coagulation rate is characterized as a function of time by the equation

$$t = Ae^{-B/T}$$

where $\underline{t}$ is the time required to reach a certain degree of coagulation, T is the absolute temperature and A and B are constants.

The rate of the process subsides in time. It rises with increasing degree of dispersion of the particles. An increase in carbon content accelerates coagulation [49].

Only a few of the largest particles grow during the fourth stage; the remainder are dissolved. The rate of the coagulation process is determined by the rate of migration of vacancies, and the process is controlled by the speed of self-diffusion of α-iron with an activation energy of 60,000 kcal/g·mole [50, 51, 52].

Influence of deformation on tempering processes. Cold deformation intensifies the segregation of carbon from the saturated α-solid solution [53] and promotes decay of the residual austenite [54]. It has been shown [55] that a 2.4% deformation reduces the relative quantity of residual austenite by 29%, an 8% deformation by another 36%, and with an 11% deformation the residual austenite is almost completely decayed. Decay of the martensite under the influence of an 18% deformation takes place just as in tempering at 100-120° [55, 56].

It would appear that deformation results in spontaneous formation of a large number of carbide nuclei. The only effect on deformation of completely decayed martensite is the appearance of lattice distortion and block crushing in the α-phase.

Influence of fast heating on tempering processes (electric tempering). V.D. Sadovskiy and his coworkers [57, 58] studied electric tempering chiefly from the standpoint of the influence of heating rate on impact strength. A rise in heating rate shifts the residual austenite decay region toward higher temperatures, and sometimes completely suppresses the decay process [57, 58]. The martensite-decay process cannot be suppressed or delayed by heating at a constant rate (up to 60,000 °C/sec) [59, 60]. The volume-decrease effect observed in the first tempering stage at ~100° with slow heating is shifted as the heating rate rises to 50°C/sec to 190-260°, while the volume-decrease effect in the third tempering stage, which is usually observed at 300°, is shifted to 370-490°. A further increase in heating rate does not result in an increase in these temperatures. Austenite decay is suppressed at a heating rate as low as 60-100°C/sec, although the residual austenite decays into a ferrite-carbide mixture after heating above 400°, even when the time of isothermal holding is short. The carbide particles are smaller after fast electric tempering than after ordinary

tempering. Lattice distortions of the second kind are retained after such treatment even at 600-650°. The size of the submicrostructure blocks is reduced considerably as compared with normal tempering, particularly above 450-500° (see also [18]).

The effect of normal tempering on properties of steel that has been quenched after high-speed electric heating was investigated by K.A. Malyshev and V.A. Pavlov [134] and I.N. Kidin [61]; the influence of self-tempering after quenching with heating by high-frequency currents was studied by K.Z. Shepelyakovskiy [66].

## 2. CHANGES IN MICROSTRUCTURE AND PROPERTIES ON TEMPERING

### Change in Microstructure

According to structural investigations using the electron microscope [62], a fine network of carbides is observed to have formed along block (subgrain) boundaries after tempering at 150-200°. These carbides dissolve when the tempering temperature is raised to 200-300°. Simultaneously, beginning with a tempering temperature of 230°, elongated carbide lamellae form along the boundaries of the martensite crystals together with lamellar and globular carbides within these crystals (Fig. 11a). The average subgrain diameter has been determined at 1.5-$2.0 \cdot 10^{-5}$ cm, and the thickness of the carbide network at 8-100 A (in a steel with 0.4-1.4% C). Solution of the carbide network and carbon impoverishment of the matrix give rise to softening of the steel. The appearance of cementite films along the boundaries of the old austenite grains may be the cause of low-temperature (~260°) tempering brittleness, which vanishes as the tempering temperature is raised due to carbon impoverishment of the matrix. Above 400°, the carbide particles within the α-phase crystals are dissolved. This process is accompanied by spheroidization and coagulation of the remaining particles. The carbide film along the grain boundaries becomes thicker by solution of

the fine carbides within the ferrite grains. It undergoes spheroidization and coalescence simultaneously (Fig. 11b). The carbide particles formed as a result of the above remain at the grain boundaries, but their number is reduced and their sizes increase. Some of the films are retained to temperatures near $Ac_1$. The processes of spheroidization, coagulation and carbon impoverishment of the matrix soften the steel. Growth of the α-phase crystals in the range from 480 to 700° is minor, obviously as a result of the inhibiting influence of the cementite along the grain boundaries of the ferrite (see also [63-65, 51]).

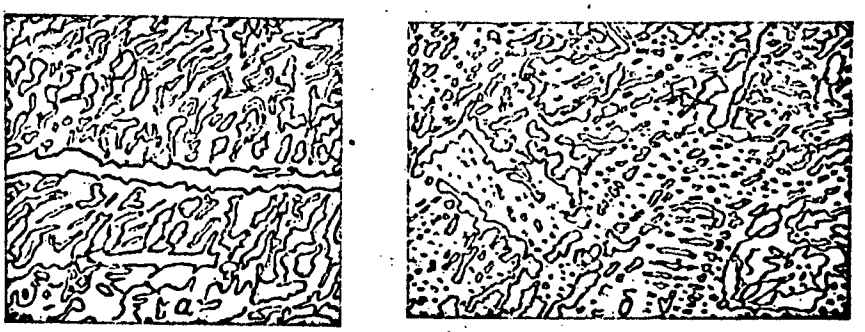

Fig. 11. Electron-microscopic structure of steel with 1.4% C after quenching from 1200° and subsequent tempering [62]: a) tempering at 260°, one hour, 15,000×; b) tempering at 480°, one hour, 5000×.

Change in Properties

Magnetic properties. The high coercive-force values of quenched steel are usually explained in terms of the premises of stress theory [68], and the secondary increase in this characteristic in the presence of residual austenite is explained by reference to the theory of inclusions [67, 68]. On tempering, coercive force decreases, particularly in the temperature interval of residual-austenite decay (see Fig. 16a) [69], and we also observe a rise in the curve (a maximum) in the temperature range from 400-450 to 475-550°, the presence of which is accounted for [4] by crushing of α-phase blocks. The temperature of

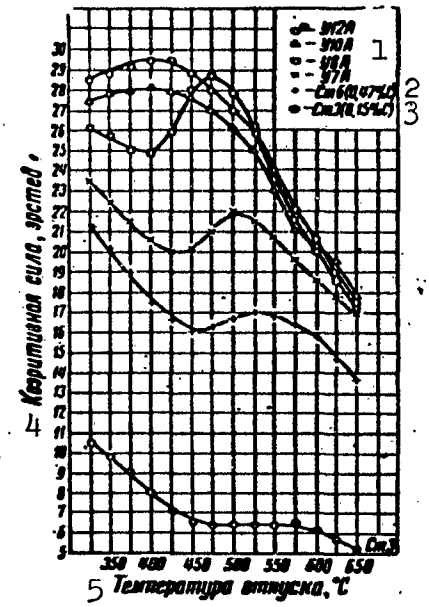


Fig. 12. Variation of coercive force as a function of carbon content in steel and tempering temperature [70]. 1) U12A, etc.; 2) St. 6 (0.47% C); 3) St. 3 (0.15% C); 4) coercive force, oersteds; 5) tempering temperature, °C.

the maximum is shifted into the region of lower tempering temperatures [70] with increasing carbon content in the steel (Fig. 12). The change in maximum magnetic permeability (see Fig. 16b) is due to the same processes [69]. The saturation magnetization (see Fig. 16c) increases sharply on decay of the paramagnetic austenite, but then decreases somewhat as a result of cementite formation [71]. The residual induction (see Fig. 16d) increases particularly rapidly in the range from 200 to 400° [72].

Electrical properties. Resistivity drops most sharply after 100 and 230° (Fig. 13), i.e., during the times of most rapid decay of the martensite and residual austenite, respectively [73]. Above 300°, resistivity changes only slightly and gradually (Fig. 16e) [74]. Thermal electromotive force changes considerably (Fig. 16f) as the carbon is precipitated from solid solution and the lattice distortions are accordingly reduced [30]. The Hall galvanomagnetic effect (Fig. 14) is a function of tempering temperature and soaking time [75].

Thermal properties. An increase in thermal conductivity is observed on decay of martensite (100-150°) and residual austenite (200-250°); the subsequent increase (see Fig. 16g) is related to the transition to the heterogeneous ferrite-carbide structure [76]; coagulation of the carbides reduces thermal conductivity insignificantly. The first effect on the heat-capacity curve is due to decay of martensite,

the second to that of residual austenite, and the third to the change in carbide state (see Fig. 16h) [45].

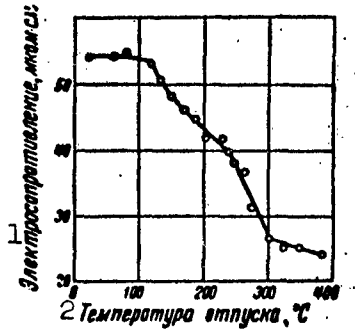


Fig. 13. Change in resistivity of steel (1.57% C) on tempering (quenching temperature 1050°) [73]. 1) Resistivity, μohms·cm; 2) tempering temperature, °C.

The latent heat of the transformations changes in the first, second and third stages of tempering (Fig. 16i) [77].

Volume changes. A decrease in specimen length corresponds to the first and third stages of tempering, and an increase to the second stage (see Fig. 16j) [78]. A significant decrease in volume can be observed for the first stage of tempering on the density curve (see Fig. 16k) [79], an increase in the second

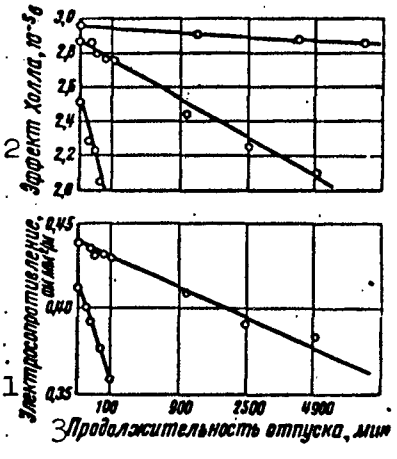


Fig. 14. Hall effect (tempering temperatures: upper curve 20°, middle curve 65°, lower curve 100°) and change in resistivity (upper curve 65°, lower curve 100°; B = 18,000 gausses) in tempering of steel with 1.18% C [8, 75]. 1) Resistivity, ohms-mm$^2$/m; 2) Hall effect, $10^{-5}$ v; 3) tempering time, minutes.

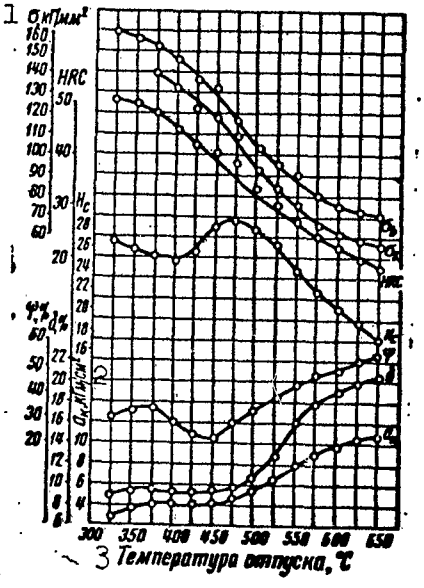


Fig. 15. Change in mechanical properties and coercive force on tempering (steel with 0.82% C) [84]. 1) σ, kgf/mm$^2$; 2) $a_k$, kgf-m/cm$^2$; 3) tempering temperature, °C.

stage and a large decrease in volume in the third stage. The volume

reduction continues to 600-650°.

Residual stresses (see Fig. 16l) diminish on tempering [80, 81].

Solubility in acids (see Fig. 16m) is characterized by a curve with two maxima [86]. The color change of the solution, which may serve as a basis for inferences concerning changes in carbide-particle size [87] is shown in Fig. 16n.

Mechanical properties. The ultimate strength diminishes more slowly in the interval from 400 to 450° than in other regions (Fig. 15) [82-84, 46, 70]. In the same temperature interval, we note a minimum of relative area reduction; the curves of relative elongation and impact strength show delayed ascent (steel with 0.8% C). The same phenomena are also detected in a steel with 0.4% C [84]. These effects are intensified when the heating rate in tempering is increased (Fig. 17). The loss in plastic properties in the range from 400 to 450° is linked with crushing of α-phase blocks [83]. On the hardness curves, we observe two maxima for decay of the martensite and austenite (see Fig. 16o) [85], and a slight increase in hardness is also noted at 450° (Fig. 15) [82, 49]. The results of microhardness determinations on martensite and residual austenite in tempering are of interest (Fig. 18) [63].

The endurance limit rises at 300-400° [88]. We note a sharp drop in wear resistance in steels tempered above 350° (see Fig. 16s) [89]. The cyclic work of deformation (damping of vibrations) diminishes in the tempering temperature range from 450 to 550° (see Fig. 16p) [82]. The data on the mechanical-property variations are in good agreement with the general conceptions of the processes that take place in steel on tempering.

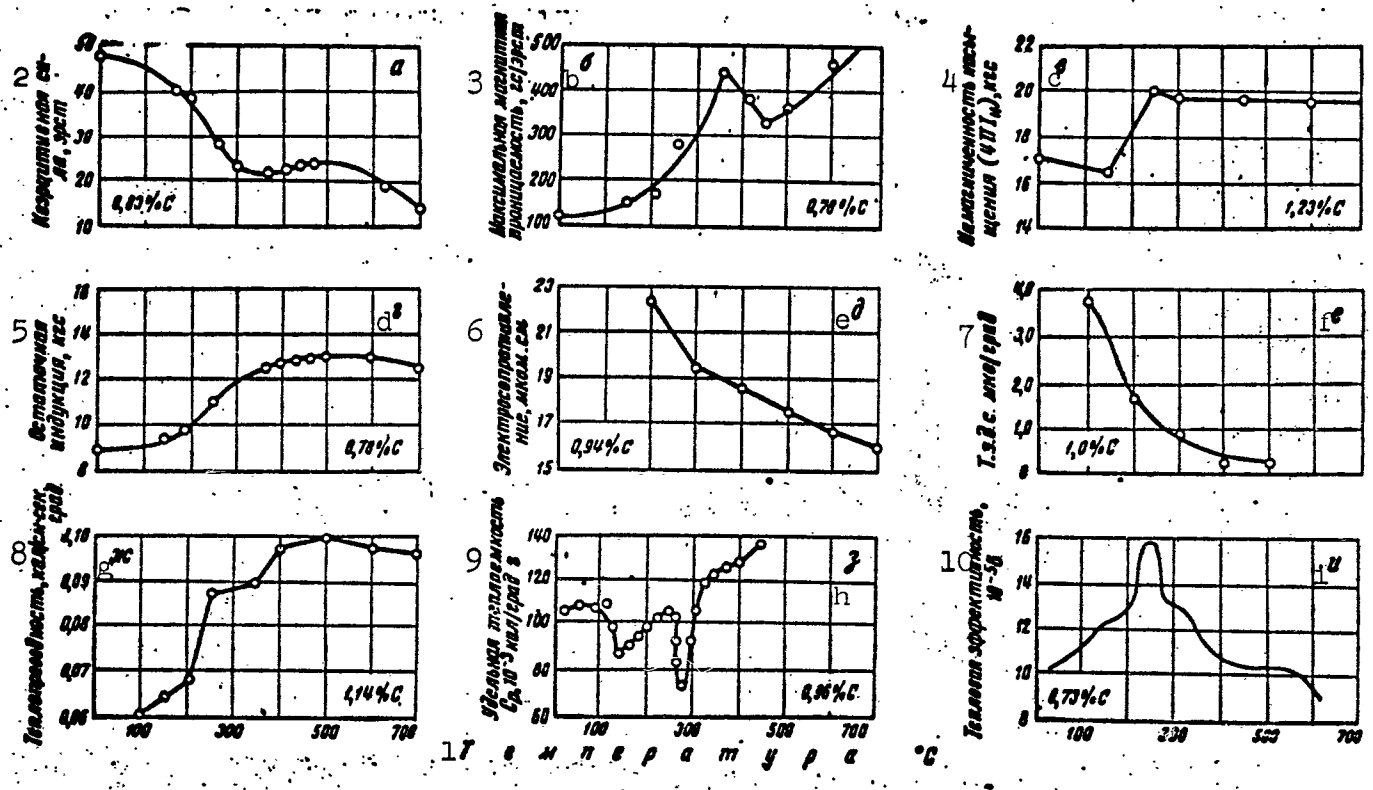
2
Коэрцитивная сила, Ja, эрст
a
0,83%C
3
Максимальная магнитная проницаемость, гс/эрст
б
b
0,70%C
4
Намагниченность насыщения (4πIs), гкс
в
c
1,23%C
5
Остаточная индукция, гкс
г
d
0,78%C
6
Электросопротивление, ом.см
е
д
0,94%C
7
Т.з.д.с. мкв/град
ж
f
1,0%C
8
Теплопроводность, кал/см.сек.град
з
g
1,14%C
9
Удельная теплоемкость Cp, 10⁻³ кал/град² в
и
h
0,96%C
10
Тепловой эффект, кг-кг
к
i
0,73%C
Температура °C

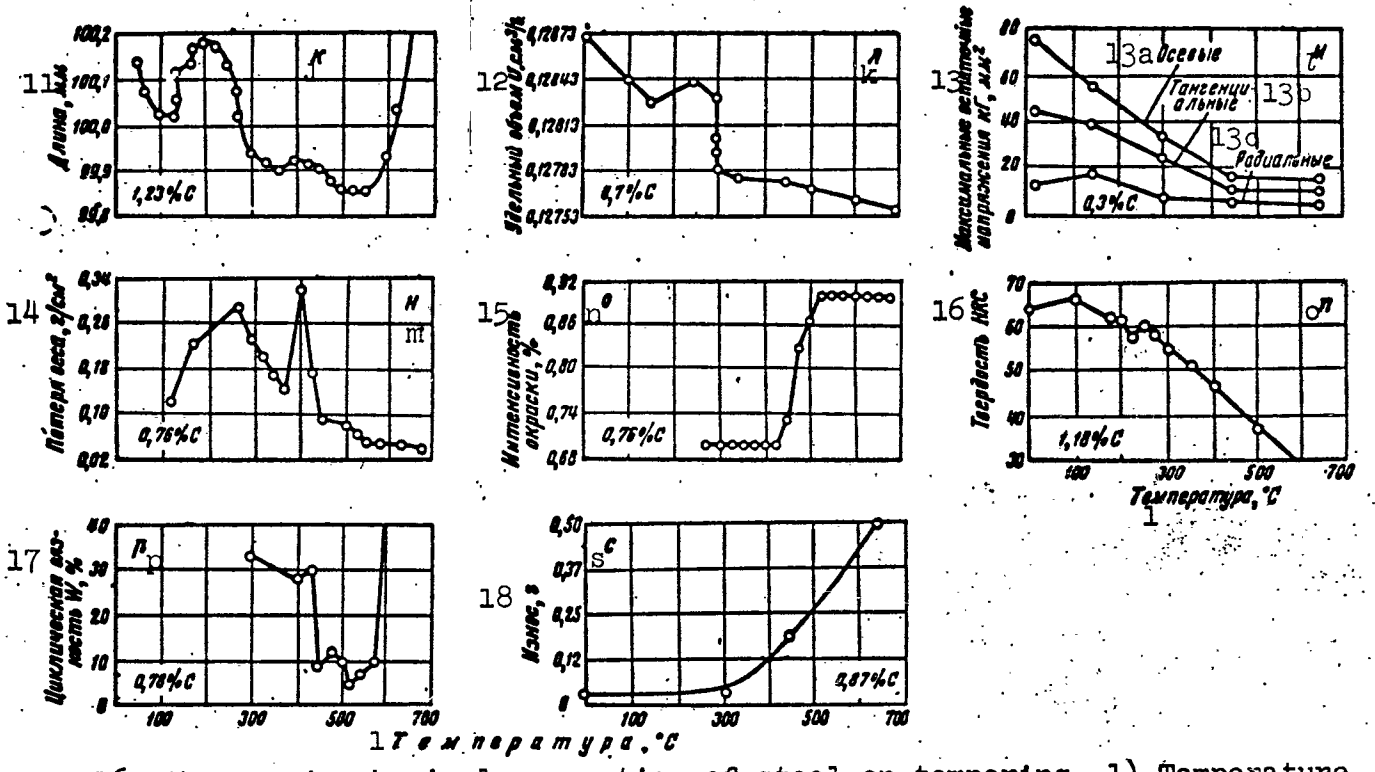


Fig. 16. Changes in physical properties of steel on tempering. 1) Temperature, °C; 2) coercive force, oersteds; 3) maximum magnetic permeability, gausses/oersted; 4) saturation magnetization ($4\pi I_n$), kilogausses; 5) residual induction, kilogausses; 6) resistivity, μohms·cm; 7) thermal electromotive force, μv/degree; 8) thermal conductivity, cal/cm·sec·deg; 9) heat capacity $C_p$, $10^{-3}$ cal/degree × × g; 10) heat effect, $10^{-5}$ v; 11) length, mm; 12) specific volume V, $cm^3/g$; 13) maximum residual stresses, $kgf/mm^2$; 13a) axial; 13b) tangential; 13c) radial; 14) weight loss, $g/cm^2$; 15) color intensity, %; 16) hardness HRC; 17) relative work of deformation W, %; 18) wear, g.

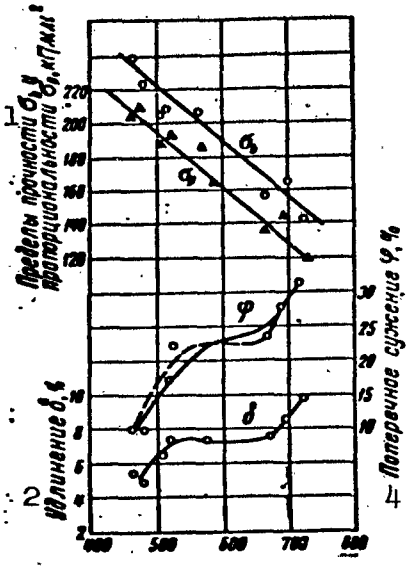


Fig. 17. Variation of mechanical properties of steel with 0.8% C after heating for tempering at a rate of 4000°C/sec (V.I. Trefilov). 1) Ultimate strength $\sigma_b$ and proportional limit $\sigma_p$, kgf/mm$^2$; 2) elongation $\delta$, %; 3) tempering temperature, °C; 4) transverse necking $\varphi$, %.

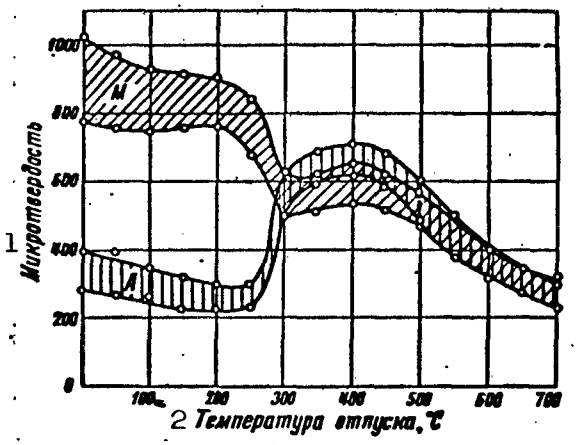


Fig. 18. Variation of microhardness of martensite (M) and residual austenite (A) as a function of tempering temperature [63]. 1) Microhardness; 2) tempering temperature, °C.

## 3. INFLUENCE OF ALLOYING ELEMENTS

First stage of tempering. Alloying elements have little influence on the rate at which carbon is precipitated in the first stage of martensite decay. The investigations of [90, 91] indicate that one hour is sufficient at 150° to bring the first stage to completion in steels with contents of 1-2% chromium, tungsten, molybdenum, or silicon. The temperature limits of the first stage in martensite decay thus undergo virtually no shift. The activation energy also shows little change. Here, the kinetics of martensite decay are determined preferentially by the rate of formation of carbide nuclei, which depends basically on

the extent to which the solution is supersaturated with carbon and to a lesser degree on the rate of atom diffusion. This is what accounts for the marked influence of carbon concentration in steel and the weak influence of alloying elements on the course taken by the decay process. In the first stage of martensite decay, redistribution of carbon concentration takes place with formation of dispersed carbide particles; here, there is no change in the distribution of alloying elements. The carbide regions that form have the same alloying-element concentrations as the initial solid solution. The redistribution of the concentrations of these elements between the martensite and the carbides begins only when the tempering temperature is elevated to 400-450° or when the tempering time is lengthened considerably [50, 93-95, 114].

Second stage of tempering. The alloying elements significantly inhibit the processes of martensite decay in this stage. The tempered-martensite state may be retained up to 400-500°. G.V. Kurdyumov [1] accounts for the inhibiting effect of alloying elements in terms of retarded growth of the carbide particles that have impregnated the solid-solution lattice. This growth process requires passage of metal atoms through the carbide/solid-solution boundary in solution of the fine particles and through the solid-solution/carbide boundary in growth of the large ones, as well as diffusion within the solid solution. Thus the rate of the second stage depends on the strength of the interatomic bonds in the solid-solution and carbide lattices, as well as on the diffusion rate of the carbon. The rate of transition of metal atoms through the solid-solution/carbide boundary in either direction is governed to a certain degree by the extent of bonding of the metallic atoms in the solid-solution lattice. This quantity may be judged on the basis of recrystallization rate. Alloying elements (W,

Mo, Cr, Co) raise the temperature and activation energy of recrystallization [96]. Thus it is obvious that alloying elements influence the kinetics of the second stage in martensite decay by strengthening the interatomic bonds in the α-solution and the carbide phase; those alloying elements that sharply inhibit solid-solution decay strengthen the bonding forces between atoms and raise the activation energy of recrystallization significantly.

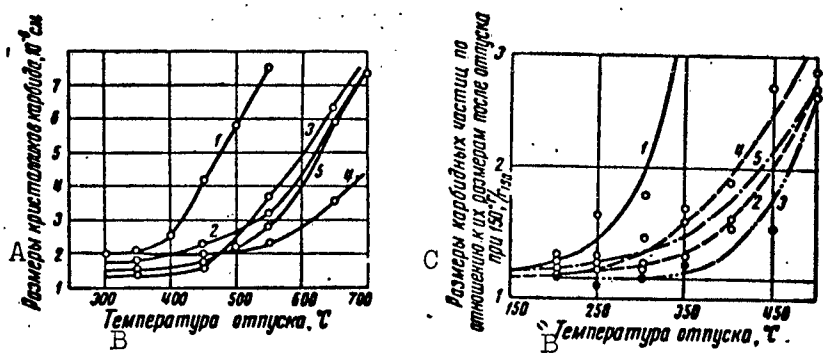


Fig. 19. Change in size of carbide crystals as a function of tempering temperature: a) for carbon steel (1), chromium steel (2), cobalt steel (3), molybdenum steel (4) and tungsten steel (5) [19]; b) for carbon (1), chromium (2), cobalt (3), zirconium (4) and silicon (5) steels [4]. A) Size of carbide granules, $10^{-6}$ cm; B) tempering temperature, °C; C) size of carbide particles as compared to size after tempering at 150°, $g/g_{150}$.

To characterize quantitatively the influence exerted by specific alloying elements, we may indicate the tempering temperatures at which the carbon content in the α-iron reaches 0.01% (on the basis of carbide analysis [50]): 500° in carbon steel (with 0.4% C), 500° in alloyed steels with 0.4% C at 1.75% Si, 500° with 3% Ni, 550° with 2.4% Mn, 650° with 2% Cr and 700° with 0.5% Mo. Increasing the extent of carbide-particle dispersion results in retention of an increased carbon concentration in the α-solution. Retention of the state of tempered martensite to higher temperatures dictates high hardness of the

steel up to 450-500°.

Decay of residual austenite in tempering. To one degree or another, alloying elements inhibit this decay [96]. In steels alloyed with carbide-forming elements, we observe two maxima on the decay curves of the residual austenite (see also [30]).

Third stage of tempering. Alloying elements increase the crystal-lattice distortions, raise the temperature at which they are eliminated, and broaden the temperature range in which the α-phase blocks are crushed [97].

Fourth stage of tempering. In alloy steels, the lowest temperature at which coagulation becomes noticeable is raised from 250 to 350-450° [19]. The growth of carbide particles in tempering of alloy steels is illustrated by Fig. 19 [19, 93]. On the basis of a quantitative study of the carbide-coagulation process in isothermal tempering, S.Z. Bokshteyn [50] proposed a method for computing the dispersion of carbide particles as a function of time, temperature, carbon concentration, and the content of alloying elements.

Redistribution of alloying elements. Carbide transformations. The onset of redistribution of alloying elements between the ferrite and carbide coincides with the last stages in martensite decay. Elements that do not form carbides remain in solution. Redistribution of carbide-forming elements takes place at higher tempering temperatures and at higher rates the stronger the bonding forces between the element and carbon. Consequently, the ferrite of vanadium steel is found to be least alloyed; it is followed by the ferrite of molybdenum and chromium steel and the ferrite of manganese steel is least heavily alloyed. The carbide transformation begins when the cementite becomes saturated with alloying elements and results in formation of the carbide of the specific element that is stable for the steel in question. At high con-

tents of molybdenum and vanadium, the specific carbides may arise directly from the solid solution [50, 98-102, 107]. Research into the influence exerted by carbide transformations (transition of one type of carbide into another) on the structure and properties of steel [50, 103-104] is of considerable interest. The investigations show that the temperature region of secondary hardness coincides with formation of the specific carbide and considerable retardation of relief of stresses of the second kind [105, 106].

4. TEMPERING BRITTLENESS*

The drop in impact strength in the tempering-temperature range from 250 to 400° is usually known as irreversible low-temperature tempering brittleness [108], while the drop in impact strength in the range from 450 to 575° is known as reversible tempering brittleness [109]. In certain grades of steels, irreversible brittleness also appears at 450-550° (high-temperature irreversible tempering brittleness) [110].*

Irreversible Low-Temperature Tempering Brittleness

Until recently, this form of brittleness was accounted for in terms of residual-austenite decay. It was also proposed [113] that the residual austenite is, so to speak, a viscous cement that binds the structure of quenched steel; its decay would only be exposing the true brittleness of the martensite. Together with this, the hypothesis had also been advanced that irreversible brittleness is caused by segregation of carbides on decay of the martensite.

V.D. Sadovskiy and his colleagues undertook a series of investigations on this question. Steels were selected in which the temperature ranges of martensite and austenite decay did not coincide. The experiments indicated that quite often, the brittleness range failed, either wholly or in part, to coincide with the temperature range of residual-

austenite decay. It was found further that the appearance of the carbide phase on tempering of martensite coincides with the development of irreversible tempering brittleness. Those alloying elements that inhibit martensite decay shift the range in which brittleness develops toward higher temperatures. Using special heat treatment, they succeeded in excluding decay of residual austenite and showing that development of the brittleness is governed by decay of martensite. As a result, it can now be affirmed that the development of irreversible tempering brittleness takes place independently of residual-austenite decay and is entirely determined by processes of carbide formation in tempering of the martensite [108].

Irreversible High-Temperature Tempering Brittleness

This form of brittleness, which develops in the range from 450 to 550°, but is not eliminated by rapid cooling, appears in steels that are sensitive to reversible brittleness and not susceptible to it. This is most distinctly manifested in steels with high contents of carbide-forming elements. In silicon-containing steels, the zones of low-temperature and high-temperature irreversible brittleness merge together. Some investigators link high-temperature irreversible brittleness to decay of residual austenite, while others associate it with segregation of disperse alloyed carbides. Alloying elements whose introduction into the steel might prevent the appearance of this form of brittleness are not known. Avoidance of dangerous temperature intervals in tempering of steels sensitive to this form of brittleness may be regarded as the only measure that can be taken to prevent it [110, 113].

Reversible Tempering Brittleness

This brittleness appears after tempering in the range from 450-575°, after tempering at 650-700° with subsequent slow cooling or when

steel is retempered in the range from 450-575° after tempering at higher temperatures with rapid subsequent cooling.

After a new tempering at 650-700° and rapid cooling, the steel recovers its resiliency. Subsequent soaking in the brittleness zone again makes the steel brittle, and so forth. Increasing the number of such cycles reduces the susceptibility of the steel to brittleness [114].

To a certain degree, a steel's tendency to reversible brittleness is determined by smelting conditions, i.e., by the processes used in producing it [110, 114, 115]. To a significant degree, the different tendencies toward reversible brittleness are accounted for in this case by fluctuations in the chemical composition of the steel, even though they may not exceed the limits tolerated by the standards.

The influence exerted by chemical composition is very strong. Phosphorus, manganese, silicon, chromium, aluminum, vanadium (as well as nickel and copper in the presence of chromium and manganese) increase the steel's tendency to reversible brittleness. Titanium, zirconium and nitrogen (as well as nickel and copper in the absence of other alloying elements) have no influence on it. Molybdenum and tungsten reduce the tendency to reversible brittleness. Phosphorus exerts the strongest influence on the development of reversible brittleness, even when present in small contents in the steel [116, 120, 109, 117, 110]. With high phosphorus contents (0.1-0.2%), a steel that is resilient after quenching and high tempering becomes brittle after exposure to air for a few hours. The phenomenon described here is reversible [118, 119, 109]. Steel with the lowest possible contents of phosphorus and manganese is virtually insensitive to brittleness [109]. Manganese in quantities above 0.5% imparts a sensitivity to reversible brittleness to carbon steel [109], but the content of this element that causes brittleness depends on phosphorus content [120, 110]. In the presence,

for example, of 1.6% Cr and 2.5% Ni, raising the manganese content from 0.25 to 0.90% increases the susceptibility of the steel to reversible brittleness by a factor of 13 [121]. Silicon at a content of 1.5% raises the tendency of chromium-nickel steel to reversible brittleness [109, 113], although its influence is weaker than that of manganese. Chromium raises the sensitivity to brittleness particularly in the presence of nickel [113], manganese and silicon [110]. In a chromium-nickel steel with 1.5% Si, chromium intensifies reversible brittleness even in the presence of molybdenum [109]. Vanadium causes a slight rise in sensitivity to reversible brittleness [123]; nickel steels, which have no tendency to brittleness of this kind, acquire susceptibility to it in the presence of phosphorus, chromium and manganese; copper steels have no tendency to brittleness [110]. According to recent data [122, 123], niobium and boron reduce reversible brittleness in steel to some extent. Aluminum is usually classified as a "neutral" element, although there are data indicating that it has some effect in reducing brittleness, apparently as a result of refinement of the steel grain [109]; according to another source [123], aluminum intensifies reversible brittleness. Reports concerning the influence of nitrogen are contradictory. Molybdenum introduced into steel in a certain quantity lowers the susceptibility to reversible brittleness; in smaller or larger contents it has a weaker influence or none at all [124]. Tungsten reduces the tendency of steel to reversible brittleness and may, in some cases, act as a rather effective substitute for molybdenum [125]. Titanium and niobium cannot be used effectively to suppress reversible brittleness; these elements can only alleviate it to a minor degree by refining the steel's grain.

Carbon increases reversible brittleness sharply; in its absence (0.003%), brittleness does not appear even in chrome-nickel steel [126].

Carbon steels are susceptible to reversible brittleness [114, 127, 128]. The temperature range of its development in a steel with 0.6% C is the same as for alloy steels (500-650°). Reversible brittleness also develops in those parts of carbon-steel products that were not quenched to martensite. The maximum brittleness is observed on cooling at 20°C/hour, and the reversible brittleness diminishes with higher or lower cooling rates. With 0.35% Mn and 0.01% P, no brittleness is detected; it is significant with 0.4% Mn and 0.05% P; it is less pronounced at 0.9% Mn and 0.01% P; the embrittlement effect has its maximum at 0.8% Mn and 0.05% P (the GOST upper limits for steels to be used for railway-car wheels) [129]. The idea of rapid embrittlement of carbon steel has not been confirmed by experiments [116, 109, 129].

The conditions of heat treatment strongly influence the development of brittleness. Reversible brittleness increases with increasing grain size in the austenite [114, 116, 130]. Chilling before quenching, which reduces stresses in the quenched steel but has no effect on the size of the austenite grain, does not alleviate brittleness [109]. A holding period at a rather low chilling temperature may help slightly [130]. Overheating sharply increases brittleness; to eliminate it, the steel must be heated above Chernov's point b, cooled and again heated to the quenching temperature [131]. Repeated quenching from the critical interval (between $Ac_1$ and $Ac_3$) reduces the sensitivity to brittleness [132]. Raising the tempering temperature inhibits subsequent development of brittleness at lower temperatures [114]. As the holding time in high tempering (650°) is prolonged, the toughness falls off, reaches a minimum, and then begins to rise again [114, 130, 133, 94, 102]. The cold-shortness threshold is shifted toward lower temperatures [125]. With increasing heating rate for quenching [134] and for tempering [55, 56] and diminishing holding times in tempering, revers-

Carbon steels are susceptible to reversible brittleness [114, 127, 128]. The temperature range of its development in a steel with 0.6% C is the same as for alloy steels (500-650°). Reversible brittleness also develops in those parts of carbon-steel products that were not quenched to martensite. The maximum brittleness is observed on cooling at 20°C/hour, and the reversible brittleness diminishes with higher or lower cooling rates. With 0.35% Mn and 0.01% P, no brittleness is detected; it is significant with 0.4% Mn and 0.05% P; it is less pronounced at 0.9% Mn and 0.01% P; the embrittlement effect has its maximum at 0.8% Mn and 0.05% P (the GOST upper limits for steels to be used for railway-car wheels) [129]. The idea of rapid embrittlement of carbon steel has not been confirmed by experiments [116, 109, 129].

The conditions of heat treatment strongly influence the development of brittleness. Reversible brittleness increases with increasing grain size in the austenite [114, 116, 130]. Chilling before quenching, which reduces stresses in the quenched steel but has no effect on the size of the austenite grain, does not alleviate brittleness [109]. A holding period at a rather low chilling temperature may help slightly [130]. Overheating sharply increases brittleness; to eliminate it, the steel must be heated above Chernov's point b, cooled and again heated to the quenching temperature [131]. Repeated quenching from the critical interval (between $Ac_1$ and $Ac_3$) reduces the sensitivity to brittleness [132]. Raising the tempering temperature inhibits subsequent development of brittleness at lower temperatures [114]. As the holding time in high tempering (650°) is prolonged, the toughness falls off, reaches a minimum, and then begins to rise again [114, 130, 133, 94, 102]. The cold-shortness threshold is shifted toward lower temperatures [125]. With increasing heating rate for quenching [134] and for tempering [55, 56] and diminishing holding times in tempering, revers-

ible brittleness is reduced and even prevented altogether. In the structures obtained as a result of isothermal decay of chrome-nickel steels, reversible brittleness develops to a lesser degree than it does in tempered martensite [116]. Raising the temperature of isothermal decay strengthens the tendency to brittleness [135]. Reversible brittleness is also observed in annealed steels [114, 136]. Its development raises the temperature of the transition to brittle failure in determinations of impact strength as a function of test temperature. Rational evaluation of a steel's tendency to brittleness is possible only as a result of series testing and determination of the shift in the critical brittleness temperature under the influence of embrittlement of the steel [109, 111, 114, 127, 120, 131 and others]. All known cases of tempering brittleness may be regarded as varieties of the cold-shortness phenomenon, although we may not yet speak of identity of the cold-shortness and tempering-brittleness problems ([109] – see also [138, 137]). A shift in the cold-shortness curves indicates the presence of tempering brittleness, but characterizes the degree of its development only highly approximately [109]. Brittleness is characterized by reduced tensile breaking strengths [139]. Failure occurs along the austenite grain boundaries of the α-phase [113, 116, 140]. Under the influence of cold plastic deformation, the susceptibility to irreversible and reversible brittleness is reduced [114, 141]. Plastic deformation in the austenitic state followed by quenching prior to recrystallization alleviates both irreversible and reversible tempering brittleness sharply [142].

It was believed for a long time that the results of mechanical tests with static load application remained the same on transition from the tough to the brittle state. Recently, however, brittleness has also been established in static testing [116, 143, 139, 138, 109

and others]; here, wear increases [144], endurance declines [145], and microhardness rises slightly [158]. Internal friction is higher in tough specimens [125].

Investigation of physical, including electrical and magnetic properties in the tough and brittle states has produced highly contradictory data [114, 116, 146 and others], since the presence of large residual stresses in the tough specimens and the varying residence times of the brittle and tough specimens in the zone of comparatively high temperatures were not taken into account. By special heat treatment, S.N. Polyakov succeeded in excluding the influence of the above factors. It was found that the coercive force of steel is 12% higher in the brittle state than in the tough state, while the hardness is 5% higher. The resistivity of tough specimens was also higher. In a steel without a tendency to tempering brittleness that was nevertheless tested in both the tough and brittle states, no property differences were observed [129].

The chemical properties of steel are different in the brittle and tough states. Thus, the rate of corrosion was found higher in specimens subjected to reversible brittleness [144].

In recent years, reagents have been suggested that make it possible to distinguish the states of reversible brittleness and toughness from the microstructure by the sharply etched grain boundaries [116, 147, 125, 148, 133 and others]. Use of the electron microscope and electron-diffraction apparatus has not yet given unequivocal results [149, 150, 116, 151, 152]. According to x-ray analysis, the major part of the carbides retains the cementite lattice [114, 150, 125, 127] on transition of the steel from the tough to the brittle state. Reports concerning the quantity of carbide phase in brittle and tough specimens are contradictory [125, 127].

It was assumed earlier that the solid solution of carbon in α-iron that forms when steel is heated to temperatures near $Ac_1$ decays so readily on cooling that it cannot be prevented even by sharp quenching. It was considered that the carbon has time to precipitate out of the α-solution even during extremely rapid cooling. But it has been shown comparatively recently by G.V. Kurdyumov and his colleagues that while the martensite crystals in quenched carbon steels with 0.2-0.6% C represent a partially decayed solid solution, all of the carbon may be fixed in solid solution at carbon concentrations lower or higher than the above [153]; there are also other reports that tend to confirm these observations [154, 155, 159].

An investigation of the solubility of carbon in α-iron alloyed with manganese or molybdenum, which also embraced the kinetics of carbon precipitation from solution [156, 129] and employed the internal-friction method showed that the presence of manganese (0.75%) and molybdenum (0.4%) lowers the solubility of carbon in iron (Fig. 20). However, with manganese alone present in the iron (with 0.03% C), the quantity of carbides precipitated is one-third as large as in iron; in the presence of molybdenum alone, the quantity of carbides was the same as in iron with 0.03% C without the alloying additives. Manganese sharply inhibits the onset of the precipitation process; addition of molybdenum does not influence its course. In a molybdenum-alloyed iron with 0.03% C,

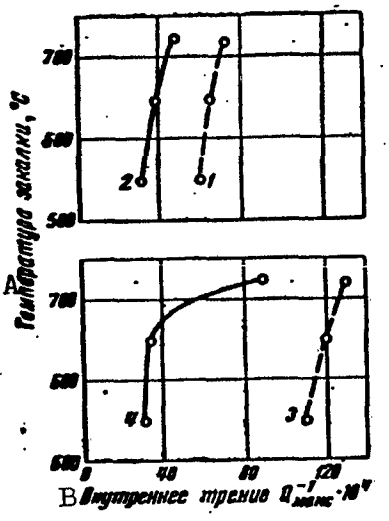


Fig. 20. Solubility of carbon in α-iron as a function of manganese and molybdenum contents. 1) Technical iron (0.03% C); 2) same, with 0.75% Mn; 3) technical iron (different composition); 4) same with 0.4% Mo [156, 129]. A) Quenching temperature, °C; B) internal friction $Q^{-1}_{maks} \cdot 10^4$.

tempering at 550-650° forms a highly stable carbide, so that virtually no solubility of carbon in the α-iron is noted. Thus, the tendency of the steel to reversible tempering brittleness is increased in the presence of manganese, apparently because this element raises the relative quantity of the precipitating phase and inhibits the coagulation process of the finely dispersed carbides; in the presence of an optimum amount of molybdenum, the relative quantity of precipitated phase does not increase, and its coagulation is not delayed. If specific carbides are formed in tempering no excess phase separates out [129].

At the present time, there are two basic viewpoints as to the nature of the phenomenon of reversible tempering brittleness.

According to one of these, reversible tempering brittleness is a consequence of a drop in brittle strength due to the segregation of certain phases at the boundaries of grains and mosaic blocks. It is generally known that on heating to 600-700°, the solubility of various components in steel rises, and that they are then separated out during slow cooling or on retempering with subsequent rapid cooling. The phase separation responsible for brittleness represents the result of the decay of solid solutions that form on heating (for high tempering or annealing). The hypothesis of internal adsorption proposed by V.I. Arkharov, according to which surface-active impurities are nonuniformly distributed in the grain volume in polycrystalline solid solutions [160, 161, 117, 131], enables us to assume the possibility of formation of supersaturated solutions in the surface layers of the granules, even in cases where the average composition of the solution is far from saturation. It appears that no unequivocal answer can be proposed for the question as to the nature of the phase whose separation produces brittleness; there is a possibility that it is different in different steels; it is also possible that in certain cases, brittleness

is caused by simultaneous precipitation of two or more phases [109]. In ordinary-type steels, phosphorus has a highly important role. The segregations may be phosphides, carbides, nitrides, and so forth [120, 157 and others]. The standpoint set forth here is confirmed by recent data on hardness and microhardness increases, an increase in internal friction and deterioration of corrosion resistance, and changes in resistivity and coercive force; also, by certain investigations carried out with the electron microscope and electron-diffraction apparatus, by data on the possibility of fixing the carbon in solid solution by rapid cooling, by data on the horophilic nature of the carbon and the concentration of its atoms at points of distortion of the α-iron lattice force field, and so forth.

According to the second point of view, reversible tempering brittleness and thermal brittleness are associated with segregation (without precipitation of a crystalline phase from the solid solution) of atoms of dissolved elements toward the grain boundaries and the distortions of the atomic crystal lattice of the solvent in the boundary sections of the grains that result from these displacements [111 and others]. Certain objections have been raised against the segregation hypothesis in the synopsis [109].

The problem of reversible tempering brittleness cannot yet be regarded as solved, since no altogether unequivocal proofs have as yet been presented for any specific point of view. It must be acknowledged, however, that both the older and the more recent data are in complete agreement with the "solution-precipitation" theory [109] when it is supplemented by conceptions as to the possibility of nonuniform distribution of surface-active elements in the solid solutions [160, 161, 117].

Manuscript Page No.

[Footnotes]

90 Editor's note: for carbon steel and a heating rate of 10°C/min.

95 I.V. Isachev found that the rhombic lattice of the carbide formed from $Fe_xC$ at 300-400° differs from the cementite lattice and comes to resemble it more closely only as the temperature of tempering is raised to 600° [43].

114 The phenomena of thermal brittleness [111], which arises on prolonged application of elevated temperature, and blue brittleness [112], which appears under static loading at 200-300° and under impact loading at 500-550°, are not considered here, although their nature has much in common with tempering brittleness [111].

REFERENCES


1. G.V. Kurdyumov, Primeneniye rentgenovskikh luchey k issledovaniyu materialov [The Use of X-Rays in Investigations of Materials], Mashgiz [State Scientific and Technical Publishing House of Literature on Machinery], 1949; Voprosy fiziki metallov i metallovedeniya [Problems of Metals Physics and Metallurgy], No. 2, Izd. AN USSR [Publishing House of the Acad. Sci. Ukrainian SSR], 1950.
2. S.T. Konobeyevskiy, Izvestiya AN SSSR, ser. khim. [Bulletin of the Acad. Sci. of the USSR, Chemistry Series, 1937, No. 5; ZhETF [J. Exp. Theor. Phys.], Vol. 13, 1943, No. 6, pages 185-200; Nos. 11-12, page 418.
3. G.V. Kurdyumov and L.I. Lysak, ZhTF [Journal of Technical Physics], 1949, No. 5, page 525.
4. L.I. Lysak, Voprosy fiziki metallov i metallovedeniya [Problems of Metals Physics and Metallurgy], No. 3, Izd. AN USSR [Publishing House of the Acad. Sci. of the Ukrainian SSR], 1952.
5. L.I. Lysak, Voprosy fiziki metallov i metallovedeniya, [Problems of Metals Physics and Metallurgy], No. 7, 1956, page 20.
6. H. Krainer, Arch. Eisenhuettenw. [Arch. Iron Metallurgy], Vol. 22, 1951, page 53.
7. C.S. Roberts, B.L. Averbach, M. Cohen, Trans. ASM, Vol. 45, 1953, page 576.
8. W. Jellinghaus, Arch. Eisenhuettenw., 1956, page 433.
9. B.S. Lement, M. Cohen, Acta Metallurgica, 1956, Vol. 4, No. 5,

page 469.

10. E.Z. Kaminskiy and T.I. Stelletskaya, Problemy metallovedeniya i fiziki metallov, Metallurgizdat, 1949, page 192.
11. G.V. Kurdyumov and L.I. Lysak, ZhTF, 1947, No. 9, page 993.
12. V.I. Arkharov, Kristallographiya zakalki stali [The Crystallography of Steel Hardening], Metallurgizdat, 1951.
13. G.V. Kurdyumov, ZhFKh [J. Phys. Chem.], 1930, p. 281.
14. M.P. Arbuzov and G.V. Kurdyumov, ZhTF, 1940, No. 13, page 1093.
15. E.Z. Kaminskiy and D.S. Kantsel'son, ZhTF, 1945, No. 3, page 182.
16. Ya.S. Umanskiy, Tekhnologicheskiye, fiziko-khimicheskiye i mekhanicheskiye svoystva stali. Trudy Moskovskogo instituta stali, Sb. 28, Metallurgizdat [Technological, Physicochemical and Mechanical Properties of Steel. Trans. of the Moscow Steel Institute, Collection 28, State Scientific and Technical Publishing House for Literature on Ferrous and Nonferrous Metallurgy], 1949.
17. Ya.S. Umanskiy, B.N. Finkel'shteyn, M.Ye. Blanter, S.T. Kishkin, N.S. Fastov and S.S. Gorelik, Fizicheskiye osnovy metallovedeniya [Physical Fundamentals of Metallurgy], Metallurgizdat, 1955.
18. F. Marion and R. Faivre, Rev. metallurgie [Metallurgy Review], Vol.55, 1958, page 459.
19. M.P. Arbuzov, Voprosy fiziki metallov i metallovedeniya, No. 3, Izd. AN USSR, 1952.
20. Yu.A. Bagaryatskiy, DAN SSSR, Vol. 73, 1950, No. 6.
21. G. Hägg. Zeitschr. Kristallogr. [J. Crystallography], Vol. 89, 1934, page 92.
22. K.H. Jack, Proc. Roy. Soc., Vol. 195, 1948, Ser. A, page 56.
23. K. H. Jack, J. Iron and Steel Inst., Vol. 169, 1951, page 26.
24. R.D. Heidenreich, L. Sturkey, H.L. Woods, Nature, Vol. 158, 1946, page 60; Appl. Phys., Vol. 17, 1946, page 127.

25. H.K. Goerlich, H. Goossens, Arch. Eisenhuettenw., 1956, page 119.
26. Yu.A. Skakov et al., DAN SSSR [Proc. of the Acad. Sci. USSR], Vol. 118, 1958, No. 2, page 284.
27. N.V. Gudkova, E.I. Levina and V.A. Tolomasov, Fizika metallov i metallovedeniye, Vol. 4, 1957, No. 3, page 500.
28. B.A. Apayev, Metallovedeniye i obrabotka metallov [Physical Metallurgy and Metalworking], 1957, No. 1, page 2.
29. N.M. Popova, Zavodskaya laboratoriya [Industrial Laboratory], 1949, No. 3, page 264; 1950, No. 3, page 280.
30. I.N. Bogachev and V.G. Permyakov, Otpusk zakalennoy stali [Tempering of Hardened Steel], Mashgiz [State Scientific and Technical Publishing House of Literature on Machinery], 1950.
31. V.G. Permyakov, ZhTF, 1955, No. 5, page 908.
32. V.G. Permyakov and M.V. Belous, Fizika metallov i metallovedeniye, Vol. 4, 1957, No. 3, page 490.
33. V.G. Permyakov, Metallovedeniye i obrabotka metallov, 1958, No. 3, page 24.
34. B.A. Apayev, Sb. Termicheskaya obrabotka metallov [Collection. Heat Treatment of Metals], Mashgiz, 1950, page 190; ZhTF, 1953, No. 7, page 1192; Fizika metallov i metallovedeniye, 1955, Vol. 1, No. 3, page 467; DAN SSSR; 1956, Vol. 107, No. 5, page 685.
35. B.A. Apayev, Metallovedeniye i obrabotka metallov, 1957, No. 1, page 2; 1957, No. 7, page 23.
36. J. Crangle, W. Sucksmith, J. Iron and Steel Inst., Vol. 168, 1951, page 141.
37. M.P. Arbuzov, Fizicheskaya priroda protesessov otpuska stali [Physical Nature of Processes of Steel Tempering], Kiev, 1954.
38. J. Iron and Steel Inst., Vol. 170, 1952, pages 251, 252, 254.
39. J.H. Andrew, H. Lee, J. Iron and Steel Inst., 1942, No. 1, page

153; Vol. 165, 1950, page 145; page 369; D.V. Wilson, Nature, Vol. 167, 1951, page 899; D.V. Wilson, Trans. ASM, Vol. 47, 1955, page 321.

40. Ye.I. Kondorskiy, DAN SSSR, 1950, Vol. 70, page 215; Vol. 74, page 213; 1951, Vol. 80, page 197; 1952, Vol. 82, page 365.

41. S.V. Vonsovskiy, Izv. AN SSSR, 1952, Vol. 16, page 4; Sovremennoye ucheniye o magnetizme [Modern Science of Magnetism], Gostekhteorizdat [State Publishing House of Theoretical and Technical Literature], 1953, page 270.

42. K.P. Belov, Uprugiye, teplovyye i elektricheskiye yavleniya v ferromagnitnykh metallakh [Elastic, Thermal and Electrical Phenomena in Ferromagnetic Metals], Gostekhteorizdat, 1957.

43. I.V. Isaichev, ZhTF, 1947, No. 7, page 839.

44. A.P. Gulyayev and N.I. Burova, Metallovedeniye i obrabotka metallov, 1955, No. 1, page 40.

45. P.L. Gruzin, G.V. Kurdyumov and R.I. Entin, Metallurg, 1940, No. 8, page 15; R.A. Abramovich, P.L. Gruzin, G.V. Kurdyumov and R.I. Entin, ZhTF, 1941, No. 12, page 1083.

46. K.F. Starodubov and V.K. Babich, Izmeneniye plasticheskikh svoystv stali pri otpuske. Izd. Ukrainskogo respulikanskogo pravleniya NTO ChM, 1957; Izvestiya vyschikh uchebnykh zavedeniy. Chernaya Metallurgiya [Change in Plastic Properties of Steel on Tempering. Publishing House of the Ukrainian-Republic Office of the Scientific and Technical Society of Ferrous Metallurgy, 1957; Bulletin of the Institutions of Higher Learning. Ferrous Metallurgy], 1958, No. 2, page 133.

47. V.K. Kritskaya, G.V. Kurdyumov and N.M. Nodia, ZhTF, 1955, No. 2, page 177.

48. E.Z. Kaminskiy, G.V. Kurdyumov and D.Kh. Leyvikova, ZhTF, 1941,

No. 12, page 1089.

49. L.S. Moroz, Tonkaya struktura i prochnost' stali [Fine Structure and Strength of Steel], Metallurgizdat, 1957.

50. S.Z. Bokshteyn, Struktura i mekhanicheskiye svoystva legirovannoy stali [Structure and Mechanical Properties of Alloyed Steel], Metallurgizdat, 1954.

51. E.D. Hyam, J. Nutting, J. Iron and Steel Inst., Vol. 184, 1956, page 148.

52. J.H. Hollomon, L.D. Jaffe, Trans. AIMME, Vol. 162, 1945, page 223; Metals Technology, Techn. Publ., No. 1831.

53. S.T. Kishkin, Izv. AN SSSR, OTN, 1946, No. 12, page 1799.

54. V.I. Prosvirin, Vliyaniye vneshnego davleniya na fazovyye prevrashcheniya v stali i chugune [The Effect of External Pressure on Phase Transformations in Steel and Cast Iron], Mashgiz, 1948.

55. L.I. Lysak, Voprosy fiziki metallov i metallovedeniya, 1956, No. 7, page 12.

56. G.V. Kurdyumov, B.D. Grozin and L.I. Lysak, DAN USSR, 1949, No. 1, page 17; Voprosy fiziki metallov i metallovedeniya, 1950, No. 2, page 43.

57. V.D. Sadovskiy and B.F. Sazonov, Trudy instituta fiziki metallov UFAN SSSR [Trans. of the Institute of Metal Physics of the Urals Branch of the Acad. Sci. USSR], 1946, Vol. 9, page 41.

58. R.M. Lerinman and V.D. Sadovskiy, Trudy instituta fiziki metallov UFAN SSSR, No. 13, 1951, page 32; Stal' 1948, No. 5, page 456.

59. V.N. Gridnev, Sb. Termicheskaya obrabotka metallov, Mashgiz, 1952, page 114; Sb. Voprosy fiziki metallov i metallovedeniya, Izd. AN USSR, 1959, page 54.

60. V.N. Gridnev, V.G. Permyakov and V.T. Cherepin, Metallovedeniye i obrabotka metallov, 1958, No. 4, page 9.

61. I.N. Kidin, Termicheskaya obrabotka stali pri induktsionnom nagreve [Heat Treatment of Steel With Induction Heating], Metallurgizdat, 1950.

62. B.S. Lement, B.L. Averbach, M. Cohen, Trans. ASM, Vol. 46, 1954, page 851; Vol. 47, 1955, page 291.

63. L. Besdek and D. Ruzicka, Sb. Problemy a vyhedy naseho hutnictvi a slevarenstvi [Problems of Metallurgy and Foundry Work], Prague, 1956.

64. R.M. Lerinman, V.D. Sadovskiy and A.M. Polyakova, Izv. AN SSSR, OFN [Bull. Acad. Sci. USSR, Division of Physical Sciences], 1951, No. 3, page 337.

65. A.P. Gulyayev and M.P. Zel'bet, Izv. AN SSSR, OTN, 1954, No. 3, page 83.

66. K.Z. Shepelyakovskiy, Samootpusk stali pri vysokochastotnoy zakalke [Self-Tempering of Steel in High-Frequency Hardening], Mashgiz, 1955.

67. M. Kersten, Phys. Zs. [Phys. J.], Vol. 44, 1938, page 63; Zs. Physik [J. Phys.], Vol. 124, 1948, page 714.

68. Ye.I. Kondorskiy, Zh. eksperim. i teor. fiz. [Journal of Experimental and Theoretical Physics], 1937, Vol. 7, page 1117; 1940, Vol. 10, page 420; DAN SSSR, Vol. 63, 1948, page 507.

69. V.S. Mes'kin, Ferromagnitnyye splavy [Ferromagnetic Alloys], ONTI, 1937.

70. K.F. Starodubov and M.A. Tylkin, Povysheniye prochnosti, plastichnosti i vyazkosti stali putem termicheskoy obrabotki [Increasing the Strength, Plasticity and Toughness of Steel by Heat Treatment], NTO ChM, 1957.

71. I.L. Mirkin and B.A. Sadikov, Khimicheskiye i termicheskiye metody obrabotki stali, Trudy Moskovskogo instituta stali [Chemical and

Thermal Methods of Steel Treatment. Trans. of the Moscow Steel Institute], Metallurgizdat, 1938.

72. V.S. Mes'kin, Trudy instituta metallov. Izd. Ukrainskogo respublikanskogo pravleniye ... tallov [Publishing House Ukr. Repub. ... Metals], Gostekhizdat, No. 10, 1930.

73. B.D. Enlund, Jernkont. Ann [not identified], Vol. 106, 1922, page 389.

74. E.D. Campbell, J. Iron and Steel Inst., Vol 92, 1915, page 164; Vol. 94, 1916, page 268.

75. W. Jellinghaus and M.P. de Andres, Arch. Eisenhuettenw., 1956, page 187; see also W. Jellinghaus, Arch. Eisenhuettenw., 1956, page 433.

76. F. Bollenrath and W. Bungardt, Arch. Eisenhuettenw., 1935, page 253.

77. S. Sato, Science Reports of the Tohoku Imperial University, Vol. 18, 1929, page 303.

78. A. von Vegesack, Jernkont. Ann., Vol. 120, 1936, pages 49, 143, 226.

79. V.N. Gridnev and A.Ts. Spektor, Trudy Instituta chernoy metallurgii [Trans. of the Inst. of Ferrous Metallurgy], Vol. 6, Izd. AN USSR, 1953.

80. H. Buehler, H. Buchholtz and E.H. Schulz, Arch. Eisenhuettenw., 1932, page 413.

81. D.M. Nakhimov, Struktura i svoystva termicheski obrabotannoy stali. Sb. Moskovskogo mekhanicheskogo instituta [Structure and Properties of Heat-Treated Steel. Collection of the Moscow Mechanical Institute], No. 2, Mashgiz, 1951, page 164.

82. K.F. Starodubov, DAN SSSR, Vol. 53, 1946, No. 3, page 217.

83. K.F. Starodubov, Sb. Problemy Metallurgii, Izd. AN SSSR, 1953,

page 442.

84. K.F. Starodubov, Nauchnyye doklady vysshey shkoly. Metallurgiya [Scientific Reports of Institutions of Higher Learning. Metallurgy], 1958, No. 1, page 266.

85. G.M. Kurdyumov and N.L. Oslon, ZhTF, 1939, No. 21, page 1891.

86. K.F. Starodubov and S.G. Chernyavskaya, DAN URSR [Proc. Acad. Sci. UkrSSR], 1956, No. 2, page 140.

87. K.F. Starodubov and S.G. Chernyavskaya, DAN URSR, 1956, No. 3, page 259.

88. A. Pomp, Stahl u. Eisen [Steel and Iron], 1924, II, September.

89. M.I. Zamotorin, Trudy Instituta mekhanizatsii sel'skogo khozyaystva [Trans. of the Institute of Agricultural Mechanization], Vol. 2, 1931.

90. G.V. Kurdyumov and G.Ya. Kozyrskiy, Voprosy fiziki metallov i metallovedeniya, No. 2, Izd. AN USSR, 1950, page 38.

91. G.V. Kurdyumov and M.D. Perkas, Problemy metallovedeniya i fiziki metallov, No. 2, Metallurgizdat, 1951, page 153.

92. L.I. Kogan and R.I. Entin, ZhTF, 1950, No. 5, page 629.

93. L.I. Lysak and G.Ya. Kozyrskiy, Voprosy fiziki i metallovedeniya, No. 3, izd. AN USSR, 1952, page 53.

94. L.I. Lysak and G.Ya. Kozyrskiy, DAN URSR, 1950, No. 4, page 293.

95. S.T. Kishkin, Izv. AN SSSR, OTN, 1941, No. 3, page 101.

96. V.D. Sadovskiy, Trudy Instituta metallofiziki i metallurgii [Trans. of the Institute of Metals Physics and Metallurgy], UFAN SSSR, No. 3, 1945.

97. L.I. Lysak and G.Ya. Kozyrskiy, ZhTF, 1953, No. 10, page 1761.

98. G.V. Kurdyumov and M.D. Perkas, DAN SSSR, Vol. 87, 1952, No. 1, page 41.

99. K. Kuo, J. Iron and Steel Inst., Vol. 173, 1953, page 363; Vol.

174, 1953, page 223; Vol. 184, 1956, page 258; Vol. 185, 1957, page 297.

100. A.P. Gulyayev, Sb. Novoye v metallovedenii [Recent Discoveries in Metallurgy], Mashgiz, 1948, page 5.

101. A.S. Zev'yalov and Ye.Ya. Paley, Sb. Metallovedeniye, Sudpromgiz [Collection. Metallurgy. State All-Union Publishing House of the Shipbuilding Industry], 1957, page 220.

102. S.T. Kishkin, Izv. AN SSSR, OTN, 1941, No. 4, page 91.

103. N.F. Lashko and M.D. Nesterova, Izv. AN SSSR, Ser. fiz., Vol. 15, 1951, No. 1.

104. Z.K. Kos'ko, DAN SSSR, Vol. 108, 1956, No. 6, page 1072; Fizika metallov i metallovedeniye, 1957, Vol. 5, No. 1, page 179.

105. L.I. Lysak and Ye.G. Nesterenko, Voprosy fiziki metallov i metallovedeniya, No. 4, Izd. AN USSR, 1953.

106. Z.K. Kos'ko, Metallovedeniye i obrabotka metallov [Metallurgy and Metalworking], 1956, No. 11, page 33.

107. V.I. Arkharov and S.T. Kiselev, DAN SSSR, Vol. 59, 1948, No. 9, page 1571; Sb. Metallovedeniye i termoobrabotka, No. 11, Mashgiz, 1949, page 191.

108. Ye.N. Sokolov and V.D. Sadovskiy, Trudy Instituta fiziki metallov [Trans. of the Institute of Metals Physics], UFAN SSSR, 1956, No. 18, page 3.

109. V.D. Sadovskiy, Metallovedeniye i obrabotka metallov, 1957, No. 6, page 24.

110. V.A. Delle, Legirovannaya konstruktsionnaya stal' [Alloyed Structural Steel], Metallurgizdat, 1953.

111. G.P. Mikhaylov-Mikheyev, Teplovaya khrupkost' stali [Thermal Brittleness of Steel], Mashgiz, 1956.

112. G.I. Pogodin-Alekseyev and M.M. Fetisova, Termicheskaya obrabotka

metallov, Sb. MVTU [Heat Treatment of Metals, Collection of the Moscow Higher Technical School (im. N.Ye. Bauman)], No. 70, Mashgiz, 1956, page 36; Metallovedeniye i obrabotka metallov, 1956, No. 8, page 31.

113. V.D. Sadovskiy and N.P. Chuprakova, Trudy Instituta metallovedenii, UFAN SSSR, No. 6, 1945.

114. G.V. Kurdyumov and R.I. Entin, Otpusknaya khrupkost' konstruktsionnykh staley [Tempering Brittleness of Structural Steels], Metallurgizdat, 1945.

115. S.M. Baranov, Stal' [Steel], 1948, No. 4, page 346; Sb. Problemy konstruktsionoy stali, Mashgiz, 1949; DAN SSSR, Vol. 83, No. 1, page 125; Metallovedeniye i obrabotka metallov, Vol. 83, No. 1, page 125; Metallovedeniye i obrabotka metallov, 1956, No. 12, page 41.

116. B.C. Woodfine, J. Iron and Steel Inst., Vol. 173, 1953, pages 229 and 240.

117. V.I. Arkharov, S.I. Ivanovskaya, N.M. Kolesnikova and T.A. Fofanova, Fizika metallov i metallovedeniye, Vol. 2, 1956, No. 1, page 57.

118. E. Houdremont and H. Schrader, Arch. Eisenhuettenw., 1950, Vol. 3/4.

119. A.M. Beyngarten, Stal', 1949, No. 10, page 920.

120. N.V. Tolstoguzov and A.D. Kramarov, Metallovedeniye i obrabotka metallov, 1957, No. 2, page 32.

121. H. Esser and H. Ellender, Arch. Eisenhuettenw., 1930, Vol. 3.

122. I.V. Bolobuyev and V.V. Gavranek, Trudy Khar'kovskogo politekhnichskogo instituta [Trans. of the Khar'kov Polytechnic Institute], 1957, No. 9, page 113.

123. M.L. Bernshteyn, Metallovedeniye i obrabotka metallov, 1956, No.

9, page 25.

124. A.A. Moiseyev and V.A. Delle, Sb. Metallovedeniye i termicheskaya obrabotka, No. 1, Metallurgizdat, 1954, page 24.

125. V.I. Prosvirin and Ye.I. Kvashnina, Vestnik mashinostroyeniya [Herald of Machine Building], 1955, No. 2, page 58. Termicheskaya obrabotka i svoystva litoy stali [Heat Treatment and Properties of Cast Steel], Mashgiz, 1955; Metallovedeniye i obrabotka metallov, 1955, No. 3, page 18; 1956, No. 2, page 34.

126. E.B. Mikus, C.A. Siebert, Trans. ASM, Vol. 50, 1958, page 682.

127. A.S. Zav'yalov and M.I. Senchenko, ZhTF, 1953, No. 3, page 479; A.S. Zav'yalov, M.I. Senchenko and L.Ya. Gol'dshteyn, Metallovedeniye i obrabotka metallov, 1957, No. 4, page 21; Sb. Metallovedeniye, Sudpromgiz, 1957.

128. J.F. Libsch, A.E. Powers, G. Bhat, Trans. ASM, Vol. 44, 1952, page 1058.

129. K.F. Starodubov and S.N. Ployakov, Izvestiya vysshikh uchebnykh zavedeniy. Chernaya metallurgiya, 1958, No. 3, page 132.

130. L.V. Smirnov and V.D. Sadovskiy, Trudy instituta fiziki metallov UFAN SSSR, No. 18, Izd. AN SSR, 1956, page 57.

131. M.L. Bernshteyn and N.N. Kuleshova (cited from 109), Metallovedeniye i obrabotka metallov, 1957, No. 6, page 36.

132. V.G. Sazonov, Metallovedeniye i obrabotka metallov, 1957, No. 4, page 30.

133. V.N. Svechnikov and V.N. Gridnev, Trudy instuta chernoy metallurgii AN USSR, 1951, page 23.

134. K.A. Malyshev and V.A. Pavlov, Trudy Instituta fiziki metallov UFAN SSSR, No. 9, 1946, page 20.

135. T.V. Sergiyevskaya, Stal', 1955, No. 1, page 63 (sr. sb. Metal-

lovedeniye i termicheskaya obrabotka. Prilozheniye k zhurnaly Stal' [Steel, 1955, No. 1, page 63 (See Collection Entitled Physical Metallurgy and Heat Treatment. Supplement to the Journal Steel], Metallurgizdat, 1958, page 95.

136. K.M. Pogodina-Alekseyeva, Metallovedeniye i obrabotka metallov, 1957, No. 3, page 36.

137. N.N. Davidenkov and G.P. Zaytsev, ZhTF, 1932, No. 5, page 477.

138. N.N. Davidenkov, ZhTF, 1953, No. 3, page 401.

139. M.M. Shteynberg and A.A. Popov, Zavodskaya laboratoriya, 1952, No. 11, page 1377.

140. A.R. Entwisle, J. Iron and Steel Inst., Vol. 169, 1951, page 36.

141. M.M. Shteynberg, V.D. Sadovskiy and A.V. Demakova, Metallovedeniye i obrabotka metallov, 1956, No. 6, page 26.

142. L.V. Smirnov, Ye.N. Sokolkov and V.D. Sadovskiy, Trudy Instituta fiziki metallov UFAN SSSR, No. 18, Izd. AN SSSR, 1956, page 36.

143. N.V. Tolstoguzov, Metallovedeniye i obrabotka metallov, 1956, No. 8, page 28.

144. V.K. Tselikov, Stal', 1947, No. 5, page 436; 1948, No. 8, page 724.

145. S.I. Ratner, DAN SSSR, Vol. 106, 1956, No. 2.

146. Dzh.F. Libsh and G.P. Konrad, Sb. Struktura metallov i svoystva, Metallurgizdat, 1957, page 215.

147. H.C. Goerlich, E. Koerfer, G. Obelode and H. Schenck, Arch. Eisenhuettenw., 1954, page 613; 1956, page 147.

148. S.F. Yur'yev and Z.I. Kusnitsyna, Fizika metallov i metallovedeniye, Vol. 3, 1956, No. 2, page 282.

149. A.I. Rizol' and L.G. Sakvarelidze, L.M. Utevskiy, DAN SSSR, Vol. 105, 1955, No. 2.

150. S.R. Maloof, Trans. ASM, Vol. 44, 1952, page 264; perev. sm.

Problemy sovremennoy metallurgii [For translation, see Problems of Contemporary Metallurgy], 1953, No. 2.

151. L.Ya. Gol'dshteyn, Metallovedeniye i obrabotka metallov, 1956, No. 11, page 36.

152. N.V. Kazakova and N.V. Koroleva, Metallovedeniye i obrabotka metallov, 1957, No. 2, page 39.

153. G.V. Kurdyumov, M.D. Perkas and A.Ye. Shamov, DAN SSSR, Vol. 92, 1953, page 955.

154. C.A. Wert, J. Appl. Phys., Vol. 20, 1949, No. 10, page 943.

155. W. Wepner, Arch. Eisenhuetenw., 1955, Vol. 2, page 71.

156. K.F. Starodubov and S.N. Polyakov, DAN URSR, 1958, No. 2, page 135.

157. V.S. Mes'kin, Metallovedeniye i obrabotka metallov, 1956, No. 7, page 24.

158. S.H. Busch, C.A. Siebert, J. Metals, 1954, No. 11.

159. A.S. Novik, Uspekhi fiziki metallov [Progr. Phys. Metals], Vol. 1, Metallurgizdat, 1956.

160. V.I. Arkharov, DAN SSSR, Vol. 50, 1945, page 293.

161. V.I. Arkharov, Trudy Instituta fiziki metallov UFAN SSSR, No. 8, 1946, page 54.

# DISTRIBUTION LIST

| DEPARTMENT OF DEFENSE | Nr. Copies |
|---|---|
| HEADQUARTERS USAF | |
| AFCIN-3D2 | 1 |
| ARL (ARB) | 1 |
| OTHER AGENCIES | |
| CIA | 1 |
| NSA | 6 |
| DIA | 9 |
| AID | 2 |
| OTS | 2 |
| AEC | 2 |
| PWS | 1 |
| NASA | 1 |
| ARMY (FSTC) | 3 |
| NAVY | 3 |
| NAFEC | 1 |
| AFCRL (CRXLR) | 1 |
| SPECTRUM | 1 |
| RAND | 1 |

| MAJOR AIR COMMANDS | Nr. Copies |
|---|---|
| AFSC | |
| SCFDD | 1 |
| DDC | 25 |
| TDBTL | 5 |
| TDBDP | 5 |
| AEDC (AEY) | 1 |
| ASD (ASYID) | 1 |